PHYSIOLOGICAL EFFECTS OF HYDRODYNAMIC FORCES ON ANIMAL CELLS

A Dissertation

Presented in Partial Fulfillment of the Requirements for

the Degree Doctor of Philosophy in the

Graduate School of The Ohio State University

By

Michael Mollet, B.S.

*****

The Ohio State University

2004

Ph.D. Examination Committee:

Dr. Jeffrey Chalmers, Adviser
Dr. Kurt Koelling
Dr. Shang-Tian Yang

Approved By:

_____

Adviser
Graduate Program in Chemical Engineering

Abstract

In biological research and in the biopharmaceutical industry, there is a continuing concern over the occurrence of cell damage in a variety of devices as a result of hydrodynamic forces. One of the parameters used to quantify hydrodynamic conditions is the local energy dissipation rate (EDR). The EDR is the irreversible rate of internal energy increase per unit volume, or, in other words, the irreversible conversion of mechanical energy to heat. It is a scalar value, has units of power per unit volume (i.e. W/m^3), and is intrinsic to any moving fluid. It can be calculated reliably using well-established equations for simple systems and computational fluid dynamics (CFD) for more complex systems. A microfluidic device was developed to determine the sensitivity of mammalian cells to locally high levels of EDR. Using this microfluidic device, the level of cell damage was measured as a function of the EDR. Two cell types were analyzed, CHO-K1 cells transfected with bcl-2, an anti-apoptosis gene, and the wild type CHO-K1 cells. These cells were evaluated for apoptosis as well as necrosis using flow cytometry. The results were then compared to the EDR cells would encounter in many bioprocess devices, such as: tubing, pipettes, rectangular channels, Fluorescence Activated Cell Sorter (FACS) instruments, and stirred tank bioreactors. The EDR in the aforementioned device was determined using analytical and experimental techniques as well as CFD simulations. With the exception of bubble rupture in

bioreactors and the FACS instrument, it was found that necrosis is unlikely in most systems. Under certain growth conditions apoptosis is possible at a lower EDR, however this lower EDR value is still at least an order of magnitude higher than what cells would typically experience in bioprocess equipment.

Dedicated to my wife,

my children, and

my parents

Acknowledgements

I wish to thank Dr. Jeff Chalmers, my adviser, for his support; his deep understanding of the fundamentals of cell culture is an invaluable resource. I am very grateful for the latitude he granted me to find unique solutions for problems in my research and in other areas as well. I would also like to thank Dr. Robert Brodkey and Dr. Kurt Koelling for their insights into fluid mechanics, and Dr. S.T. Yang for his advice.

I am also thankful for the help Dr. Ningning Ma gave me in learning cell culture and FLUENT. I especially appreciate all of the help, advice, and long hours Ruben Godoy, Weiwei Hu, and Bhavya Mehta gave me over the course of several experiments.

Finally, I wish to thank my parents for their unfaltering love and support, and I would like to thank Amy Mollet, my wife. Her unconditional love and incredible patience have truly been a godsend. Most of all I would like to thank God for giving me the ability and perseverance to finish.

Vita

March 18, 1977…… Born – Saint Louis, Missouri

2000……...B.S. Chemical Engineering,
University of Missouri–Rolla

2000-2001…… Departmental Fellowship,
The Ohio State University

2001-2002……. Graduate Research Associate,
The Ohio State University

2003-present……..Research Associate,
The Ohio State University

Publications

Mollet, M., Ma, N., Zhao, Y., Brodkey, R., Taticek, R., and Chalmers, J. 2004. Bioprocess Equipment: Characterization of Energy Dissipation Rate and its potential to Damage Cells. *Biotechnology Progress*. **20(5)**: 1437-1448.

Bhattacharya, G., Herman, J., Delfi´n, D., Salem, M., Barszcz, T., Mollet, M., Riccio, G., Brun, R., and Werbovetz, K. 2004. Synthesis and Antitubulin Activity of N^1- and N^4-Substituted 3,5-Dinitro Sulfanilamides against African Trypanosomes and Leishmania*, J. Med. Chem.* **47**: 1823-1832.

Ma, N., Mollet, M., Chalmers, J. "Aeration, Mixing and Hydrodynamics in Bioreactors." Cell Culture Technology for Pharmaceutical and Cellular Therapies Ed. Ozturk, S. and Hu, W. New York, NY: Marcel Dekker, 2004.

Fields of Study

Major Field: Chemical Engineering

Minor Field: Biotechnology, cell culture

Table of Contents

Page
Abstract……ii
Dedication……...iii
Acknowledgements……..v
Vita……..vi
List of Tables……..xi
List of Figures……xii

Chapter

1 Introduction……..1

2 Literature Review……5

2.1 Biology of Cell Death……5
2.1.1 Necrosis……5
2.1.2 Apoptosis……6
2.2 Calculating Hydrodynamic Stress……..7
2.3 Previous Studies Relating Cell Damage To Fluid Forces……..8
2.4 Hydrodynamic Stress in Bioprocess Equipment……..13
2.4.1 Hydrodynamic Stress in Bioreactors……13
2.4.1.1 Impellers……...14
2.4.1.2 Bubble Rupture……17
2.4.2 Cell damage in Other Bioprocess Equipment……...18
2.4.2.1 Cell damage in pumps……...18
2.4.2.2 Cell Death in Filtration Systems and Centrifuges…….19
2.4.2.3 Cell Damage in Turbulent Flow……...21
2.4.2.4 Cell Damage in FACS Instruments……...21

3 Characterization of Energy Dissipation Rate in Bioprocess Equipment……..27

3.1 Introduction……..27
3.2 Analytical Analysis……..32
3.3 Computational Fluid Dynamics (CFD) Analysis……36
3.4 Empirical Studies……38

3.5 Experimental Values ofEnergy Dissipation Rate in a Bioreactor……....40
3.6 Discussion……47

4 Apoptosis in Bioprocess Equipment……66

4.1 Introduction……..66
4.1.1 Modes of Cell Death: Necrosis……66
4.1.2 Modes of Cell Death: Apoptosis……..67
4.1.3 Means of Initiating and blocking Apoptosis……69
4.1.4 Means of Representing Hydrodynamic Stress……70
4.1.4.1 Shear Stress……70
4.1.4.2 The Energy Dissipation Rate (EDR)……...71
4.1.5 Micro-fluidic Contractional Flow Device……72
4.2 Materials and Methods……74
4.2.1 Stainless Steel Contractional Flow Device……..74
4.2.2 Computational Fluid Dynamic (CFD) Simulations……74
4.2.3 Cell Culture……..75
4.2.4 Contractional flow device experiments ……..76
4.2.4.1 Annexin V/7-AAD experiments……76
4.2.4.2 Mitochondrial Activity: Rhodamine 123……...77
4.2.4.3 Bcl-2 Expression Detection……...78
4.3 Results……..78
4.3.1 CFD Simulations……..78
4.3.2 AV/7-AAD Experiments……79
4.3.3 Other Flow Cytometric and Fluorescence Microscopy Data…...80
4.4 Discussion……81
4.4.1 Early Apoptosis……81
4.4.2 Late apoptosis/necrosis……82
4.4.3 Other Flow Cytometric and Fluorescence Microscopy Data…...83
4.5 Conclusion……...…84

5 Cell Damage in FACS Instruments……100

5.1 Introduction……100
5.2 Materials and Methods……...105
5.2.1 CFD Simulations……105
5.2.2 FACS Experiment……..106
5.3 Results……107
5.3.1 CFD Simulations……107
5.3.2 FACS Experiment……..108
5.4 Discussion……..109
5.4.1 CFD Simulations……109
5.4.2 FACS Experiment……..109
5.5 Conclusion and Future Work……110

6 Conclusions……123

Bibliography……127

Appendix A: User Defined Function (UDF) to calculate EDR……...136

A.1: Calculating the EDR in three dimensions……...136

A.2: Calculating the EDR in two dimensions……138

Appendix B: Particle Tracking in FLUENT……...139

Appendix C: Perl script to determine the maximum EDR for each particle....……..141

Appendix D: Annexin V (AV) assay procedure……144

List of Tables

Table		Page
3.1	Dimension and number of nodes used in simulation of pipettes……...50	
3.2	Geometry of bioreactor and impeller and properties of liquid and tracer used in the experiments……..50	
3.3	Experimental conditions for PTV studies……..51	
3.4	Values for parameters used in the AGW ES analysis of data……52	
3.5	Summary of several variables obtained for each of the three experimental conditions……...…53	
4.1	Summary of median maximum particle EDR for each of the simulated flow rates……85	
5.1	Summary of maximum EDR produced in a 100 μm diamter FACS nozzle……...111	
5.2	Summary of maximum EDR produced in a 70 μm diameter FACS nozzle……...112	
5.3	FACS core stream diameters determined analytically and from FLUENT…….113	

List of Figures

Figure Page

2.1 Velocity vector profile for laminar fluid flow in a pipe……...……..24

2.2 (A) FACS instrument nozzle and deflection plates schematic;
(B) FACS instrument nozzle, internal flow……25-26

3.1 Maximum energy dissipation rate as a function of flow rates, geometries, and dimensions. Specifically, pipe, annulus, parallel plates, and square channels (A-D, respectively) are presented. The variable k is the ratio of the inner to outer radius……..54-57

3.2 (A) Representative histogram of the simulated maximum energy dissipation rate each particle experienced flowing through a wide pipet at 2 mL/s.
(B) Plot of the maximum energy dissipation rate calculated for the three types of pipets over a range of flow rates……..58

3.3 (A) Diagram of the vessel in which studies were conducted,
(B) the triggering mechanism used to synchronize impeller position with image acquisition, and (C) schematic diagram of the experimental apparatus used obtain images for PTV analysis……...59-60

3.4 Gray scale plot of five slices of the energy dissipation rates (W/m^3) in the impeller region at 195 rpm. Also included is a diagram indicating the location of the five slices……...61

3.5 Locations of nodes with highest values of energy dissipation from experimental condition B and the same impeller position: (a-c) highest five node points, (d-f) highest 20 node points, and (g-i) top 100 node points…...62

3.6 Histogram of the energy dissipation for (a) the whole vessel and (b) impeller region for the 73 rpm studies and (c) the impeller region for the 195 rpm study…….63

3.7 (A) Top and (B) perspective view of the volume used to create the "square ring" in the impeller discharge region……..64

3.8 Calculated maximum (—) and mean (···) energy dissipation rate in the Applikon bioreactor, containing four baffles, as a function of rpm. The single points correspond to experimental measurements in this study without baffles……...65

4.1 Photograph of the contractional device……..86

4.2 Microscope picture of the constricted region of the contractional device…….86

4.3 Representative particle tracks colored by EDR (in W/m³), from FLUENT simulation……..87

4.4 Histogram of simulated maximum EDR each particle received for every flow rate; median values are included……...87

4.5 Representative dot plot of 7-AAD vs. AV-PE, from WT CHO-K1 cells cultured in T-flasks with 10% FBS, events in the lower left quadrant are healthy, events in the lower right quadrant are early apoptotic, and events in the upper right quadrant are late apoptotic or necrotic……88

4.6 Early Apoptosis (lower right quadrant): WT CHO-K1 cells cultured in T-flasks with 10% FBS……..89

4.7 Early apoptosis (lower right quadrant): WT CHO-K1 cells cultured in a spinner flask, 0% FBS……90

4.8 Early apoptosis (lower right quadrant): WT CHO-K1 cells cultured in a bioreactor, 0% FBS……90

4.9 Early apoptosis (lower right quadrant): CHO-bcl2 cells cultured in T-flasks with 10% FBS…….……...91

4.10 Early Apoptosis (lower right quadrant): bcl2-CHO cells cultured in a bioreactor, 0% FBS……91

4.11 Late apoptosis/necrosis (upper right quadrant): WT CHO-K1 cultured in T-flasks with 10% FBS……..92

4.12 Late apoptosis/necrosis (lower right quadrant): WT CHO-K1 cells cultured in a spinner flask, 0% FBS……92

4.13 Late apoptosis/necrosis (lower right quadrant): WT CHO-K1 cells cultured in a bioreactor, 0% FBS…….93

4.14 Late apoptosis/necrosis (lower right quadrant): bcl2-CHO cultured in T-flasks with 10% FBS……..93

4.15 Late apoptosis/necrosis (lower right quadrant): bcl2-CHO cells cultured in a bioreactor, 0 % FBS……94

4.16 Summary of necrosis data, relative to each sample's corresponding control……94

4.17 Relative median Rhodamine 123 fluorescence as a function of time for WT CHO-K1 cells cultured in spinner flasks with 0% FBS…….95

4.18 Rhodamine 123 fluorescence (FL1-H) vs. Draq5 fluorescence (FL4-H), for the WT CHO-K1 cells cultured in serum free media and in suspension in a 250 mL spinner flask…….95

4.19 Forward vs. Side scatter dot plot of the events in the Draq5 "bright" gating region of figure 4.18……..96

4.20 Forward vs. Side scatter dot plot of the events in the Draq5 "dim" gating region of figure 4.18……..96

4.21 Histogram overlays of bcl2 over expressing cells stained with an anti-human bcl2 antibody conjugated to PE…….97

4.22 (A and B) Fluorescent Microscope pictures, taken at 100X, of bcl-2 expressing cells, red color is the anti-bcl-2 PE antibody, and the blue is the Hoechst 33342 nuclear stain……...98

4.23 Percentage of necrotic WT and bcl2 expressing CHO cells, as a function of EDR (in kW/m^3). Data recorded shortly after cells' passage through the contractional flow device……99

5.1 Schematic detailing the fluidics of a FACS instrument; the gray areas are sheath and the blue are the sample fluid (A) cutaway of the FACS nozzle, (B) sheath tank, and (C) sample tube…….…….114

5.2 Geometry and mesh of node points for FACS instrument nozzle, (A) entire geometry, (B) magnified exit……115-116

5.3 Measured volumetric flow rate versus sheath pressure for a BD FACS Vantage…….117

5.4 Measured sample uptake rate versus sample differential pressure, for the 70 μm diameter nozzle……..117

5.5 Measured sample uptake rate versus sample differential pressure, for the 100 μm diameter nozzle……...118

5.6 Representative histogram of maximum particle EDR versus count for the 70 μm diameter nozzle at 25 psi sheath pressure for various sample differential pressures……119

5.7 Counter plot of particle tracks, colored by EDR at the exit of the 70 μm diameter nozzle with a 35 psi sheath pressure and a 1.0 psi sample differential pressure…….120

5.8 Representative dot plot of 7-AAD relative fluorescence (FL3-H) versus Annexin V-PE relative fluorescence (FL2-H), events in the lower left quadrant are healthy, events in the lower right quadrant are early apoptotic, and events in the upper right quadrant are late apoptotic or necrotic……..……121

5.9 Percent of early apoptotic (lower right quadrant) versus time (hr.) since sorting or passage through the contractional flow device……121

5.10 Percent of late apoptotic/necrotic (upper right quadrant) versus time (hr.) since sorting or passage through the contractional flow device……..122

Chapter 1

Introduction

Most of the new therapeutic compounds in clinical trials (approximately 67%) are protein-based drugs, which are also called biologics or biopharmaceuticals (Arnst *et al.*, 2004). Typically biologics are produced in genetically modified mammalian cells, because of the post translational modifications required to make the therapeutic compound effective *in vivo* (Molowa, 2002). Unfortunately, producing proteins from mammalian cell culture is more difficult than producing proteins using bacterial or yeast fermentation, primarily because mammalian cells do not grow as fast and are less robust due to a lack of a rigid cell wall.

There has been a continuing concern regarding cell death in bioprocess equipment, e.g. bioreactors, pumps, tubing, filtration systems, etc. The productivity of the bioprocess is affected by the cell viability, the percentage of live cells (Rose *et al.*, 2003). Simply stated, dead cells do not produce much protein. Cells die via two methods, necrosis and apoptosis. Necrosis is passive cell death, or "cell murder", whereas apoptosis is active cell death or "cell suicide". Many engineers and scientists in the biopharmaceutical community have been led to believe that mammalian cells are

extremely sensitive to hydrodynamic stress, and because of this belief, many bioprocesses may be operating at a sub-optimal level. An example of this sub-optimal performance is that the agitation rate in many bioreactors is very low, which affects nutrient mixing and gas dispersion.

The primary focus of this work is cell death in bioprocess equipment as a result of hydrodynamic forces. This focus is divided into two areas: determining the amount of hydrodynamic force cells can withstand before the onset of apoptosis or necrosis and determining the amount of hydrodynamic force cells encounter in bioprocess equipment. A contractional flow microfluidic device was developed to determine the amount of hydrodynamic stress suspended cells could withstand; the design and use of this device are described in chapter 4. The amount of hydrodynamic stress cells encounter in bioprocess equipment was determined using analytical and experimental techniques; the techniques and the results are described in chapter 3. Chapter 5 contains computer simulations and experimental data pertaining to hydrodynamic stress and cell death in Fluorescence Activated Cell Sorters (FACS) instruments.

The maximum local energy dissipation rate (EDR) is the parameter used throughout this study to characterize hydrodynamic stress. The EDR is a scalar value that accounts for both extensional and shear forces, and has units of power per volume (i.e. W/m^3). The EDR is the amount of mechanical energy that is "lost" due to viscous dissipation, or as described by Bird *et al.* (1960), the irreversible conversion of mechanical energy to heat. Shear stress is the most widely used measure of hydrodynamic stress, however extensional flows are more damaging to cells than pure shear flows (Gregoriades *et al.*, 2000). Also, the maximum local EDR is better

suited to predict cell damage than the average or overall EDR, because the maximum EDR is two to three orders of magnitude greater than the average EDR in some flow systems (Zhou and Kresta, 1996a; Wernersson and Tragardh, 1999). The EDR can be calculated analytically for laminar flow through simple geometries, such as pipes and annuli; computational fluid dynamics (CFD) is required for laminar flow through more complex geometries, such as converging or diverging channels. CFD may also be utilized to determine the EDR in transitional or turbulent flows, however extensive experimental validation is required before the CFD results of turbulent or transitional flows can be trusted (Bernard and Wallace, 2002).

As described above, the maximum local EDR is determined for a variety of simple laminar flow geometries using well-established equations in chapter 3. The maximum EDR for a pipette and a FACS instrument's nozzle were determined using FLUENT, a commercial CFD program, see chapters 3 and 5 respectively. Particle tracking velocimetry (PTV) was used to calculate the maximum local EDR in a stirred tank bioreactor operating in the transitional or turbulent flow regimes. PTV is an experimental technique that simultaneously tracks several thousand particles in a given volume to map the velocity vectors, and the local EDR is calculated from the velocity vector map. With the exception of the flow in a FACS nozzle, the maximum local EDR cells would encounter in most bioprocess equipment is not sufficient to cause necrosis or apoptosis, based on data from Ma *et al.* (2002) and chapter 4. The level of EDR produced in a FACS instrument's nozzle is significant and appears to damage cells.

A microfluidic device was used in this study to determine cells' sensitivity to hydrodynamic force. Two different Chinese Hamster Ovary (CHO) cell lines

were pumped through the device and then a flow cytometric assay was implemented to determine the percentage of apoptotic and necrotic cells. The effect of serum concentration and culture conditions, attached versus suspended, were also investigated. Cells cultured in serum containing media were more susceptible to apoptosis, whereas cells cultured in serum free media were more likely to die via necrosis. The same apoptosis and necrosis detection assay was applied to determine percentage of apoptosis and necrosis following cell sorting with a FACS instrument. The sorted cells responded in a similar manner as the cells that were pumped through the contractional flow device, the sorted cells displayed approximately the same level of necrosis and apoptosis.

Chapter 2

Literature Review

2.1 Biology of Cell Death

2.1.1 Necrosis

As mentioned in chapter 1, necrosis is passive cell death, meaning an external force kills the cell. Necrosis is initiated after the cell receives a high level of stress and does not have time to respond. This stress can be extreme temperature, pH, hydrodynamic force, etc (Cotter and Al-Rubeai, 1995). Usually, the integrity of necrotic cell's plasma membrane is compromised and the cell swells (Darzynkiewz *et al*., 1997). Eventually, the cell membrane ruptures and the cells' internal components are released into the surrounding environment. *In vivo* these components initiate an immune response (inflammation), and in terms of industrial cell culture, some of the components that are released are proteolytic enzymes, which may degrade the therapeutic protein (Darzynkiewz *et al*., 1997).

Necrosis is determined by measuring the number of cells with a compromised cell membrane or by measuring the activity of an intracellular enzyme in the surrounding fluid. Cell membrane integrity is usually determined using a dye that does not enter healthy cells. Typically these dyes are hydrophilic and/or charged; hydrophilic or charged molecules do not cross the cell membrane unassisted. Cells with

damaged plasma membranes allow these types of dyes to enter, and the number of stained cells is counted with the aid of a light microscope or a flow cytometer. One of the commonly utilized enzyme assays for necrosis measures lactate dehydrogenase (LDH) activity. LDH is located on the cell's interior; therefore any LDH activity in the fluid surrounding the cell must have come from ruptured cells. With the proper controls, an accurate measurement of cell viability can be determined (Ma *et al.*, 2004a).

2.1.2 Apoptosis

Unlike necrosis, cells have an active role in apoptosis. An outside event initiates a signal pathway within the cell, which ultimately leads to its death. *In vivo*, apoptosis is a means of disposing of aged, damaged, infected, or surplus cells; the apoptotic cells are phagocytosed to limit the release of their inflammatory contents (Walsh *et al.*, 1998). *In vitro*, apoptosis is initiated by sub-optimal pH and temperature, nutrient starvation, hypoxia, and hydrodynamic force (Cotter and Al-Rubeai, 1995; Mastrangelo *et al.*, 1998). Cells undergoing apoptosis display a series of morphological changes during the apoptotic pathway: first the cell volume decreases, then the membrane blebs (spherical bulges formation), the nucleus fragments, and finally the blebs break away from the membrane forming apoptotic bodies (Mastrangelo *et al.*, 1998). There are several biochemical milestones along the apoptotic pathway as well. For non-receptor mediated apoptosis, cytochrome C is released from the mitochondria, which initiates the caspase cascade and phosphatidylserine (PS) translocates from the interior of the cell membrane to the exterior. The caspase cascade ultimately initiates endonuclease activity within the nuclease and the enzymatic degradation of the cytoskeleton.

2.2 Calculating Hydrodynamic Stress

There are several means of representing the amount of hydrodynamic stress a fluid element would experience, examples include shear stress, rate of strain, and energy dissipation rate (EDR). All of the aforementioned parameters are functions of the velocity gradient, ∇U. The most common means of representing hydrodynamic stress is shear stress. Pure shear flows are one half extensional and one half rotational, so in addition to being elongated, a fluid element also rotates. Pure shear flow is created by fluid flowing past a boundary, which forms a velocity gradient orthogonal to the direction of flow (see figure 2.1). Shear stress is the most common method for representing hydrodynamic stress because analytically calculating the velocity gradient in a pure shear flow is relatively straightforward; most of the equations are found in standard fluid mechanics textbooks. Unfortunately, fluid flow through any sort of contraction or expansion as well as turbulent flow in a mixing vessel are not pure shear flow – many of these types of flows will have a more pronounced extensional component. Another parameter used to characterize hydrodynamic stress is the energy dissipation rate (EDR). The EDR is a scalar value and accounts for both the shear and extensional components of any given fluid flow, and has been used in the fluid mechanics research community to characterize stirred tank mixing tanks. It is measured in terms of power per unit volume or in SI units, W/m^3. For an incompressible, Newtonian fluid, the EDR (ε) is determined using the following equation:

$$\varepsilon = \tau : \nabla U = \mu[\nabla U + (\nabla U)^T] : \nabla U = \mu \sum_i \sum_j [\nabla U + (\nabla U)^T]_{ij} \nabla U_{ji} \qquad (1)$$

where μ is the viscosity, τ is the stress tensor, ∇U is the velocity gradient tensor and ∇U^T is the transpose of ∇U. In Cartesian coordinates, ∇U is defined as:

$$\nabla U = \begin{bmatrix} \frac{\partial U_x}{\partial x} & \frac{\partial U_y}{\partial x} & \frac{\partial U_z}{\partial x} \\ \frac{\partial U_x}{\partial y} & \frac{\partial U_y}{\partial y} & \frac{\partial U_z}{\partial y} \\ \frac{\partial U_x}{\partial z} & \frac{\partial U_y}{\partial z} & \frac{\partial U_z}{\partial z} \end{bmatrix} \qquad (2)$$

As can be seen in equations (1) and (2), once velocity vectors are known for every point throughout the geometry, the energy dissipation rate can be calculated for every point throughout the system. This is known as the local EDR. Knowing the local EDR is important, because the average or overall EDR for the system may be significantly less than maximum local EDR. There are relations available for the velocity vectors in simple geometries, for complex systems computational fluid dynamics (CFD) is necessary to calculate the velocity vectors. If, however, the flow is no longer in the laminar flow regime, then experimental measurements are needed to validate the CFD results. For a more complete discussion regarding calculating the EDR, see chapter 3.

2.3 Previous Studies Relating Cell Damage To Fluid Forces

In general, there are two broad categories for determining cells' response to fluid forces: single cell techniques and rheological techniques. The single cell techniques, such as micropipette aspiration and micromanipulation, examine one cell at a time to

determine physical characteristics such as Young's modulus and tensile strength. The rheological techniques involve the use of viscometers to determine the effects of hydrodynamic forces on a population of cells. Each method has its drawbacks. The single cell techniques only examine one cell at a time, meaning many experiments are needed to create statistically meaningful data. Also most of the single cell studies only investigate catastrophic cell death. The rheological techniques typically only investigate shear stress and only over relatively long periods of time. Ideally, one would like a method that would examine a large population of cells, one cell at a time, in a well-characterized fluid flow environment, and at a time scale relevant to the biotechnology industry.

The single cell techniques like micropipette aspiration, cell squeezing, and cell poking, are typically used to determine the physical properties of single cells. These techniques are done in a relatively short time frame (a few seconds). Micropipette aspiration is the most common of these techniques, in this technique a cell is forced into a glass tube (a micropipette) that is slightly smaller than the cell itself. This process is recorded by a video camera attached to a microscope. The vacuum pressure of the micropipette and the movement of edge of the cell into the micropipette are measured (Hochmuth, 2000). The cell's Young's modulus and the cell's viscosity are calculated using this information. Unfortunately, investigators have not determined if cells act like viscous liquids (Hochmuth, 2000) or solids (Jones *et al.*, 1999), which affects the equations one needs to use to determine the physical constants. Apparently, certain cell types (i.e. endothelial cells) act like solids, whereas other act like viscous fluids (i.e. neutrophils). Miyazaki *et al*. (2000) used two opposed micropipettes to determine

the tensile strength of rabbit fibroblasts, and found that the cells can withstand a maximum load of 0.9 μN and can be stretched 4× their original diameter. The tests Miyazaki *et al.* (2000) utilized lasted less than 5 s. There is little in the available literature regarding micropipette aspiration experiments performed on cells relevant to the biotechnology industry (e.g. CHO, Sf-9, Hybridoma, etc.). Another single cell method involves the use a micromanipulator that squeezes a cell between two parallel plates and records the imposed force (Thomas *et al.*, 2000). Thomas *et al*. (2000) tested hybridoma cells in the aforementioned apparatus, and found that the hybridoma cells can endure approximately 2 μN of compressive force prior to rupture (Thomas *et al.*, 2000). The tests Thomas *et al.* (2000) performed on the cells lasted approximately one second. In the cell poking technique, a microneedle is used to deform the cell's membrane. Veselska and Janisch (2001) qualitatively examined changes in the human fibroblast cell's cytoskeletal as a function of time, the force imposed on the cell was not reported. Veselska and Janisch (2001) noticed the actin filaments formed "knots" where the needle pressed the cell, whereas the microtubules passively deformed.

The rheological techniques utilize rheometers to determine the cellular response to varying levels of shear stress. Rheometers, such as cone and plate viscometers, produce a pure shear flow and have been used for many years to characterize cells response to hydrodynamic forces. In theses studies, typically cells attached to a substrate are exposed to shear stress over an extended period of time in viscometers (Dewey *et al.*, 1981; Martin *et al.*, 1979; Davies *et al.*, 1984). This approach is adequate for most biomedical studies because most cells *in vivo*, with the exception of blood cells, are not freely suspended and the only type of hydrodynamic stress most of these cells

would encounter is shear stress. For the biotechnology industry, however, this is a major drawback since most cells are grown in suspension. Also these viscometer experiments take place over a relatively long time scale, usually on the order of minutes to hours – much longer than the time scale of maximum hydrodynamic forces that cells would experience in a bioreactor. Cells in a bioreactor and other bioprocess equipment experience more than just pure shear forces, the cells encounter a complex mixture of extensional and shear forces. Since the cells in a bioreactor are usually suspended in the fluid, they can rotate away from the principle axis of stress. In a viscometer, the cells are anchored to the surface of the viscometer and cannot rotate to reduce the strain.

Since viscometers have been used for several years to study hydrodynamic forces on cells, a lot of information has been collected for anchorage-dependent cells in pure shear flows. Unfortunately, there is not a high level of agreement between the different studies. There are several proposed methods that cells detect and respond to shear stress. These so called mechanotransduction pathways include ion channels, G-protein linked receptors, tyrosine kinase receptors, and integrins (Papadaki and Eskin, 1997). Changes in the permeability of certain ions, in particular calcium and potassium, cause a rapid cellular response, on the order of a few seconds (Papadaki and Eskin, 1997). All of the other mechanotransduction pathways require much longer to produce a measurable response. It is unclear whether a sustained level of shear stress was required to produce a response, or if the cellular machinery took several minutes/hours to respond. So some of the response seen in the viscometer studies may be a response to a "build-up" of stress over time and thus may not be relevant to the short bursts of stress cells in a stirred tank bioreactor or other pieces of bioprocess equipment experience.

A third type of cell damage study is capillary experiments (McQueen *et al*., 1987; McQueen and Bailey, 1989; Al-Rubeai *et al.*, 1995). Most of the capillary tubing experiments involved pumping cell suspensions through capillaries of varying diameter, or with a sudden constriction - similar to an orifice meter (McQueen *et al*., 1987), or with a converging-diverging region - similar to a venturi meter (McQueen and Bailey, 1989), and then measured the percent of cells killed as a function of the wall shear stress. All of these studies focused on the wall shear stress, and did not account for the possible extensional flow effects on the cells.

Gregoriades *et al*. (2000) and Ma *et al*. (2002) studied cell death of cells attached to microcarriers and suspended cells, respectively, as a function of the maximum, local energy dissipation rate. Gregoriades *et al.* (2000) utilized an opposed piston system to force Chinese Hamster Ovary (CHO) cells attached to microcarriers through a small orifice. The opposed piston geometry was simulated in FLUENT, a commercial computational fluid dynamics (CFD), and the simulation data was exported to a separate C program, which calculated the local EDR. Gregoriades *et al.* (2000) found that the CHO cells were removed from the microcarriers at approximately 10^3 W/m³. Ma *et al.* (2002) developed a microfluidic contractional flow device to test the robustness of suspended cells from various cell lines as a function of the maximum local EDR. Ma *et al.* (2002) produced the microfluidic device using a photolithography technique, and simulated the fluid flow through the device using FLUENT. Ma *et al.* (2002) discovered suspended cells do not show statistically significant levels of necrosis below 10^7 W/m³.

2.4 Hydrodynamic Stress in Bioprocess equipment

2.4.1 Hydrodynamic Stress in Bioreactors

Hydrodynamic stress originates from two primary sources in bioreators: the action of the impeller and sparging. There are novel bioreactors used in research that do not use an impeller to facilitate mixing or use membranes introduce oxygen into the cell suspension, however these systems are not widely used in industry. A majority of the bioreactors used in mammalian cell culture use impellers to mix the cell suspension and sparging to supply oxygen and remove carbon dioxide. Mixing is needed to keep the cells from settling and to facilitate heat and mass transfer. However, due to historical concerns regarding mammalian cells' sensitivity to hydrodynamic stress, most bioreactors were agitated just enough to keep the cells in suspension (Varley and Birch, 1999). Due to this low level of mixing, large concentration gradients of pH, oxygen, and other nutrients existed within the reactor. Ozturk (1996) demonstrated this experimentally by adding base to a poorly mixed bioreactor. The base was added to the top of the bioreactor, and because of the poor mixing within the bioreactor, the base was not mixed throughout the system, creating a region at the top of the bioreactor with a high pH. The cells in this region ruptured, forming a "snow ball" of cellular debris in the vicinity of the base inlet. Increasing the agitation rate would improve the mixing time and the oxygen transfer in the bioreactor (Nienow *et al.*, 1996; Nienow, 1997).

2.4.1.1 Impellers

Stirred tanks, and bioreactors in particular, have been investigated extensively to comprehend their fluid mechanics, but a complete understanding of their hydrodynamics is unavailable. Bioreactors usually operate outside of the laminar flow regime, and therefore cannot be modeled analytically due to the closure problem – there are more unknown variables than available equations. Empirical correlations exist that describe mixing at the macro-scale (Brodkey and Hershey, 2001), however such relations do not apply at the microscopic level of a cell. Experimental techniques are stymied due to their low spatial resolution. Laser Doppler Anemometer (LDA) (Yianneshis *et al.*, 1987; Stoots and Calabrese, 1995; Wu and Patterson, 1989; Zhou and Kresta, 1996) and Constant Temperature Anemometry (CTA) (Rao and Brodkey, 1972; Wernersson and Tragardh, 1999) are two of the most frequently used techniques, but can only investigate one point at a time. Particle Tracking Velocimetry (PTV) allows one to measure the full velocity field simultaneously. However, due to the modest resolution of the velocity map, the velocity vectors acquired at different time points must be ensemble averaged (Zhao and Brodkey, 1998). More information regarding PTV can be found in chapter 3.

Many of the studies of fluid mechanics in bioreactors, used the local energy dissipation rate (EDR) as a parameter to characterize mixing at microscopic scales. In general, the mixing community considers using parameters, such as the local EDR, to be a better approach to mixing research than empirical unit operations approaches (Kresta *et al.*, 2004). Power introduced to a bioreactor via the impeller(s) is not evenly distributed throughout the vessel, 30-70% of the total power input is dissipated in a small region around the impeller that is less than 10% of the total vessel volume (Zhou and

Kresta, 1996). Also, the variation between the highest and lowest measured local EDR can be as much as two to three orders of magnitude (Zhou and Kresta, 1996; Mollet *et al.*, 2004). Due to the heterogeneity in local EDR, cells circulating in the bulk fluid will not be exposed to one value of local EDR for an extended period of time and, because the majority of the energy dissipated by the impeller occurs in a relatively small volume, cells will not experience the highest levels of local EDR very frequently (Ma *et al*. 2002). Wernersson and C. Tragardh (1999) examined a 22,000 L stirred tank operating at 120 rpm and Zhou and Kresta (1996) examined a 11 L stirred tank operating at 714 rpm and both sets of researchers reported maximum local energy dissipation rates of less than 10^5 W/m³, which is approximately two orders of magnitude lower than the value Ma *et al.* (2002) found to cause cell lysis. The agitation rates Wernerson and Tragardh (1999) and Zhou and Kresta (1996b) utilized in their studies are significantly higher than what is typically employed in biopharmaceutical production.

Given this data, one can logically conclude that the action of the impeller alone is not causing cell lysis in bioreactors. However, the belief that mammalian cells are extremely fragile and can be damaged by agitation is persistent throughout the biopharmaceutical community. A possible source of the biopharmaceutical community's belief in mammalian cell fragility stems from the fact that cells attached to microcarriers are not very robust, and much of the early work in mammalian cell culture utilized cells attached to microcarriers (Gregoriades *et al.,* 2000). Recently, a paper was published examining the effects of increasing agitation on CHO cells producing human tissue-type plasminogen activator protein (tPa) in an unbaffled, 1.5 liter bioreactor agitated with a pitched blade impeller (Senger and Nazmul, 2003). Senger and Nazmul

(2003) increased the agitation rate from 40 to 200 rpm in 40 rpm increments and discovered that the cell viability decreased considerably at 200 rpm. The maximum local energy dissipation rate measured in a similar vessel, with a high shear impeller at 195 rpm, was 1.34×10^3 W/m³ (see chapter 3). This value is several orders of magnitude less than what Ma *et al.* (2002) discovered to cause necrosis and several orders of less than what was found to cause apoptosis in CHO cells (see chapter 4). A possible explanation for this discrepancy is as follows: unbaffled stirred tanks tend to have a central vortex form at high agitation rates, if the vortex extends down to the impeller, small air bubbles may become entrained in the bulk fluid, and small air bubbles are a cause of cell death in bioreactors (see below). To test this hypothesis, the rotation rate of a similarly configured 1.25 liter, unbaffled bioreactor was to 200 rpm; a central vortex formed and a few small bubbles were entrained in the bulk fluid. When the rotation rate was increased to 250 rpm a significant number of small bubbles were entrained in the bulk fluid. Kioukia *et al.* (1992) discovered similar phenomena when they investigated cell damage in highly agitated bioreactors, which they were able to attribute to the air bubbles emanating from the central vortex. This observation is further supported by the work of Michaels *et al*. (1992) and Kunas and Papoutsakis (1990), where a bioreactor without a gas-liquid interface, which eliminated bubbles forming from the central vortex, was agitated at over 400 rpm without a decrease in cell viability.

2.4.1.2 Bubble rupture

Sparging is the most efficient and cost effective way to introduce oxygen and remove carbon dioxide from the bioreactor (Ma *et al.*, 2004b). Sparging introduces bubbles into the bioreactor and, unlike agitation, bubble rupture has been shown to damage cells (Handa *et al*., 1987; Bavarian *et al*., 1991; Trinh *et al.*, 1994). Due to hydrophobic interactions between cells and bubbles, cells have a tendency to adhere to bubbles as the bubbles rise through the media (Chattopadhyay, *et al.*, 1995a; Chattopadhyay, *et al.*, 1995b). When the bubbles reaches the surface of the air-media interface and ruptures, a energy jet is produced, killing the cells attached to the bubble (Ma *et al.*, 2004b). Boulton and Blake (1993) and Garcia-Briones *et al*. (1994) independently simulated bubble rupture using computation fluid dynamics and found that bubble rupture produced maximum local energy dissipation rates on the order of 10^7 – 10^8 W/m³. Also the maximum local EDR increased with decreasing bubble diameter (Boulton and Blake, 1993; Garcia-Briones *et al*., 1994). Trinh *et al.* (1994) collected the cells contained in the upward jet created by a ruptured bubble and found that approximately 1000 cells were killed per 3.5 mm diameter bubble. When surfactants, such as Pluronic F-68, are added to the media cell-bubble attachment is thermodynamically unfavorable (the Gibbs free energy, ΔG, is greater than zero) (Chattopadhyay, *et al.*, 1995b). Garcia-Briones and Chalmers (1992) demonstrated Pluronic F-68 eliminates cell-bubble attachment experimentally. However, at high cell concentrations (10^7 cells/mL), even large concentrations of Pluronic F-68 (> 1 g/L) will not keep cells from becoming "trapped" in the foam layer (Ma *et al.*, 2004a).

2.4.1 Cell damage in Other Bioprocess Equipment

The biopharmaceutical industry utilizes several other pieces of equipment that would expose suspended cells to hydrodynamic forces. Examples of such equipment include pumps, filtration units, and fluorescent activated cell sorters (FACS). Cell death resulting from cells flowing through pipes, square channels, and cones (pipettes) will be discussed in chapter 3 and cell death resulting from flow through FACS instruments will be discussed in chapter 5.

2.4.2.1 Cell Damage in Pumps

Data regarding cell death in pumps used in bioprocesses is scarce; most literature investigating cell death in pumps is empirical or concerned with blood cell lysis in centrifugal pumps. Merten (2000) found that insect cells' viability decreased after continuous pumping through a peristaltic pump operating as part of a perfusion bioreactor. Fan and Graf-Hausner (2002) studied peristaltic, membrane, centrifugal, and gear pumps with respect to cell damage and found that peristaltic pumps caused the least amount of cell death. Jaouen *et al*. (1999) investigated the effects of various pumps types on the loss of motility of microalgae. Jaouen *et al*. (1999) found that after twelve passes through a centrifugal pump, operating at 1 L/min, all of the microalgae were immobile, whereas after 48 passes through a peristaltic or diaphragm pump, operating at 1 L/min, approximately 30% to 40% of the microalgae were immobile, and after 72 passes through a monoscrew pump less than 10% of the microalgae were immobile. Jaouen *et al.* (1999) also found that increasing the volumetric flow rate of the cells through the pumps had a deleterious effect: operating the monoscrew pump at 12 L/min

immobilized all of the microalgae in 300 passes whereas 25% of the microalgae were immobilized at 300 passes when the volumetric flow rate was 6 L/min. Song *et al*. (2003) modeled the flow in a centrifugal pump used as a possible bridge-to-transplant treatment for patients with heart disease and congestive heart failure, and reported that 2% of the red blood cells would have been lysed in the process, based on the shear stress produced within the pump and clinical observations. Song *et al*. (2003) mentioned that the pump operated in the turbulent flow regime, but did not mention what model of turbulence they utilized (i.e. Reynolds Averaged Navier-Stokes, Large Eddy Simulation, or Direct Numerical Simulation). Since Song *et al*. (2003) used CFX, a commercial computational fluid dynamics program, the authors most likely used Reynolds Averaged Navier-Stokes, and the results of which should be viewed with a healthy amount of skepticism (Bernard and Wallace, 2002). Also the authors assumed blood was a Newtonian fluid, however blood has a shear dependent viscosity and is therefore non-Newtonian (Macosko, 1994).

2.4.2.2 Cell Death in Filtration Systems and Centrifuges

Cell death in flirtation and centrifugation systems is a concern of practicing bioprocess engineers, because host cell proteins released during cell lysis may complicate the downstream protein purification (Iverson, 2003; Castilho and Anspach, 2003; Tebbe *et al.*, 1996). Unfortunately, very little information is available in the literature regarding cell death in these unit operations. Iverson (2003) recommends operating tangential flow filtration systems such that the shear rates are less than 3000 s^{-1}, which corresponds to an EDR of 9×10^{3} W/m^3 for a simple shear flow of pure water. Vogel and Kroner

(1999) reported a large number of Baby Hamster Kidney (BHK) cells were lysed, determined via LDH assay, in a crossflow filtration system at a shear stress of 2.5 N/m² (6.25×10^3 W/m³) over the course of three hours. Castilho and Anspach (2003) designed a novel dynamic filtration system to filter mammalian cells, simulated the device using FLEUNT, and compared the shear stress values calculated by FLUENT to lethal levels of shear stress determined experimentally using CHO cells cultured in serum free media and a cone and plate viscometer. Castilho and Anspach (2003) found that for time durations of less than five minutes, significant decreases in viability were observed only at high levels of shear stress, 200 Pa, or approximately 10^7 W/m³, which is consistent with data from Ma *et al.* (2002). Castilho and Anspach were able to operate their dynamic filtration system successfully at relatively high feed flow rates (61 L m^{-2} h^{-1}) and cell concentrations (2×10^6 cells/mL) with minimal loss of cell viability. Tebbe *et al*. (1996) measured LDH activity in the fluid surrounding hybridoma cells separated using a modified pilot scale disc stack centrifuge, and found that with the original design and under normal operating conditions (2200 to 5700 × g and 90 kg/hr cell suspension), between 50 and 100% of the hybridoma cells were killed, based on an LDH assay. Using a modified feed system, Tebbe *et al*. (1996) measured a less than 2% increase in cell death at the same operating conditions (2200 to 5700 × g and 90 kg/hr cell suspension). The modification Tebbe *et al*. (1996) incorporated into the centrifuge, which they called the hydrohermetic feed system, essentially eliminated the possibility of air bubble entrainment in the feed distributor. Tebbe *et al.* (1996) attributed the improved cell viability to an elimination of "shear forces due to intensive gas liquid mixing in the inlet area".

2.4.2.3 Cell Damage in Turbulent Flow

In addition to stirred tank bioreactors, suspended cells may encounter turbulence in other flow systems, such as turbulent flow in pipes and free turbulent jets. Chisti (2001) reviewed the level of shear stress and energy dissipation created in turbulent pipe flow and free turbulent jets, and reported that damaging levels of hydrodynamic force is possible in extreme cases of pipe flow ($N_{Re} = 4\times10^4$) and is likely in free turbulent jets. Chisti (2001) showed that the maximum shear stress in a free turbulent jet is several times the wall shear stress of the pipe leading up to the expansion. Chisti (2001) stated that "damage to fragile cells may occur during transfer operations such as inoculation of a bioreactor even though the velocity in the transfer pipe may be relatively low," and stated further that "These effects can be avoided by discharging the jet above the level of the receiving fluid such that the liquid flows down the vessel wall".

2.4.2.4 Cell Damage in FACS Instruments

Flow cytometry is a rapid method for simultaneously measuring multiple parameters of a single cell suspension. A suspension of cells flows single file through a nozzle. Each cell is illuminated with a laser; if the cell is stained with the appropriate dye or fluorescently labeled antibody, the cell will fluoresce. This fluorescence is filtered using a combination of dichroic mirrors and bandpass filters, and then measured using photo multiplier tubes (PMT). The analog signal from the PMTs is digitized and sent to a computer for storage and analysis. Over 10,000 cells per sample are examined

typically. Fluorescence activated cell sorters (FACS) are flow cytometry analyzers with the added ability to sort cells based on their florescence. Like the flow cytometers described above, cells are pumped single file through a nozzle and interrogated with one or more lasers. However the nozzle vibrates at a high frequency, creating droplet formation downstream from the stream-laser intercept. These droplets are then charged depending on if the cell(s) within them meet certain criteria set by the operator. The charged drops are then deflected into collection tubes by electrically charged (usually 3000-6000 V) deflection plates (see figures 2.2 a and b). The operator sets the frequency, phase, and amplitude of the nozzle vibration, the charge on the droplets, the voltage on the deflection plates, and the pressure of the sheath fluid empirically. There are few combinations of these parameters that allow for acceptable operation and only a small subset of those combinations are stable. There has not been a report of anyone modeling the fluid dynamics of a FACS instrument using CFD. Part of this work is to model the nozzle of a commercially available flow cytometer, and determine if cell damage is possible under normal operating conditions (see chapter 5).

Information regarding cell damage in FACS instruments is limited. Seidl *et al*. (1999) examined necrosis and apoptosis in normal human skin fibroblast cell line N1 and human breast carcinoma cells BT474 after FACS sorting. Seidl *et al*. (2001) discovered both cell lines displayed relatively high levels of necrosis after sorting, approximately 10 to 15% above the controls, based on the flow cytometric propidium iodide dye exclusion assay. The authors employed the Annexin-V/PI apoptosis assay on the sorted cells and discovered correspondingly high percentages of apoptotic BT474 cells, but not the skin fibroblast cells. These results are somewhat surprising since cells BT474

overexpress bcl2, an anti-apoptosis gene (Halder *et al.*, 1994). Seidl *et al.* (2001) did not add Fetal Bovine Serum (FBS) to the collection tubes, a practice widely reported within the flow cytometry community to improve the viability of sorted cells (Trotter, 2003; Atzberger, 2000). Aslam *et al*. (1998) checked the viability of sorted human sperm cells using a trypan blue dye exclusion assay, and reported that the viability of the sorted sperm cells was approximately 99%. Aslam *et al*. (1998) did not mention if they added FBS to the collection tubes.

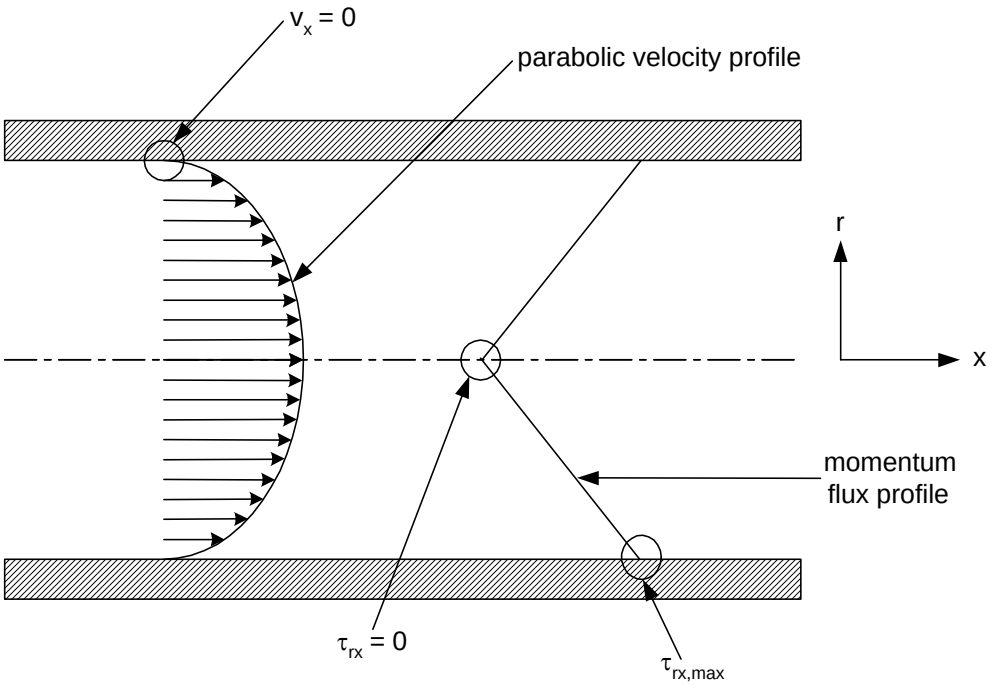

Figure 2.1: Velocity vector profile for laminar fluid flow in a pipe

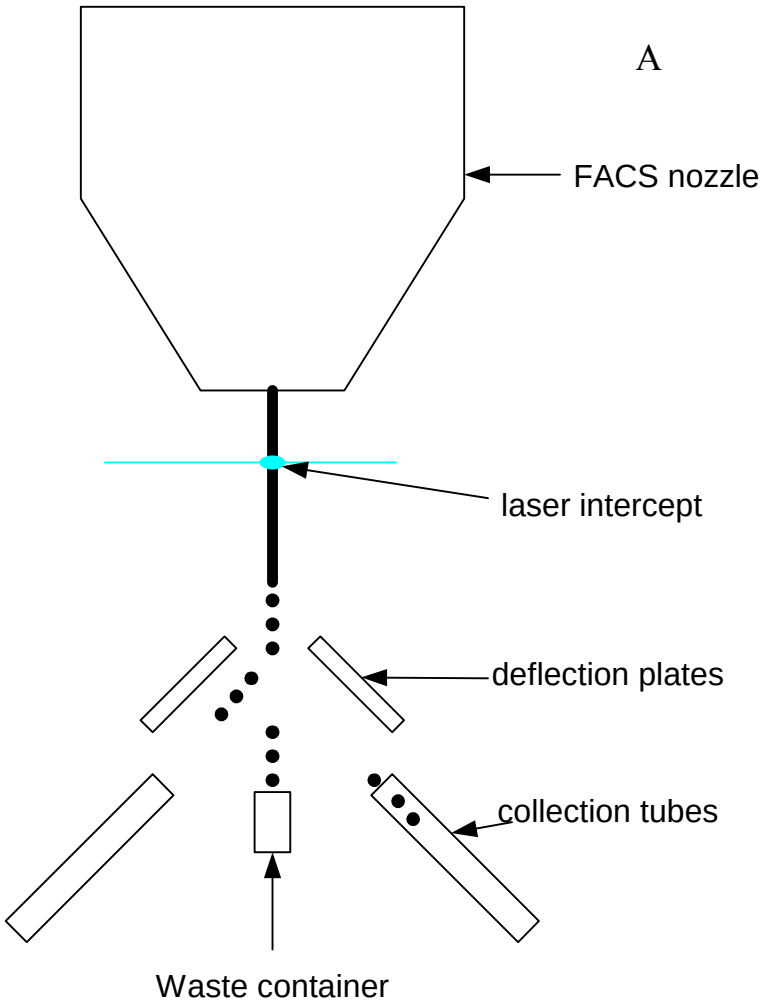

Continued

Figure 2.2: (A) FACS instrument nozzle and deflection plates schematic;
(B) FACS instrument nozzle, internal flow.

Figure 2.2 Continued

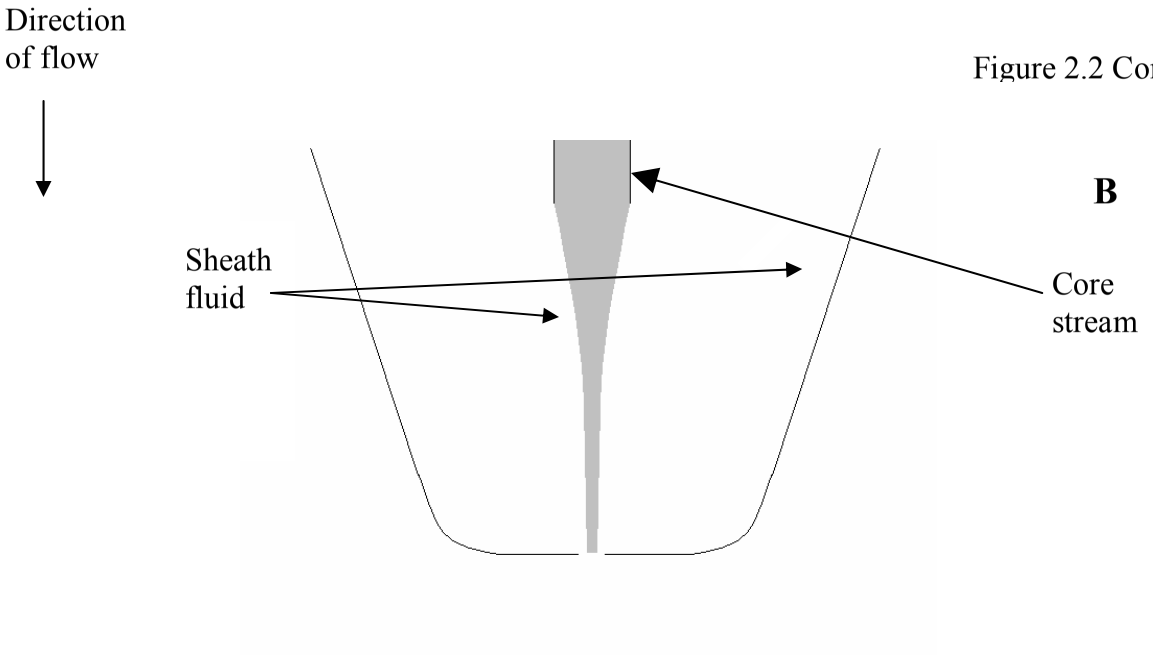

Chapter 3

Characterization of Energy Dissipation Rate in Bioprocess Equipment

The content of this chapter was published previously: Mollet, M., Ma, N., Zhao, Y., Brodkey, R., Taticek, R., and Chalmers, J. 2004. Bioprocess Equipment: Characterization of Energy Dissipation Rate and its potential to Damage Cells. *Biotechnology Progress*. **20(5)**: 1437-1448. Ningning Ma produced the data presented in section 3.5.

3.1 INTRODUCTION

One of the more controversial subjects in large scale animal cell cultivation, historically, has been the perceived "shear sensitivity" of the cells. In the early days of large scale animal cell culture, it was routinely reported that suspended animal cells were too sensitive to be grown on a large scale. Nevertheless, a significant number of highly successful, commercial products are currently being produced in suspended animal cell culture at scales on the order of 10,000 liters.

There are a number of reasons for this confusion and/or contradiction, and these reasons can be categorized as: 1) the difficulty in characterization and quantification of the bulk and local (micron scale) hydrodynamic forces in the vessel, 2) the lack of a complete relationship(s) to relate the lethal and non-lethal effects of hydrodynamic forces on cells to both the magnitude and time of exposure of specific hydrodynamic forces, and 3) the lack of a model which relates the first two points (Gregoriades *et al*.,

2000; Thomas and Zhang, 1998). Ideally, this/these relationships would also consider the differences in the "shear sensitivity" between different cell types and the mode of growth (i.e. suspended or anchorage dependent).

Shear stress has been and continues to be one of the most commonly used predictors of adverse cell affects as a result of hydrodynamic forces. Many cell lines have been tested in parallel plate apparatuses or viscometers at varying levels of shear stress and over extended periods of time. However, the flow in parallel plate systems as well as viscometers usually approaches pure shear flows, which is half rotational and half extensional (Aris, 1962). It has been suggested that pure shear flows are not as damaging to cells as flows that are fully extensional, because in a shear flow the cells rotate as a result of the non-zero vorticity; consequently no one point on a cell encounters the maximum strain for a very long period of time (Garcia-Briones *et al*. 1994).

An alternative to the use of shear stress, is the use of the term local energy dissipation rate, *EDR*. This term has been used to characterize the flow conditions acting on cells for over thirty years (Blustein and Mockros, 1969) and has been extensively used in the fluid mechanical/mixing community for even longer (Kresta *et al*. 1998).

The *EDR*, which is a scalar value with units of power per unit volume (i.e. W/m^3), is the irreversible rate of internal energy increase per unit volume (Bird *et al*., 1960), or the irreversible conversion of mechanical energy to heat. A key clarification in the discussion and study to follow is the concept of local versus average *EDR*. Since in some systems the difference between average and local *EDR* can be over three orders of magnitude, such a distinction is significant.

Fundamentally, the *EDR* , ε, can be determined using the following equation (Bird *et al*., 1960; Brodkey, 1995):

$$\varepsilon = \tau : \nabla U \tag{1}$$

where τ is the stress tensor and ∇U is the velocity gradient tensor. The velocity gradient tensor is defined by:

$$\nabla U = \begin{bmatrix} \frac{\partial U_x}{\partial x} & \frac{\partial U_y}{\partial x} & \frac{\partial U_z}{\partial x} \\ \frac{\partial U_x}{\partial y} & \frac{\partial U_y}{\partial y} & \frac{\partial U_z}{\partial y} \\ \frac{\partial U_x}{\partial z} & \frac{\partial U_y}{\partial z} & \frac{\partial U_z}{\partial z} \end{bmatrix} \tag{2}$$

Equation 1 can be derived from first principles using the second law of thermodynamics. More specifically, Equation 1 emerges from the loss term in the energy balance equation. Much like the Navier-Stokes equation, Equation 1 is valid for any flow regime, be it laminar, transitional, or fully turbulent.

For an incompressible Newtonian fluid Equation 1 becomes (Brodkey, 1995):

$$\varepsilon = \mu\left(\nabla U + \nabla U^T\right) : \nabla U \tag{3}$$

where μ is the viscosity and ∇U^T is the transpose of ∇U. Alternatively, Equation 3 can be written in terms of the second invariant

of the rate of deformation tensor, 2D (Bird *et al*., 1960).

$$\varepsilon = -\mu II_{2D} \tag{4}$$

The second invariant and the rate of deformation are defined as (Bird *et al*., 1960):

$$\begin{aligned} 2D &= \nabla U + \nabla U^{T} \\ II_{2D} &= \tfrac{1}{2}\left[(tr2D)^2 - tr(2D)^2\right] \end{aligned} \tag{5}$$

where tr2D is the trace of the rate of deformation tensor. As can be seen from Equations 3 through 5, once the velocity vectors are known at every point in a given flow system, the energy dissipation rate at every point (the local EDR) can be determined.

There are analytic equations for the velocity vectors in laminar flow systems for a number of specific geometries: pipes, annuluses, rectangular channels, and parallel plates. For more complicated laminar flow geometries, a computational fluid dynamics (CFD) program, such as FLUENT, can be used to determine the velocity vectors. For systems that operate in the transitional or turbulent flow regimes (i.e. stirred tank bioreactors), CFD results typically require experimental validation and accurate resolution on the order needed to understand cell fluid interactions are not possible.

Alternatively, a number of experimental technologies have been used to attempt to quantify turbulence (complex flow) in general, and mixing vessels, specifically. Several of these techniques provide a single point measurement of the velocity (either in one or two dimensions) as a function of time. Two examples are Laser Doppler Anomometer (LDA) (Yianneskis *et al*., 1987; Stoots and Calabrese, 1995; Zhou

and Kresta, 1996a, 1996b) and constant temperature anemometry (CTA) (Rao and Brodkey, 1972; Wernersson and Tragardh, 1999).

However, while LDA is a powerful technique to evaluate Equation 1 in absolute terms one needs accurate measurements of spatial gradients (in 3-D) of instantaneous velocities. Recently, three-dimensional particle tracking techniques have been developed which allow a significant number of randomly distributed, instantaneous, 3-D velocity vectors to be measured (Guezennec *et al*., 1994; Venkat *et al*., 1996a, 1996b; Zhao and Brodkey, 1998). However, while this technique has certain specific advantages over LDA, it suffers from having modest spatial resolution, due to the overlapping of particles when high particle concentrations in the projected images are used. Therefore, one cannot obtain the spatial gradients of the instantaneous velocities needed to solve Equation 1 at the most fundamental level.

In terms of EDR and cell death and/or lysis, Ma *et al*. (2002) used a transient, contractional flow device to characterize the effect of a rapid exposure to a range of high levels of EDR on suspended CHO, HB-24, SF-9 and MCF-7 cell lines. The results from their study indicated that all of the cell lines were able to withstand relatively intense, rapidly transient energy dissipation rates, up to 10^7-10^8 W/m^3. It is the purpose of this manuscript to estimate the energy dissipation rate for a variety of hydrodynamic geometries and conditions that animal cells will be expected to encounter in bioprocessing equipment.

3.2 Analytical Analysis

Under laminar flow conditions, one can define a number of fundamental geometries common in bioprocess equipment: pipe flow, duct flow (of both square and rectangular cross-section), annular flow, flow between parallel plates, and contracting (nozzle) flow. Analytical solutions to the basic flow equations for pipe flow, annular flow, and rectangular flow exist. Consequently, these analytical solutions can be used to directly solve Equation 3 or 4 to obtain values of ε as a function of specific dimensions and flow conditions.

Flow in a Pipe. The velocity profile equation for fully developed laminar flow in a pipe is (Bird *et al*., 1960; Brodkey, 1995)***:***

$$\frac{dU_z}{dr} = \frac{-4Qr}{\pi R^4} \tag{6}$$

where Q is the volumetric flow rate, r is the radial position, and R is the radius of the pipe. Applying (6) to either (3) or (4) yields:

$$\varepsilon = \mu\left(\frac{dU_z}{dr}\right)^2 = \mu\frac{16Q^2r^2}{\pi^2R^8} \tag{7}$$

The value of $\frac{dU_z}{dr}$ is largest at the wall of the pipe, $r = R$, so the maximum local EDR in this case is:

$$\varepsilon_{max} = \mu \frac{16Q^2}{\pi^2 R^6} \tag{8}$$

Figure 3.1a is a plot of Equation 8 in the form of ε versus the pipe radius for various volumetric flow rates. The horizontal dashed line corresponds to the level of the local maximum EDR Ma *et al.* (2002) found to cause a "catastrophic loss of cell membrane integrity" for suspended animal cells while the doted line corresponds to levels of EDR shown to damage animal cells attached to microcarriers (Gregoriades *et al*. 2000).

Flow in an Annulus. Similarly, the velocity profile equation for fully developed laminar flow in an annulus is (Bird *et al*., 1960):

$$\frac{dU_z}{dr} = \frac{4Q}{\left(1-\kappa^4 - \frac{(1-\kappa^2)^2}{\ln\left(\frac{1}{\kappa}\right)}\right)\pi R^3}\left(\frac{r}{R} - \frac{1-\kappa^2}{\ln\left(\frac{1}{\kappa}\right)}\frac{R}{r}\right); \qquad \kappa = \frac{R_{inner}}{R} \tag{9}$$

where R is the outer radius and Q is the volumetric flow rate. The ε_{max} occurs at the outer radius, $r = R$. Solving for $r=R$, one obtains:

$$\varepsilon_{max} = \mu\left(\frac{4Q}{\left(1-\kappa^4-\frac{\left(1-\kappa^2\right)^2}{\ln\left(\frac{1}{\kappa}\right)}\right)\pi R^3}\left(1-\frac{1-\kappa^2}{\ln\left(\frac{1}{\kappa}\right)}\right)\right)^2 \tag{10}$$

Figure 3.1b is a plot of Equation 10 as function of the outer radius for a flow volumetric flow rate of 1 ml/min. Since, as can be observed in Equation 10, the ε_{max} is a function of Q^2, the ε for flow rates other than 1 ml/min can be obtained by simply squaring the ratio of the flow rate of interest to 1 ml/min.

Flow between Parallel Plates. The velocity distribution for steady state laminar fluid flow between two large, parallel plates is given by (Brodkey, 1995):

$$U_x = \frac{3}{2}\left(\frac{Q}{WH}\right)\left[1-\left(\frac{2y}{H}\right)^2\right] \tag{11}$$

where Q is the volumetric flow rate, W is the width of the plate, and H is the distance between the plates. Appling (11) to equations (1), (2), and (3) yields:

$$\varepsilon = \frac{144Q^2y^2\mu}{W^2H^6} \tag{12}$$

The maximum energy dissipation rate occurs at plate-fluid interface (y=H/2), so:

$$\varepsilon_{max} = \frac{36Q^2\mu}{W^2H^4} \tag{13}$$

Figure 3.1c is a plot, in a similar format to Figures 3.1a and 3.1b, of the ε_{max} as a function of distance between parallel plates for a range of fluid flow rates. In this plot, a value of *W* of 1 meter was assumed. Note the squared dependence on width, consequently, a 10 fold decrease in plate width would result in a 100 fold increase in ε.

Rectangular Channel. For flow in a rectangular channel, the equation for the velocity profile is (White, 1974)***:***

$$U_x = C \sum_{i=1,3,5\ldots}^{\infty} (-1)^{\frac{i-1}{2}} \left(1 - \frac{\cosh\left(\frac{i\pi z}{2a}\right)}{\cosh\left(\frac{i\pi b}{2a}\right)} \right) \frac{\cos\left(\frac{i\pi y}{2a}\right)}{i^3} \qquad (14)$$

where

$$C = \frac{96Q}{\pi^3 ba \left(1 - \frac{192a}{\pi^5 b} \sum_{i=1,3,5\ldots}^{\infty} \frac{\tanh\left(\frac{i\pi b}{2a}\right)}{i^5} \right)} \qquad (15)$$

and *a* is the channel dimension along the y-axis and b is the channel dimension along the z-axis.

Taking the partial of U_x with respect to *y* and the partial of U_x with respect to *z* gives:

$$\frac{\partial U_x}{\partial y} = C \sum_{i=1,3,5\ldots}^{\infty} (-1)^{\frac{i-1}{2}} \left(1 - \frac{\cosh\left(\frac{i\pi z}{2a}\right)}{\cosh\left(\frac{i\pi b}{2a}\right)} \right) \frac{-\sin\left(\frac{i\pi y}{2a}\right)\left(\frac{i\pi}{2a}\right)}{i^3} \tag{16}$$

$$\frac{\partial U_x}{\partial z} = C \sum_{i=1,3,5\ldots}^{\infty} (-1)^{\frac{i-1}{2}} \left(1 - \frac{\sinh\left(\frac{i\pi z}{2a}\right)\left(\frac{i\pi}{2a}\right)}{\cosh\left(\frac{i\pi b}{2a}\right)} \right) \frac{\cos\left(\frac{i\pi y}{2a}\right)}{i^3} \tag{17}$$

The velocity profile is steepest at the walls, so partial of U_x with respect to y and with respect to z will attain their maximum value at $y = a$ and $z = b$ respectively. Using these partials, the energy dissipation rate for flow in a rectangular duct can be calculated using, since $U_z = U_y = 0$ and $U_x \neq f(x)$:

$$\varepsilon = \mu \left(\left(\frac{\partial U_x}{\partial y} \right)^2 + \left(\frac{\partial U_x}{\partial z} \right)^2 \right) \tag{18}$$

Figure 3.1d is a plot, again in a similar format to Figures 3.1a-3.1c, of the maximum energy dissipation in a square channel as a function of width of the channel, and a range of fluid flow rates.

3.3 Computational Fluid Dynamics, CFD, Analysis.

For laminar flow in more complex flow geometries, analytical solutions for the velocity vectors are not available. For these scenarios, the velocity vectors were determined using the commercial computational fluid dynamics software,

FLUENT (Lebanon, NH). The energy dissipation rate was determined using a user defined function within FLUENT. The simulation used pure water as the model fluid; the presence of cells in the fluid will not significantly affect the results of the simulation unless the volume fraction of cells is larger than 1%, which corresponds to a cell concentration on the order of 2×10^8 cells/ml. (The viscosity of water with a 1% particle volume fraction increases less than 2%, and the relation is linear up to a 10% particle volume fraction; Hiemenz and Rajagopalan, 1997).

Contracting flow. One of the more commonly encountered complex flow geometries in bioprocess equipment is that of a contracting flow, such as a pipette. The standard, large-orifice, and 10 ml pipettes were simulated using a two-dimensional axisymetric model. The pipette dimensions as well as the number of node points used in the simulations are listed in the Table 3.1. One thousand 10 μm diameter particles were tracked through the simulated flow. The particle tracking was performed in the uncoupled mode, which assumes that the particles do not affect the fluid flow. The maximum energy dissipation rate each particle encounters in the pipette is recorded. Figure 3.2a is a representative histogram of the simulated maximum energy dissipation rate each particle experienced flowing through a wide pipette at 2 ml/s. Figure 3.2b is a plot of the maximum energy dissipation rate calculated for the three types of pipettes over a range of flow rates. It should be noted that these are extreme flow rates: i.e. the "narrow" pipette has a volume of 200 μl; consequently, a flow rate of 1 ml/s would mean that one would have to empty the pipette in 0.2 seconds.

3.4 Empirical Studies

Mixing Vessels, Literature Analysis. With respect to the flow in a mixing vessel, there exists predictable flow patterns and structures (Tatterson, 1991; Roberts *et al*. 1995). In addition to the macroscale circulation patterns consistent with the typical marine, Rushton, or pitched blade turbines, in most conditions there exists an intense trailing vortex emanating from the tips of the blades (Van't Riet and Smith, 1975; Stoots and Calabrese, 1995; Tatterson, 1991; Yianneskis, *et al*., 1987).

While the general flow patterns are well recognized, the quantification of turbulence, especially in a mixing vessel is more difficult. This difficulty arises from two primary reasons: the inability to predict the turbulent flow on a "micro" basis from first principles, and a lack of sufficiently high resolution experimental techniques. This difficulty has lead to the development of a number of models, scaling arguments and experimental correlations to explain turbulence in mixing vessels. One of the recurring concepts in these approaches is the use of energy dissipation rate.

This lack of both theoretical and experimental approaches to fundamentally define turbulent flow in mixing vessels has lead researchers interested in quantify mixing vessels to make a number of "engineering assumptions". For example, Zhou and Kresta (1996a, 1996b) assumed *local isotropic turbulence* in the impeller discharge region close to the impeller blade using one generally accepted correlation which used their experimentally determined 2-D velocity data. With this approximation method, Zhou and Kresta (1996a, 1996b) conducted a number of relevant studies.

Specifically, in one study, Zhou and Kresta (1996a) presented the difference in the distribution of *average energy dissipation rates* in the impeller region

for three types of impellers (Rushton turbine, RT; pitched blade turbine, PBT; and the fluidfoil turbine, A310) in a mixing vessel of "typical" geometry (liquid height equal to tank diameter, four equally spaced baffles 1/10 the tank diameter). In a second study, Zhou and Kresta (1996b) investigated the impact that tank geometry has on the ***maximum*** *local energy dissipation rates* for the three impellers used in the previous study as well as the high efficiency turbine, HE3. From all of these studies, one can make significant applications with respect to the analysis and scale-up of animal cell culture bioreactors.

First, the energy dissipation rate is always relatively high in the *impeller discharge stream*. Specifically, 43.5 % of mechanical energy added to the vessels is dissipated in the impeller discharge region of a RT, and 70.5% in a PBT. In addition, the "average" energy dissipation rate is over an order of magnitude higher in the impeller region when compared to bulk average for the whole vessel. ***Second***, and probably most significant, for a given impeller type, the ***maximum***, *local energy dissipation rate* in the impeller region can be approximated using a non-dimensional constant and to a specific, non-dimensional location relative to the impeller. This non-dimensional constant, *E*, (our notation) is given by:

$$E = \varepsilon_{\max} / N^3 D^2 \qquad (18)$$

where *D* is the impeller diameter and *N* is the impeller speed with units of s^{-1}. If specific geometric ratios are held constant (including the type of impeller), "*E*" did not vary significantly over a large range of impeller speeds. If the *D/T* (impeller diameter/vessel diameter) or *C/T* (off-bottom clearance/vessel diameter) ratio changed,

within certain limits, up to a 46% increase in the value of E was observed when working with a RT. These observations also held for the PBT, impeller.

3.5 Experimental Values of Energy Dissipation Rate in a Bioreactor.

While the previous, semi-empirical relationship provides estimates of the ε_{max} in turbulent mixing vessels, it does not provide information on the distribution of ε. In addition, a significant number of bioreactor studies have been, and continue to be, conducted in animal cell bioreactors without traditional baffles (i.e. Kunus and Papoutsakis, 1990; McDowell and Papoutsakis, 1998; Aloi and Cherry, 1996; Cruz et al. 1998). To address these concerns, experimental studies using Particle Tracking Velocimetry, PTV, were conducted on a bench scale bioreactor.

Vessel A two-liter bioreactor (Applikon, Foster City, CA) with a standard Rushton Turbine impeller was used for the experimental aspect of this study (Figure 3.3a). For the particle tracking velocimetry, PTV, studies, the vessel was filled with 1.6 liters of distilled water, and either one or no baffles were used. To decrease the optical distortions caused by its curved wall, the reactor was placed in a transparent, rectangular plastic box, which was filled with distilled water. Table 3.2 presents the specifics on the geometry and configuration of the bioreactor.

Particle tracking velocimetry In contrast with LDA, PTV (Guzennec *et al*., 1994) is a 3-dimensional, full-field velocity measurement technique, which is able to track up to a thousand particles at a time, depending on the resolution of the image and the size of the tracers in the image. However, even a thousand 3-D velocity vectors cannot map a turbulent velocity field well enough to obtain meaningful estimates of

local energy dissipation. To overcome this restriction, a process which is a combination of Adaptive Gaussian Windows, AGW, and ensemble averaging, ES, was used (Venkat *et al*. 1996) to develop high density, 3-D velocity maps of the bioreactor.

Tracers. The 3-D PTV technique requires particles seeded in the flow of interest. Microcarriers, 200 μm in diameter, (Solohill Engineering Inc., MI) were used as flow markers. To improve the image contrast between the particle and background, the particles were dyed with fluorescent yellow dye (Pylam Products Company, Inc., NY). Since the tracers have a density slightly higher than water, magnesium sulfate u. s. p. (Revco D. S. Inc., OH) was added to increase the density of the water used to match the particle density.

Image acquisition equipment. A schematic diagram of the experimental apparatus used to obtain images is presented in Figure 3.3c. Images were acquired by two black and white progressive scan CCD cameras (TM-6701 AN, Pulnix American, Inc., CA), using two Fuji zoom lens (Fuji Photo Optical Co., Japan). The CCD cameras could be operated at 60, 120, 125, and 200 frames per second; however, due to the bandwidth restriction, the image size at 200 fps is only 496×97 pixels while at 60 fps it is 496×450 pixels. The images from each camera were then sent to separate PCs where the images were digitalized using an image grabbing board (Dipix technologies Inc., Canada) and then loaded directly onto the computer hard disk. The flow volume of interest was illuminated by two strobe lights (Chadwick Helmuth, CA) which were synchronized with the cameras.

In order to guarantee that the vectors grouped together are from images of the same phase during AGW and ES, a trigger system was built that sent a pulse

to the computers which initiated the recording operation when one particular blade came to a specific position. The trigger system, as shown in Figure 3.3b, included a disk, a photodetector and a power supply. The disk, rotating with the shaft, had a radial slot; when its leading edge passed the fixed photo detector, a signal was sent to the control box and then the computer.

A total of four control boxes were utilized. The main control box, which coordinated all the components involved in the image acquisition process, received the external trigger signal, and the two strobe lights controllers (Chadwick Helmuth, CA). The fourth control box (Applikon, Schiedam, Holland) controlled the rotation speed to the impeller.

Image processing and calibration. The processing of two sets of sequential images (left and right view) into 3-dimensional location and velocity data has been reported previously (Guezennec *et al*., 1994; Venkat et al., 1996; Zhao and Brodkey, 1998). Every PTV reported particle has a 3-D coordinate in the real world domain and two sets of 2-D coordinates in the image world, one set for the left image and the other set for the right image. Calibration interrelates these two world domains and corrects for potential image distortions. Consequently, the calibration process should involve the full image region studied. In the work reported below, two regions were calibrated and these regions are presented in Figure 3.4a and 3.4b.

The actual calibration procedure consists of a support holder, which had six slots, that was placed inside the vessel. A calibration board was then mounted in each slot sequentially. The calibration board consisted of a two dimensional matrix of small holes into which optical fibers were placed. The other end of the optical fibers, which

were collected into a single group, were attached to a high intensity illuminator (Dolan-Jenner Industries, Inc., MA). Images were then made with the 3-D PTV system of the calibration board in each of the six slots. Since the location of each optical fiber was known in three dimensions of the "real world" and in 2-D images in the image, a "correction" file was created and incorporated into the 3-D PTV algorithm (Choi and Guezennec, 1992).

Experimental conditions. Experiments were conducted at two impeller speeds, 73 rpm and 195 rpm. There was no baffle in the 73 rpm runs, but in the 195 rpm situation, one set of experiments were preformed without, and another with one baffle inside the vessel. In each case, multiple sets of images, 20 frames per set, were recorded and each recording process was initiated by a signal from the triggering system. Consequently, each frame corresponds to a specific impeller position (phase locked). The time gap between each set of images was randomly distributed between 1 and 10 minutes. In this way, it was assumed that the effect of low frequency fluctuation was minimized. For the 195 rpm experiments, the cameras were operated at 200 frames per second. Because of the small image size (496×97 pixels), only the impeller region was targeted. For the 73 rpm case, 120 frames per second was chosen and the corresponding image size (496×240 pixels) provided a high enough resolution to map the larger region shown in Figure 4a. Table 3 summarizes the experimental conditions.

Three different experimental conditions were studied and are identified as A, B, and C (Table 3.3). For condition A, an average of 444,000 randomly distributed velocity vectors were obtained for each of 16, phase locked, distinct impeller locations.

For condition B, 87,000 velocity vectors were obtained for each of the 16 impeller locations, and for condition C, 78,000 velocity vectors were obtained for each of 16 impeller locations. Vectors for only 16, and not 20, locations were obtained because the PTV codes requires five sequential frames to assign velocity vector data to the middle (or third) frame; hence in a 20 frame sequence, data is obtained for frames 3 through 18. AGW and ES methodology was used to obtain high-resolution, 3-dimensional maps of fluid velocity in the flow visualization region. Contour plots of the local EDR were made from these velocity maps. (Venkat *et al*. 1996).

The AGW interpotation of the ensemble averaged velocity data yields mean, 3-D velocity vectors at specific node locations. The performance of the AGW and ES methodology is determined by three primary parameters: L, the characteristic length of the flow (chosen in this case to be the impeller diameter), δ, the mean nearest distance between velocity vectors, and $h/2$, the distance between the nodes. Once L and δ are set, one then chooses the value of h which determines not only the distance between nodes but also the total number of nodes in a given volume. Obviously, the smallest value of h is most desirable and its choice is governed by a set of characteristic curves developed by Spedding and Rignot (1993), which relate the root mean square error (RMSE) associated with a given set of L, δ and h values. For both rpm settings we chose a value of node spacing of 1 mm which results in a RMSE of between 2-3%. The complete summary of values chosen are presented in Table 3.4. As a point of clarification, only one impeller location was chosen to perform the AGW and ES methodology on the large number of sets of 20 frame sequences acquired.

Velocity vectors. Figures 3.4c and 3.4d presents the results of one 2-D

"slice" of AGW ES averaged data for one of the 16 impeller locations for the 73 rpm experiments, and the unbaffled 195 rpm study, respectively. As expected, the magnitude of the velocity vectors (in this case indicated by arrow length) is significantly higher in the impeller region as observed in Figure 3.4c. However, some higher values can also be observed in the bulk region away from the impeller.

Local EDR plots and maximum values . As Figures 4c and 4d indicate, it is difficult to interpret 2-D velocity vector plots with respect to the effect that hydrodynamic forces have on cells. Since 3-D velocity data exists at regularly positioned locations, it is possible to estimate the ∇U term used in the equation for energy dissipation (Equation 1) at a specific node location using the finite volume differential method. Figure 3.5 is a gray scale plot of the local energy dissipation (W/m^3) for the same "slice" presented in Figure 3.4c. Figure 3.6 presents local energy dissipation plots of five slices shown in the impeller region at 195 rpms without baffle. An alternative to the use of gray level plots is a "scatter plot" in which only the node locations with the highest values of energy dissipation are presented of the total 19,152 nodes. Figure 3.7 presents three views (perspective, top, and side) for the location of the top five node points, with respect to energy dissipation, (Figures 3.7a, 3.7b, and 3.7c), the location of the top 20 node points (Figures 3.7d, 3.7e and 3.7f), and the location of the top 100 node points (Figures 3.7g, 3.7h and 3.7i). Alternatively, Table 3.5 presents ε_{max}, ε in the impeller region, and ε for the whole vessel based on the power number of the impeller.

EDR histograms. Figures 3.4 through 3.6 only present data from several two dimensional "slices" of the complete set of three dimensional data. To present a more complete picture of the data, histograms were created which present the energy

dissipation rate values at every single node location in the three dimensional control volumes in the form of frequency of occurrence versus the magnitude of the energy dissipation. Figure 8a presents the local energy dissipation rate for the whole vessel at 73 rpm, Figure 8b presents the local energy dissipation rate in the impeller region (square ring) at 73 rpm, and 8c presents the local energy dissipation rate in the impeller region (square ring) for the 195 rpm experiment without baffle.

Comparison of Values of Energy Dissipation to Studies of Others. Zhou and Kresta (1996a) choose a number of control volumes around the impeller including one in the "impeller discharge" region around a RT. This impeller discharge region is in a very similar location to that used in this study except that in our current study the region is a rectangular box. To allow a more accurate comparison, we have changed the geometry of our control volume (through the omission of specific node points) to create a control volume which is one sixth of a "square ring" which encircles the impeller (Figure 3.9). This "square ring" contains 5.74 % of the total liquid in the vessel; yet 27.8% of the total energy dissipated in the vessel occurs within this volume. This estimate of the ratio of the total energy dissipated was obtained by summing the experimentally determined values at each node and dividing the total energy delivered to the system using a power number correlation. This estimate of the total energy dissipated in this region compares favorably to the report of Zhou and Kresta (1996a) in which the impeller discharge region was 4.87% of the total volume and 28.2% of the total energy was dissipated in this volume.

A second comparison between this currently presented work and that of Zhou and Kresta (1996a) is that of the maximum energy dissipation rate as a function of

operating conditions. Specifically, geometric ratios Zhou and Kresta (1996a) state are important with respect to the use of Equation 18; namely impeller diameter, D, to tank diameter, T, D/T, the off bottom clearance, C, to T, C/T, and the baffle width, B, to tank width, B/T are very similar between the Applicon Bioreactor used in this study and the vessel used by Zhou and Kresta. Consequently, ε_m as a function of rpm can be calculated using Equation 18 and a value of E of 13.7 (mean of all of the values reported for a Rushton Turbine by Zhou and Kresta; 1996a). The mean energy dissipation rate can also be determined for the Applicon Bioreactor using the power number correlation and a value of the power number of 4.2 (Brodkey 1988). Figure 3.10 is a plot of the calculated (solid line) and experimentally measured (dots) mean and maximum energy dissipation rate in the Applikon bioreactor as a function of impeller rpm.

3.6 Discussion

The first observation one can make from the presented calculations and experimentally derived values is that it requires extreme conditions to obtain an energy dissipation rate that has been shown to cause immediate, catastrophic rupture of typically used suspended animal cells, i.e. an ε of 1×10^7 W/m^3 (Ma et al. 2002). This observation is consistent with current industrial and bench scale experience and practice.

However, the presented calculations and experimentally derived values also indicate that it is significantly easier to reach a value of ε of 1 x 10^3 W/m^3, a value which has been reported to result in damage to animal cells attached to microcarriers (Venkat et al. 1996a, Gregoriades et al. 2000). This four order of magnitude difference between values of ε shown to damage suspended versus attached animal cells helps to explain the continued confusion and/or controversy over the shear sensitivity of animal cells.

However, it should be noted that these cited values of ε that cause cell damage are only levels of catastrophic cell damage. It is highly likely, and has been experimentally demonstrated on cells of biomedical interests attached to surfaces (Ranjan et al. 1996) that lower levels of ε can have non-lethal metabolic and physiological effects.

A second observation is that despite concerns raised by some assay kits, it is not possible to damage cells in pipette tips from purely hydrodynamic forces unless unreasonably high flow rates are used to ejected the fluid in the tips. Similar observations can be made with respect to flow in tubing. i.e. highly atypical flow conditions are needed to achieve levels of energy dissipation rate that are of concern.

A third observation is the effect, or the lack thereof, of baffles on the value of ε_m. In 1950, Rushton et al. presented one of the first studies on the power characteristics of mixing impellers. In one figure, experimental correlations of the relationship between Power number and the impeller Reynolds number with and without baffles using a "flat blade turbine" were presented. This "flat blade turbine" has since come to be known as a Rushton turbine. At an impeller Reynolds number of 2,500 (the value obtained at 73 rpm in the Applikon bioreactor), Rushton (1950) reports a power number of 1.9, while at a Reynolds number of 6,700 the power number is approximately 1.3 (for the case with no baffles present). While the case of a single baffle is not presented, it is highly likely that the power number would be somewhere between a value of 1.3 and 4.2 (the case with four baffles present).

Despite the difference in power numbers, Table 3.5 and Figure 3.10 show a surprisingly close agreement between ε_m is this study (both with no baffle and one baffle) and the correlations of Zhao and Kresta for the case when four baffles are present.

Since it is a well know and well documented observations that baffles greatly increase bulk mixing in an agitated vessel, whenever an impeller is used to mix a bioprocess, baffles should be used to maximize the bulk mixing in the vessel.

A final word of caution is in order. While commonly used suspended animal cells, such as CHO, insects, and hybridoma cells are robust with respect to hydrodynamic forces, it is not clear if such observations are true for most animal cells. Current studies in our lab also indicates that clusters of cells, such as porcine pancreas islets are at least as sensitive as animal cells attached to microcarriers, and potentially significantly more sensitive. As biotechnology continues to progress and broaden, an increasing wide range of cell types will be studied and used in cultures larger than tissue culture flasks; consequently care should be taken in the extrapolation of the observations of currently used cells lines to others.

description	exit diameter (in.)	exit diameter (mm)	entrance diameter (in.)	entrance diameter (mm)	length (in.)	length (mm)	node count
"narrow"	0.016	0.406	0.218	5.54	1.988	50.5	4.8×10^4
"wide"	0.059	1.29	0.218	5.54	1.967	50.0	1.01×10^5
10 mL	0.061	1.55	0.25	6.35	1.458	37.0	2.5×10^5

Table 3.1: Dimension and number of nodes used in simulation of pipettes

tank diameter, T	0.129 m
liquid height, H	0.135 m
impeller type	6 bladed, Rushton turbine
impeller diameter, D	0.0454 m
off bottom clearance, C	0.0426 m
impeller width, W	0.0120 m
liquid	distilled water
liquid volume	1.6 L
tracer diameter	200 μm
tracer density	1.02 Kg/L

Table 3.2: Geometry of bioreactor and impeller and properties of liquid and tracer used in the experiments

	A	B	C
baffle	0	0	1
rotation speed (rpm)	73	195	195
tip speed (m/s)	0.173	0.463	0.463
Reynolds number	2.51×10^3	6.70×10^3	6.70×10^3
frame speed (fps)	120	200	200
image size (pixels)	496×197	496×97	496×97

Table 3.3: Experimental Conditions for PTV studies.

symbol	parameter	value	comments
L	characteristic length	0.0454 m	impeller diameter
δ	mean nearest distance	0.00067 m	based on vector concn of 560/cm^3
h	twice grid distance	0.002 m	
σ	Gaussian window width	0.00083 m	
RMSE	error function	2−3%	

Table 3.4: Values for parameters used in the AGW ES analysis of data

	A	B	C
ϵ_{max} (W/m^3), measured	57.1 ± 12[a]	1.34 × 10^3 ± 190[a]	1.00 × 10^3 ± 290[a]
ϵ_{max} (W/m^3), eq 19	49	970	970
average energy dissipation rate in the impeller region (W/m^3)	4.23 ± 0.15[a]	74.9 ± 5.4[a]	41.1 ± 11.2[a]
average energy dissipation rate in the whole vessel (W/m^3)	0.856	NA	NA
average energy dissipation rate in the whole vessel based on power number (W/m^3)	0.4	5.4	5.4 to 17.0

[a] Data from 16 sets of results.

Table 3.5: Summary of several variables obtained for each of the three experimental conditions

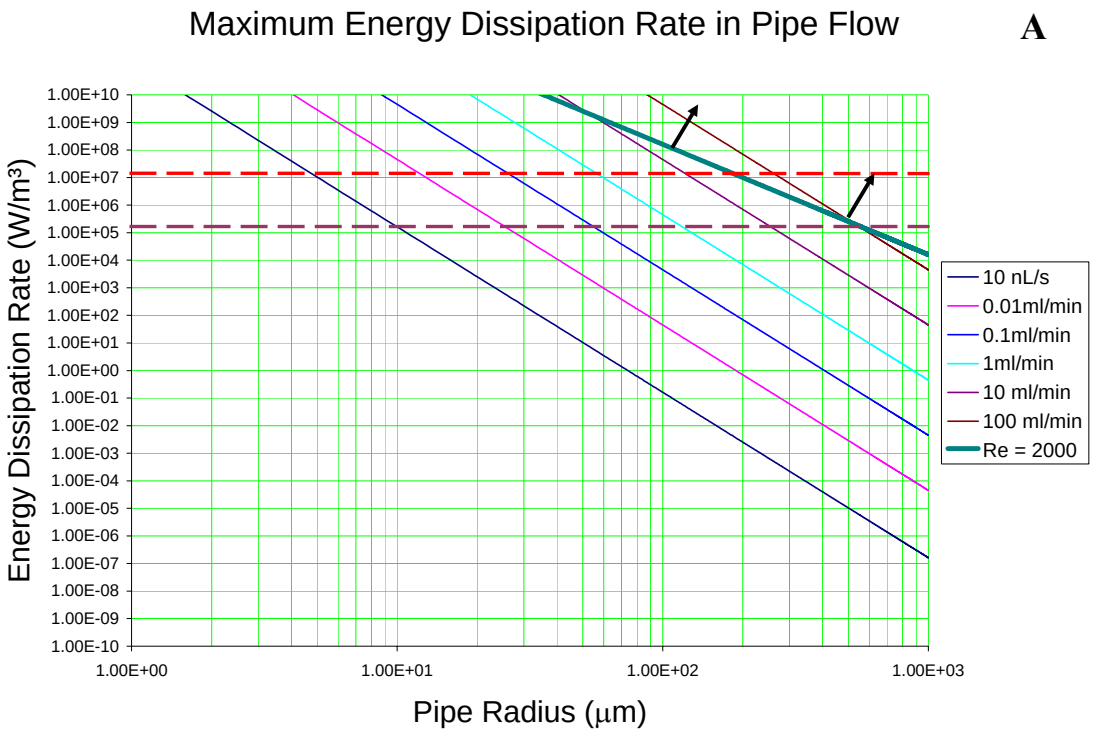

Continued

Figure 3.1: Maximum energy dissipation rate as a function of flow rates, geometries, and dimensions. Specifically, pipe, annulus, parallel plates, and square channels (A-D, respectively) are presented.

Figure 3.1 continued

B

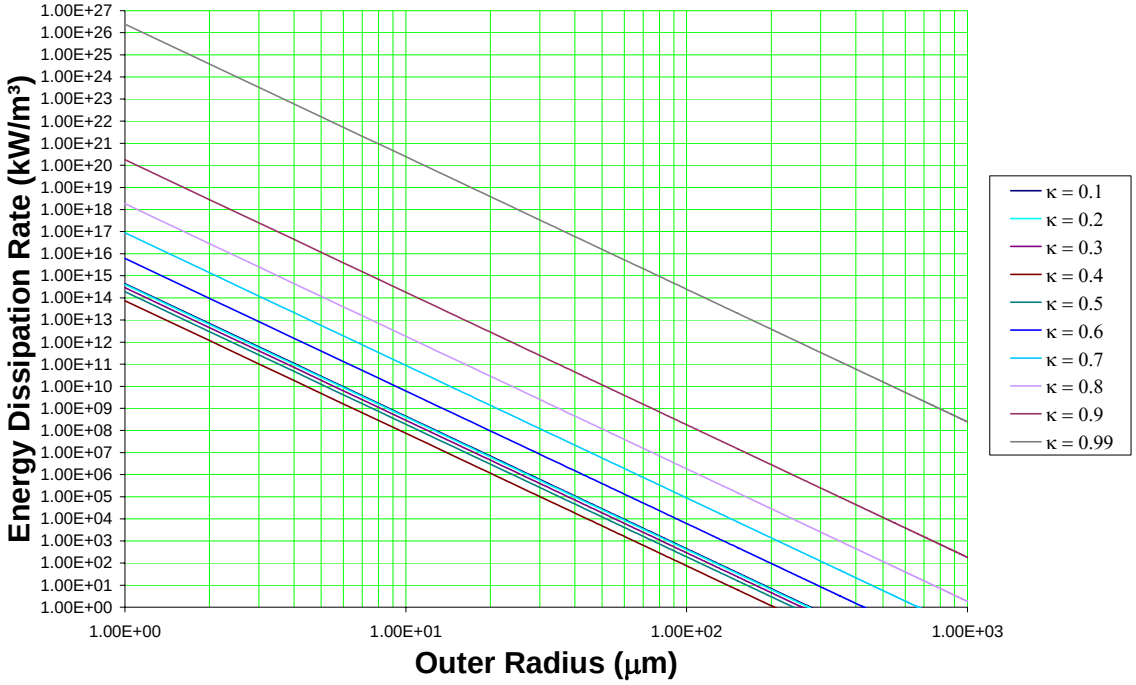

Continued

Figure 3.1 continued

C

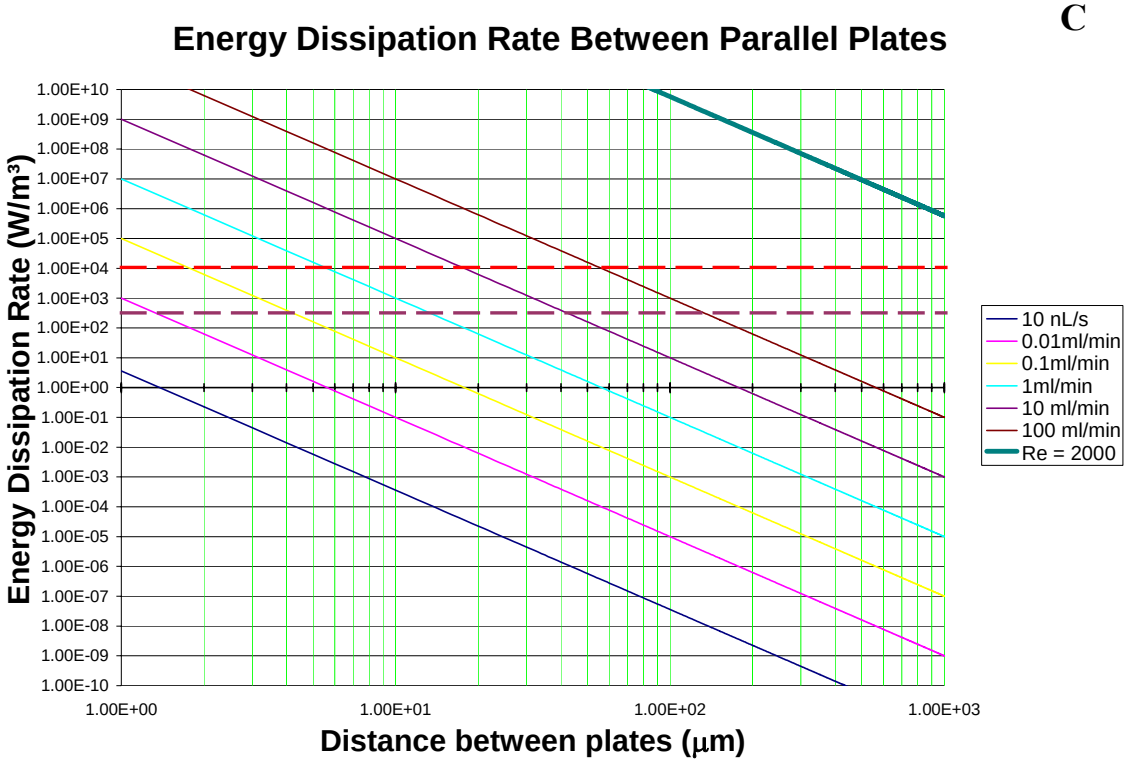

Continued

Figure 3.1 continued

D

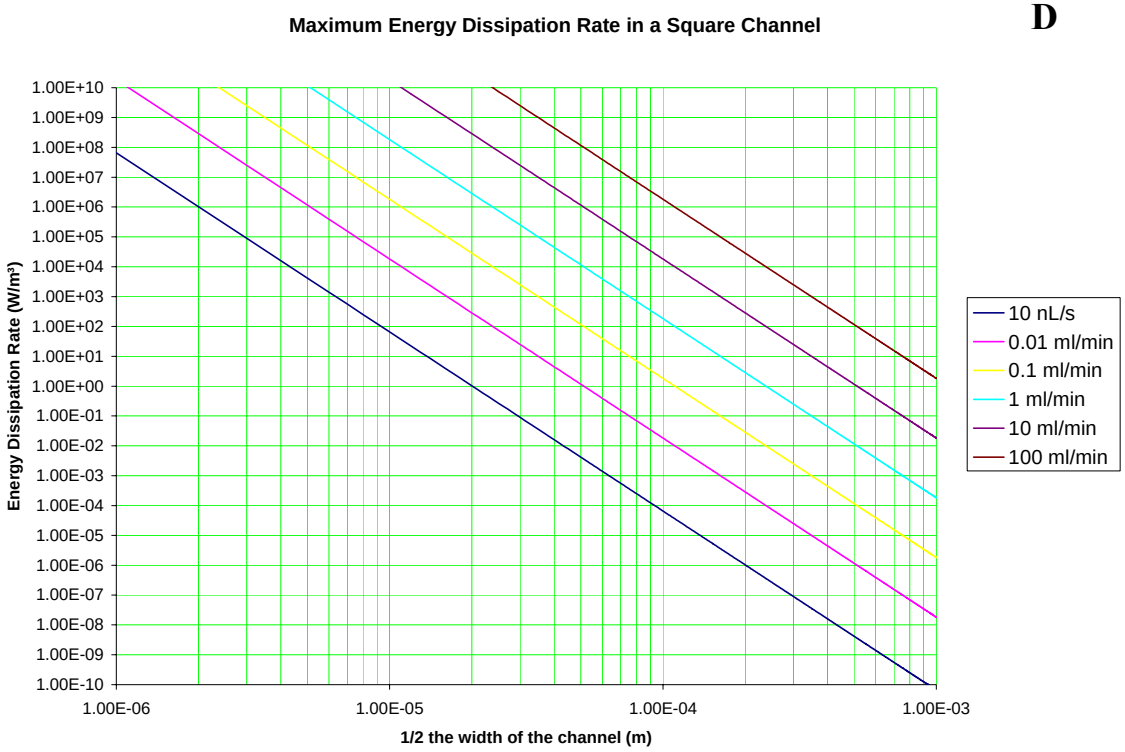

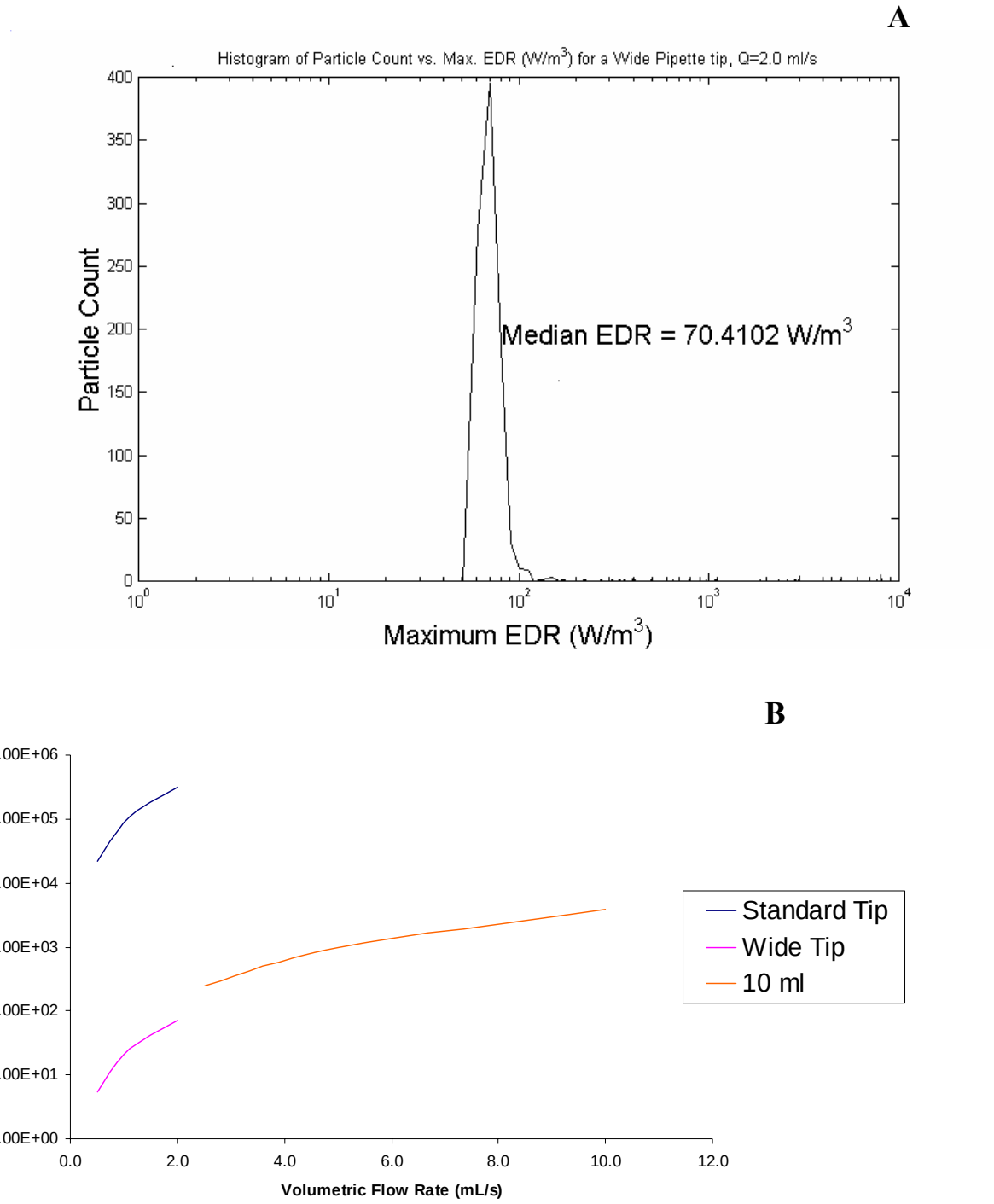

Figure 3.2: (A) Representative histogram of the simulated maximum energy dissipation rate each particle experienced flowing through a wide pipet at 2 mL/s. (B) Plot of the maximum energy dissipation rate calculated for the three types of pipets over a range of flow rates

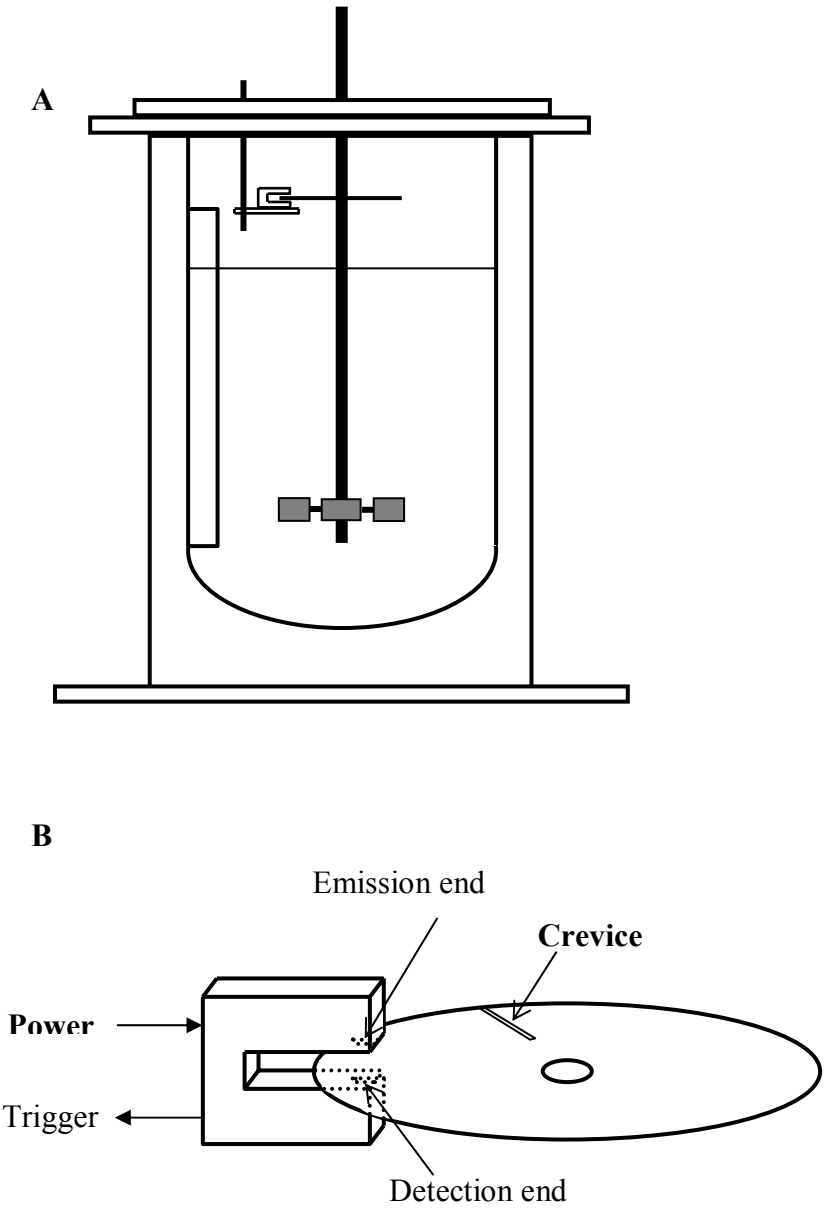

Continued

Figure 3.3: (A) Diagram of the vessel in which studies were conducted, (B) the triggering mechanism used to synchronize impeller position with image acquisition, and (C) schematic diagram of the experimental apparatus used obtain images for PTV analysis

Figure 3.3 continued

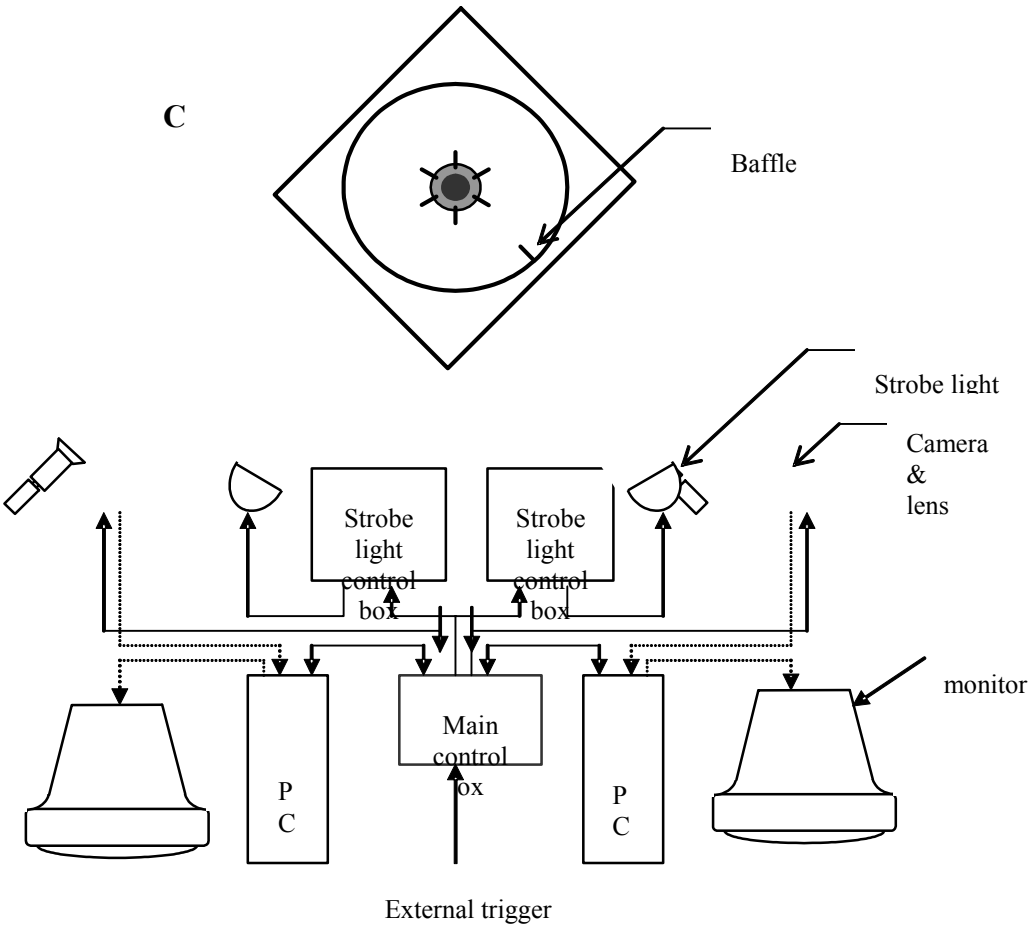

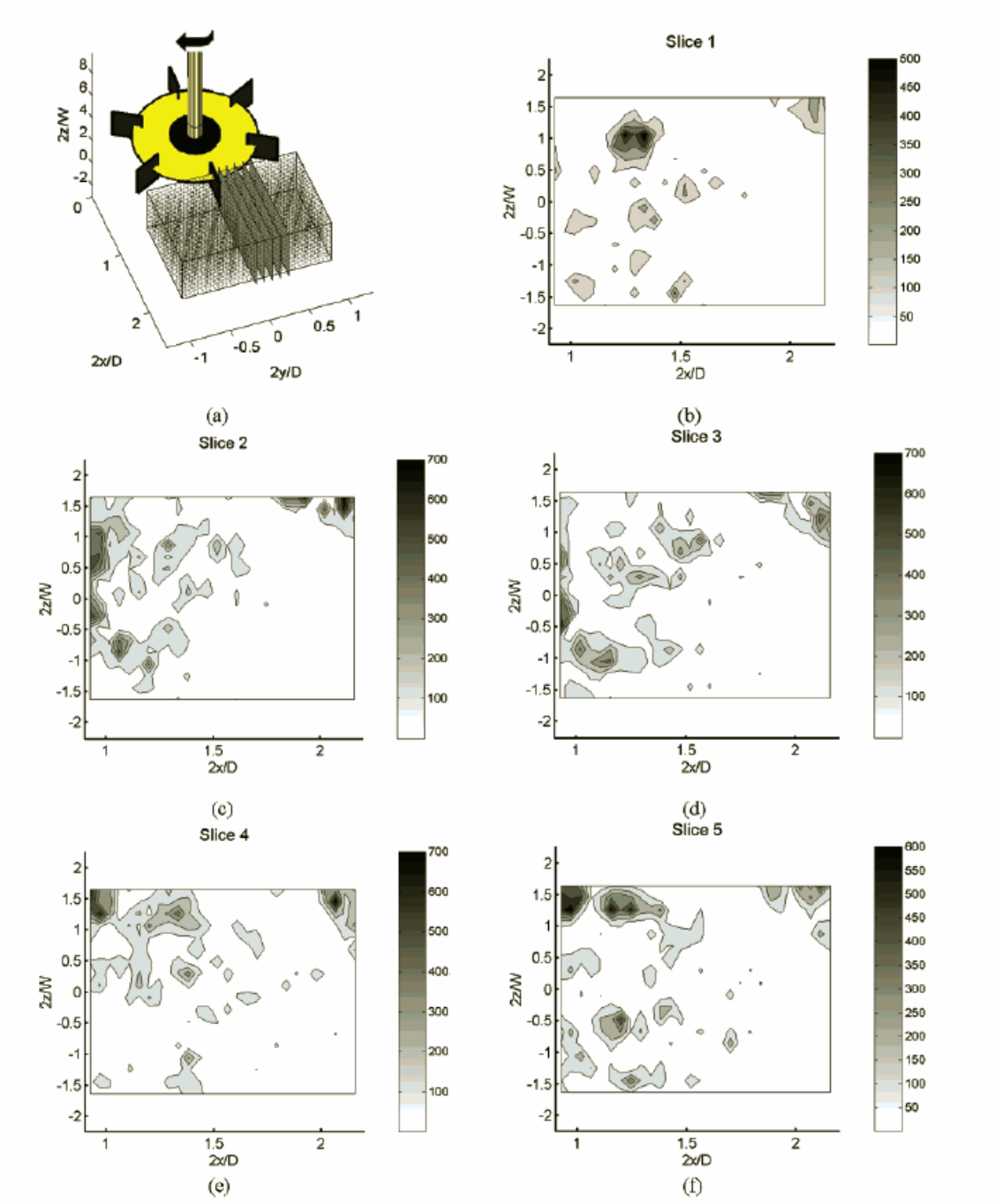

Figure 3.4**:** Gray scale plot of five slices of the energy dissipation rates (W/m^3) in the impeller region at 195 rpm. Also included is a diagram indicating the location of the five slices.

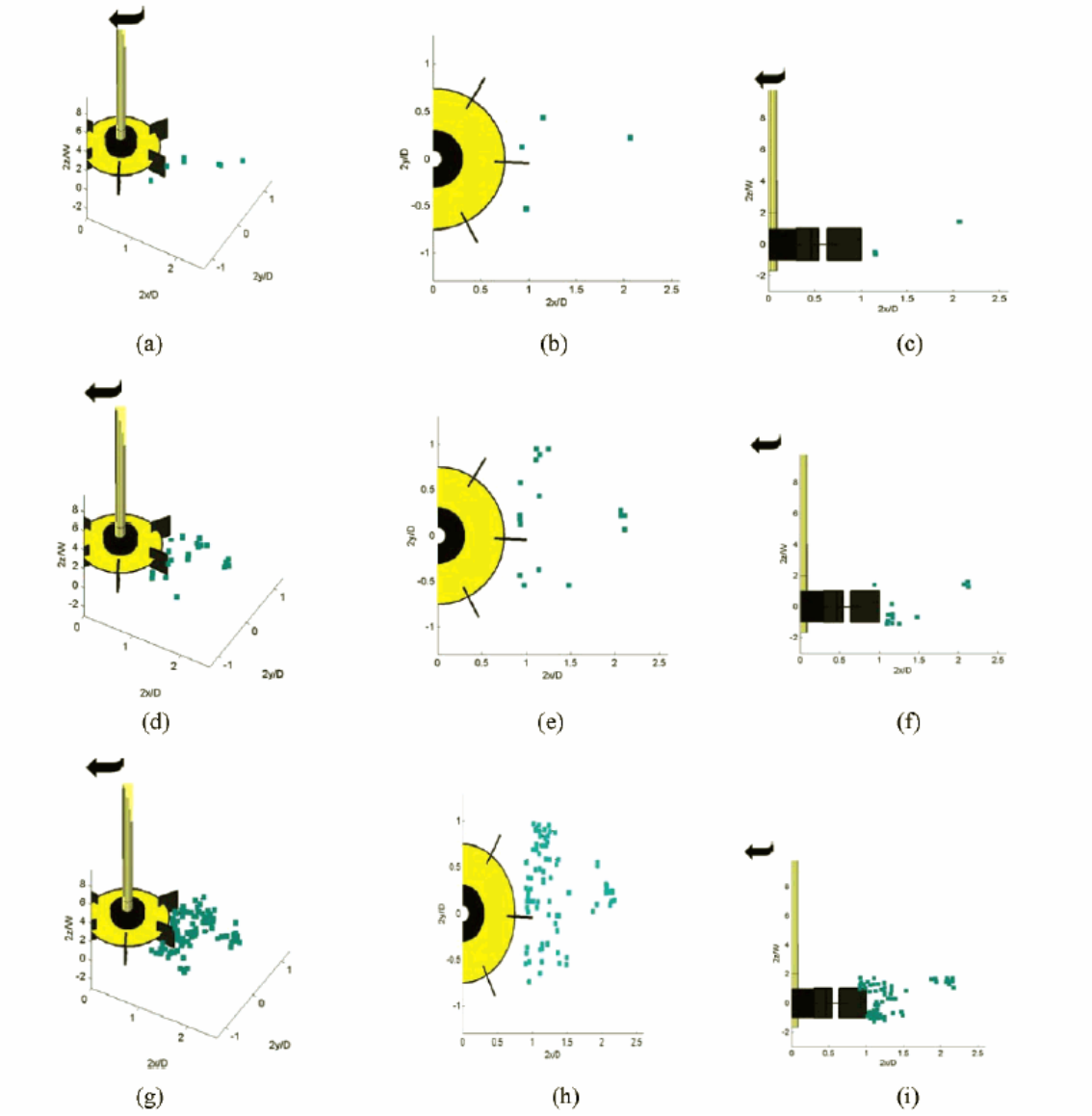

Figure 3.5: Locations of nodes with highest values of energy dissipation from experimental condition B and the same impeller position: (a-c) highest five node points, (d-f) highest 20 node points, and (g-i) top 100 node points

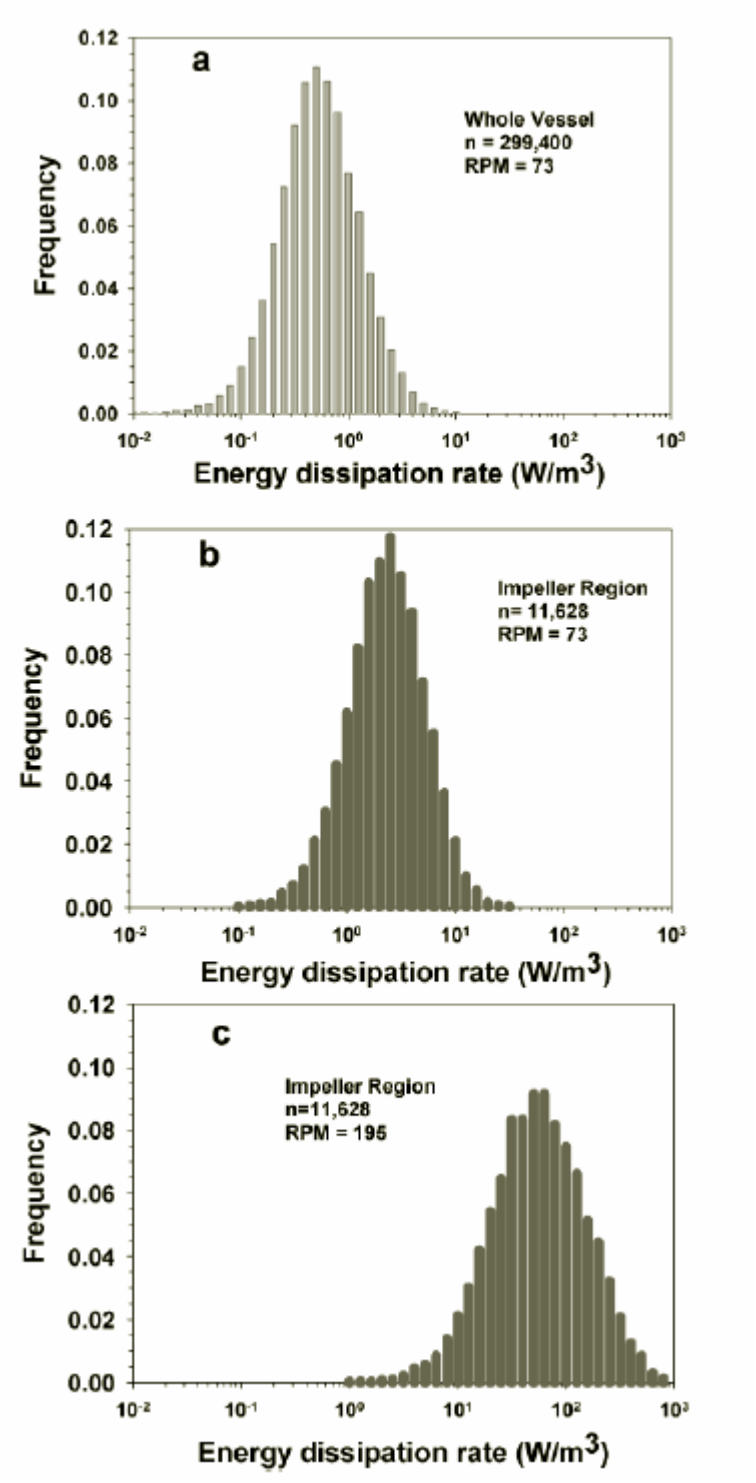

Figure 3.6: Histogram of the energy dissipation for (a) the whole vessel and (b) impeller region for the 73 rpm studies and (c) the impeller region for the 195 rpm study.

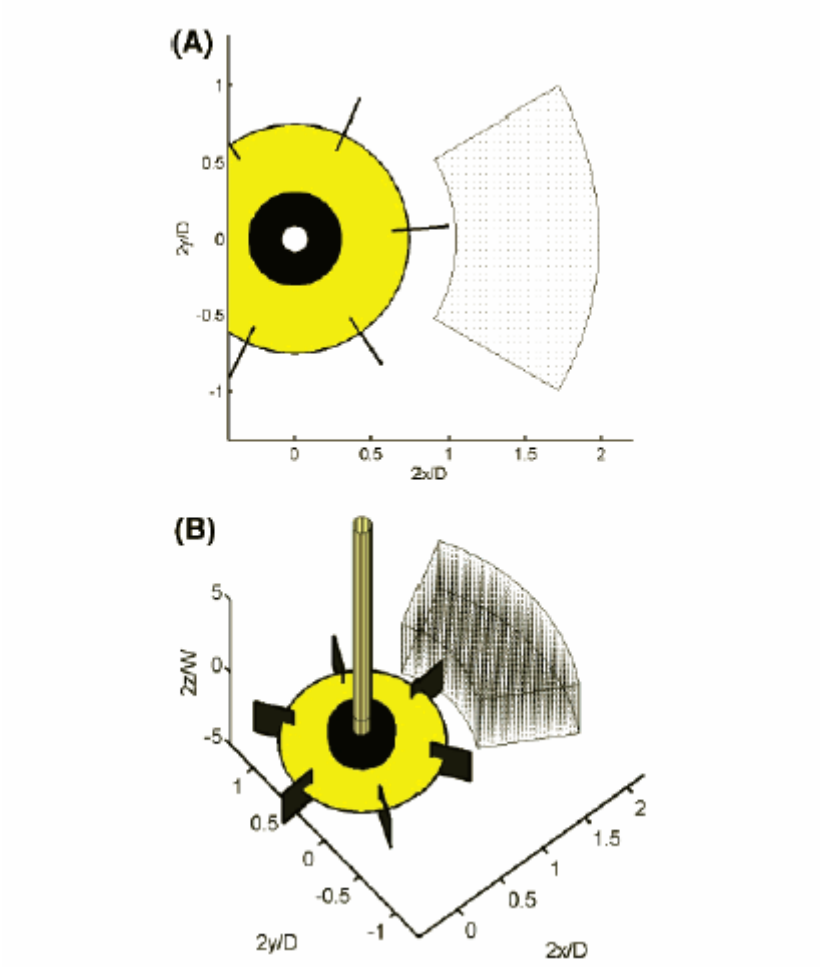

Figure 3.7: (A) Top and (B) perspective view of the volume used to create the "square ring" in the impeller discharge region

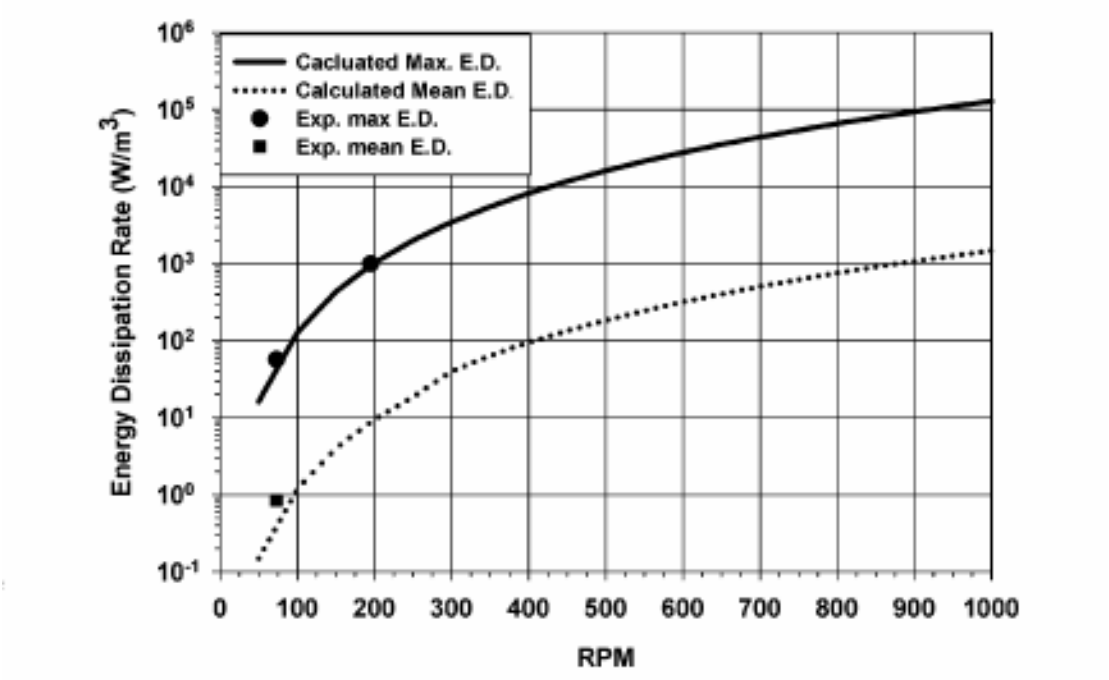

Figure 3.8: Calculated maximum (—) and mean (···) energy dissipation rate in the Applikon bioreactor, containing four baffles, as a function of rpm. The single points correspond to experimental measurements in this study without baffles.

Chapter 4

Apoptosis in Bioprocess Equipment

4.1 Introduction

Many of the newly developed pharmaceuticals are large molecules, and unlike most of the older, small molecule pharmaceuticals, the large molecule therapeutics requires mammalian cell culture for production. One of the major challenges facing engineers during the production of large molecule pharmaceuticals is maintaining a high level of cell viability in bioreactors as wells as in other pieces of bioprocess equipment such as tubing and filtration systems. In addition to the obvious need to keep cells viable to produce the compound of interest, dead cells tend to release proteolytic enzymes (Darzynkiewz *et al*., 1997). These proteolytic enzymes may degrade the protein product the cells are secreting.

4.1.1 Modes of Cell Death: Necrosis

There are two primary modes of mammalian cell death, necrosis and apoptosis. Necrosis is passive cell death; some external force suddenly destroys the cell's membrane or cytoskeleton. Most of the methods that are used to measure necrosis are based on tests of cell membrane integrity. Typically a dye is selected that does not usually enter

healthy cells. After a small amount of dye is added to the cell suspension, the number of stained cells are counted using a light microscope and hemacytometer, if trypan blue dye is used, or a flow cytometer if a fluorescent viability dye such as propidium iodide (PI) or 7-aminoactinomycin D (7-AAD) is used. Another method of detecting necrosis measures lactate dehydrogenase (LDH) activity in the suspending fluid. LDH is released from dead cells and is detected using a spectrophotometeric assay. Apoptosis, on the other hand, is active cell death whereby a cell carries out a process that ultimately leads to its death. Apoptosis is used in multicellular organisms' immune system (i.e. the destruction of viral infected cells) and during development (i.e. tadpoles losing their tail).

4.1.2 Modes of Cell Death: Apoptosis

Apoptosis is initiated by a specific signal, such as the binding of a cytokine to a receptor, or an event, such as nutrient starvation, extreme pH, hypoxia, etc. There are several milestones along the apoptotic pathway. For non-receptor mediated apoptosis, cytochrome C is released from the mitochondria, which initiates the caspase cascade and, simultaneously, phosphatidylserine translocates from the interior of the cell membrane to the exterior (Givan, 2001). The caspase cascade ultimately initiates endonuclease activity within the nucleus and enzymatic degradation of the cytoskeleton. Eventually the cell membrane starts to form bulges or "blebs", these blebs break away from the membrane forming apoptotic bodies containing intact organelles and small pieces of DNA, approximately 180 bp long (Cotter and Al-Rubeai, 1995).

There are several methods to detect apoptosis. One of the more basic is to look for the presence of blebs of the cell membrane using a light microscope.

Another method is to stain the cells with a DNA stain such as DAPI or Hoechst 33342, and examine the cells using a fluorescent microscope. Normal cells' nuclei will be diffusely stained, whereas apoptotic cells' nuclei will appear more intensely stained due to the chromatin condensation (Mastrangelo, *et al.*, 2000a; Mastrangelo, *et al.*, 2000b). Both microscopic techniques are excellent methods for detecting apoptosis qualitatively; however analyzing large number of cells to attain statistically relevant data is difficult. Another apoptosis detection technique involves extracting and analysis of the cells' DNA using an agarose gel. If the cells were apoptotic, then a DNA "ladder" will be present (Cotter and Al-Rubeai, 1995). This method is also an excellent means of detecting apoptosis qualitatively, but it is labor intensive and cannot examine large number of cells individually. There are several flow cytometric apoptosis techniques that allow for the analysis of large numbers of cells. One of the primary methods involves fixing the cells in cold, 70% ethanol, staining with PI, and performing a cell cycle analysis on the cell population. Apoptotic cells in this analysis would appear just before the G1 peak of the cell cycle; unfortunately cells that became apoptotic during the G2-M phase or are part of an aneuploid or tetraploid population would not appear as part of the sub-G1 peak. Also, unless a large percentage of the cells are apoptotic, determining where the sub-G1 peak occurs can be highly subjective, even with the appropriate peak deconvoluting software such as Modfit. Another flow cytometric apoptosis detection method involves measuring the mitochondrial activity using dyes such as Rhodamine 123 or MitoTracker (from Molecular Probes), because mitochondrial activity decreases during apoptosis (Darzynkiewz *et al*., 1997). However, a large number of cells need to be apoptotic to see a noticeable decrease in overall Rhodamine 123 fluorescence. A third

flow cytometric method to detect apoptosis, takes advantage of the fact that PS translocates to the exterior of the cell membrane; annexin V (AV) conjugated to a fluorochrome such as FITC or PE, binds to the translocated PS. When using this method, cells should also be stained with a fluorescent viability dye such PI or 7-AAD to distinguish necrotic cells from apoptotic cells. The biggest drawback to this method is that the expression of PS on the exterior of the cells' membrane is transient; typically cells' enter later stages of apoptosis within 24 hours of expressing PS. Because of this, a time course experiment is highly recommended to perform this analysis.

4.1.3 Means of Initiating and blocking Apoptosis

Several researchers have found that the primary cause of cell death in bioreactors is apoptosis or programmed cell death (Goswami, *et al*. 1999; Al-Rubeai, *et al*., 1995, Zanghi, *et al.* 2000; Laken and Leonard, 2001; Mastrangelo, *et al.*, 2000a; Mastrangelo, *et al.*, 2000b). There are certain gene products that are capable of blocking apoptosis. Bcl-2 and bcl-x_L are two commonly used genes that block apoptosis by interfering with the signal transduction pathway that initiates apoptosis, specifically bcl-2 blocks the release of cytochrome C from the mitochondria. From a practical perspective, several research groups have observed that cell viability in bioreactors is increased when the cells were infected with a virus containing the bcl-2 gene (Mastrangelo *et al.*, 2000a; Mastrangelo *et al.*, 2000b; Simpson *et al*., 1997; Suzuki *et al*., 1997). In addition to extremes in pH, low oxygen saturation and low glucose levels, some have found that cells also become apoptotic in highly agitated bioreactors (Al-Rubeai *et al*., 1995; Perani *et al*., 1998).

4.1.4 Means of Representing Hydrodynamic Stress

4.1.4.1 Shear Stress

In the past, most of the experiments regarding cells' tolerance of mechanical stress were performed either with viscometers or with capillary tubing systems. The viscometer experiments were typically done over a relatively long period of time (>15 minutes) and with medically relevant cells (usually endothelial cells). The cells used in these experiments have to be anchored to a substrate due to the viscometers' operation. Most bioprocess equipment however utilize suspended cells. Viscometers have only simple shear flow; hence the flow is half rotational and half extensional (Gregoriades *et al.,* 2000; Ma *et al*., 2002; Aris, 1962). Extensional flows are thought to be more lethal to cells than pure shear flows (McQueen, *et al*., 1987; McQueen and Bailey, 1989). This theory is based on G. I. Taylor's (1934) research. In the 1930's Taylor examined the disruption of oil droplets in pure shear and extensional flow using a four-roll mill. The apparatus was submersed in water and a drop of oil was placed at the center. Depending on the operating conditions, a pure shear or pure extensional flow was formed. It was found that the oil droplet broke apart at a lower rate of strain in the extensional flow as compared to the shear flow. This was explained as follows: due to the non-zero vorticity of the shear flow the oil drop rotated in the fluid flow therefore no one point along the oil-water interface experienced the maximum strain for very long, whereas in the pure extensional flow large amounts of strain could build-up at a few points at the interface (Clay, 1997), see figure 4.1. In terms of suspended cells, for pure extensional flows it is possible for a relatively large amount of strain to occur at one point on a cell,

whereas for pure shear flow the cells can rotate away from the principle straining direction (Clay, 1997; Gregoriades, *et al.,* 2000). In the capillary tubing experiments, cell suspensions were pumped through capillaries of varying diameter, or with a sudden constriction (McQueen *et al*., 1987), or with a converging-diverging region (McQueen and Bailey, 1989); the percent of dead cells were measured as a function of the wall shear stress. The aforementioned investigations focused on the wall shear stress, and did not account for the possible extensional flow effects on the cells.

4.1.5.2 The Energy Dissipation Rate (EDR)

Another parameter one can use to measure hydrodynamic stress is the energy dissipation rate (EDR). The EDR is a scalar value that is intrinsic to any moving fluid, and has units of energy per unit time per unit volume (i.e. $J/s*m^3$), or power per unit volume (i.e. W/m^3). The energy dissipation rate represents the rate at which work is done on a fluid element or, for this research, a cell (Clay, 1997). Bird *et al*. (1960) defined the energy dissipation rate as the irreversible rate of internal energy increase per unit volume. Depending on the system geometry and the flow regime, the energy dissipation rate can be calculated via computer simulations, experimental data, or analytical solutions of the Navier-Stokes equation. The energy dissipation rate accounts for both shear and extensional components of the flow; therefore regardless of the type of flow cells encounter the energy dissipation rate can be used as a predictor of cell damage. In terms of a stirred tank, the average energy dissipation rate is the amount of power introduced to the liquid by the impeller divided by the volume of the tank, whereas the local energy dissipation rate is the amount of power encountered in small volumes throughout

the stirred tank. The local energy dissipation rate is better suited for predicting cell damage because the local energy dissipation can be 100 times higher than the average energy dissipation rate in stirred tanks (Wernersson and Tragardh, 1999; Zhou and Kresta, 1996). For an incompressible, Newtonian fluid, such as water, the following equation can be used to calculate the EDR:

$$\varepsilon = \tau : \nabla U = \mu[\nabla U + (\nabla U)^T] : \nabla U = \mu \sum_i \sum_j [\nabla U + (\nabla U)^T]_{ij} \nabla U_{ji} \qquad (1)$$

where μ is the viscosity and ∇U is the velocity gradient tensor and ∇U^T is the transpose of ∇U. In Cartesian coordinates, ∇U is defined as:

$$\nabla U = \begin{bmatrix} \frac{\partial U_x}{\partial x} & \frac{\partial U_y}{\partial x} & \frac{\partial U_z}{\partial x} \\ \frac{\partial U_x}{\partial y} & \frac{\partial U_y}{\partial y} & \frac{\partial U_z}{\partial y} \\ \frac{\partial U_x}{\partial z} & \frac{\partial U_y}{\partial z} & \frac{\partial U_z}{\partial z} \end{bmatrix} \qquad (2)$$

For a more complete explanation of how to calculate the EDR see Mollet *et al.* (2004) or chapter 3.

4.1.5 Micro-fluidic Contractional Flow Device

Ma *et al.* (2002) developed a micro-fluidic contractional device to determine the maximum amount of energy dissipation cells can withstand before the onset of necrosis. The channel resembles a flattened hourglass (see figure 4.2), and was made using a

photolithography technique. The shape of the channel was formed from a layer of negative photoresist (Su-8) on a piece of glass; a photomask (a transparency with the shape of the channel printed on it) is positioned over the photoresist, and then exposed to UV light. The unexposed portion of the photoresist is removed with a solvent and the remainder is baked in an oven. The dimensions of the channel are measured using a microscope and a micrometer; these dimensions are then entered into FLUENT to model the fluid flow at various volumetric flow rates. The velocity vectors were exported from FLUENT into a C++ program, which calculated the maximum local EDR. Cell suspensions were pumped through the channel at the flow rates tested in FLUENT and the cell viability was determined using a lactate dehydrogenase assay. Ma *et al.* (2002) performed several experiments on CHO, HB-24, SF-9 and MCF-7 cell lines, and found that the cells can withstand high levels of energy dissipation, approximately 10^4-10^5 kW/m³ (or 10^7-10^8 W/m³). With the exception of the SF-9 cells, all of the other cells were anchorage-dependent and all of the cell lines tested were cultured with 10% (v/v) fetal bovine serum.

The primary goals of this portion of the study were to improve the design and characterization of the contractional flow device, to determine if hydrodynamic stress can trigger apoptosis, and to compare anchorage dependent cells cultured in serum containing media to suspended cells cultured in serum free media. The contractional flow device used in this study was fabricated out of stainless steel and was characterized using a particle tracking technique in FLUENT.

4.2 Materials and Methods

4.2.1 Stainless Steel Contractional Flow Device

The contractional flow device used in this study was made out of 30 gauge (304 μm thick) stainless steel using wire discharge machining, a nontraditional machining technique, which utilizes a controlled electrical spark to remove material. Wire EDM works by guiding, via computer, a piece of metal submersed in de-ionized water into a thin (100 μm diameter), electrically charged wire. As the metal approaches the wire an arc is produced and a small amount of the metal is vaporized. Using this machining technique an accuracy of ±5 μm can be achieved, also the cut surface is perfectly vertical. One of the drawbacks of using the photolithography technique utilized by Ma *et al.* (2002) is that the walls of the device were not perfectly vertical. After the device was produced, it was inspected with a light microscope to determine the surface roughness and the actual dimensions (see figures 4.2 and 4.3).

4.2.2 Computational Fluid Dynamic (CFD) Simulations

The flow through the contractional device was simulated using FLUENT, a commercial computational fluid dynamics (CFD) program. The dimensions of the stainless steel contractional device were determined using a microscope. These dimensions were entered into Gambit, the preprocessor included with FLUENT, to create the geometry and mesh of node points of the contractional device. Due to the symmetry of the contractional device, one quarter of the actual geometry was simulated. 186,000 node points were utilized in the simulations with a grid spacing of approximately 5 μm at

the constriction; five different volumetric flow rates were simulated: 10, 30, 50, 70, and 90 mL/min. After FLUENT converged on a solution for each flow rate, an execute on demand user defined function (see Appendix A) was implemented to determine the EDR at every point in the simulated geometry. Because of the relatively small dimensions of the contractional device, the flow remained in the laminar flow regime for all of the flow rates simulated. (See Appendix B for a more detailed simulation procedure.)

4.2.3 Cell Culture

Two cell lines were investigated, wild type CHO-K1 and CHO-K1 transfected with the human bcl-2Δ gene. See Mastrangelo *et al.*, (2000a) and Levine *et al*. (1993) for more information regarding the transfection process. The bcl-2 gene product inhibits non-receptor mediated apoptosis by blocking the release of cytochrome c from the mitochondria; this is the only known function of bcl2. Initially both cell lines were cultured attached to tissue culture flasks using Dulbecco's Modified Eagle's Medium (DMEM) with 10% (v/v) Fetal Bovine Serum (FBS) (both from Hyclone, Logan, Utah). The serum concentration was gradually reduced to 1%, and then the two cell lines were cultured in with Hyclone's SFM4CHO with 1% FBS. After the cells' growth stabilized, the cells were cultured in suspension in 250 mL spinner flasks with Hyclone's SFM4CHO with 1% FBS. The spinner flasks were placed in a 37°C incubator with 5% CO_2 and the agitation rate was set at 80 rpm. After the growth of the cells in the spinner flask stabilized, the FBS was eliminated. The cells cultured in spinner flasks were used to inoculate a 1.25 L working volume stirred tank bioreactor, a Bioflo 3000 from New

Brunswick Scientific (Edison, NJ). The temperature was set at 37ºC, the pH at 7.0, the dissolved oxygen at 70%, and the agitation rate at 100 rpm; the bioreactor was operated in batch mode.

4.2.4 Contractional flow device experiments

4.2.4.1 Annexin V/7-AAD experiments

Regardless of the cell type and growth conditions, cells were harvested during the mid-exponential portion of their growth phase. Cells cultured in tissue culture flasks were trypsinized and suspended in DMEM at a cell concentration of 1.5×10^5 cells/mL. The cell suspensions were pumped through the contractional flow device at various volumetric flow rates using a syringe pump (Harvard Apparatus, Holliston, MA). The effluent from the contractional device was collected, (if necessary) the appropriate volume of FBS was added to bring the concentration to 10% (v/v) FBS, and the cells were placed in a 37ºC incubator-shaker. Each flow rate and the control suspension were performed in triplicate, meaning three separate volumes of cell suspension were pumped through the device, in a random order, and the three separate control cell suspensions remained static. Approximately every two hours, a 5 mL aliquot of cell suspension was taken, washed twice with PBS, and then washed with 1X Annexin V binding buffer. 10^5 cells in 100 μL of binding buffer were stained with 5 μL of Annexin V (AV) conjugated to PE (phycol erythrum) and 5 μL 7-aminoactinomycin-D (7-AAD); both reagents were purchased from BD Biosciences (San Jose, CA). AV is a recombinant protein that binds tightly to phosphatidylserine (PS). PS "flips" from the interior of the cytoplasmic membrane to the exterior of the membrane early during the apoptotic pathway

(Givan, 2001). 7-AAD is a viability dye that enters cells with a compromised cell membrane, and binds to nucleic acids. The samples were analyzed using a BD FACS Calibur flow cytometer, and at least 10,000 gated events were recorded. The appropriate single-color controls were produced using heat-shocked cells. A similar procedure was followed for cells cultured in spinner flasks and the bioreactor, with the obvious exception that the trypsinization was not required, serum was not added to the cell suspensions after passage through the contractional flow device, and the cells were analyzed using a Coulter XL (Fullerton, CA) flow cytometer. (Please see Appendix D for more information regarding this procedure.)

4.2.4.2 Mitochondrial Activity: Rhodamine 123

The bcl2 transfected CHO cells grown in T-flasks were stained with 5 μg/mL/10^6 cells of Rhodamine 123. Rhodamine 123 is a cationic lipophilic green fluorescent dye, which is an indicator of relative mitochondrial activity. A Rhodamine 123 gradient is produced across the mitochondrial membrane due to the large potential difference between the mitochondria and the cytoplasm (Shapiro, 2003). The interior of the mitochondrion is negatively charged, which attracts the positively charged Rhodamine 123 dye molecules. The more metabolically active the cell's mitochondria are the more Rhodamine 123 is localized in the mitochondria, which produces a higher relative fluorescence. These cells were also stained with DiD oil, a red fluorescent dye which binds to the cell membrane stoichiometrically. During cell division the dye molecules are distributed evenly among the two daughter cells and the fluorescent intensity halved

for the two cells. This dye was used to indicate cell proliferation during the course of the experiment. Both the Rhodamine 123 and the DiD oil were purchased from Molecular Probes (Eugene, OR).

The WT CHO-K1 cells cultured in serum free media and in suspension in a 250 mL spinner flask were stained with Rhodamine 123 as well as AV-PE and 7-AAD. These cells were also stained with Draq5, a cell permeant DNA stain that will stain all nucleated cells, in this study it was used to differentiate cells from debris.

4.2.4.3 Bcl-2 Expression Detection

Bcl-2 over-expressing cells cultured in bioreactor using serum free media were fixed with a 3.7% formaldehyde solution and then stained with an anti-human bcl-2 antibody conjugated to PE (from BD Biosciences). A separate sample was stained with an isotype antibody, also conjugated to PE. Bcl-2 over-expressing CHO cells cultured in tissue flasks and in serum containing media were also stained in a similar manner. These anti-human bcl-2 antibodies labeled cells were counter stained with Hoechst 33342, a DNA stain, and examined using a Nikon (Melville, NY) Optiphot-2 fluorescence microscope.

4.3 Results

4.3.1 CFD Simulations

During the course of mesh optimization, a singularity in the EDR calculation appeared at the “corner” of the constricted region of the device (the circled area of figure 4.3). The EDR value at this point continued to increase as the mesh density

increased, however the EDR values more than 10 μm away from this point remained constant. To circumvent this potential problem and to better model the conditions cells experience in the device, a particle tracking technique was employed. One thousand 10 μm diameter particles were released at the inlet of the device and the EDR that each particle encountered at every point throughout the device was recorded. (See figure 4.4 for an example of the particle tracks.) These simulations were performed in the uncoupled mode; meaning FLUENT did not model the particle-to-particle interactions. The particle data was exported and the maximum EDR value each particle experienced was determined using a program written in Perl by Ruben Godoy (see Appendix C); this data was then imported into Excel to create histograms of the maximum EDR each particle received and to calculate the median maximum particle EDR value for every flow rate (see figure 4.5 and table 4.1).

4.3.2 AV/7-AAD Experiments

As was previously mentioned, early in the apoptotic pathway phosphatidylserine, PS, translocates from the interior to the exterior of the cell membrane (Givan, 2001). AV conjugated to PE binds tightly to PS. Cells are simultaneously stained with the fluorescent viability dye 7-AAD. Figure 4.6 is a typical dot plot of 7-AAD vs. AV-PE, each dot represents fluorescence data collected from a single cell. Debris is excluded in this analysis using a gating region in the forward and side scatter dot plot. Cells in the lower left quadrant of figure 4.6 are negative for both dyes and are healthy. Cells in the lower right quadrant are positive for AV only and are thereby in the early stages of apoptosis. Cells in the upper right quadrant are positive for both AV and 7-

AAD and are either in the late stages of apoptosis or are necrotic. One cannot be certain how cells in the upper right quadrant died, because if the cells' membrane is sufficiently degraded to allow 7-AAD into the cell, the membrane may also allow AV into the cell to bind to PS on the interior of the cells' membrane (Morrone, 1997). The flow cytometer cannot distinguish between AV bound to internal or external PS. Figures 4.6 through 4.10 are the percentage of cells in lower left quadrant of 7-AAD vs. AV-PE dot plot as a function of time from when the cells were pumped through the contractional device. The error bars represent one standard deviation above and below the mean value. Figures 4.11 through 4.15 are the percentage of late apoptotic/necrotic cells as a function of time from when the cells were pumped through the contractional device. Figure 4.16 is a summary of the necrosis data; each data point shown in Figure 4.16 is the difference between the percentage of necrosis in the "abused" cells and the corresponding control values.

4.3.3 Other Flow Cytometric and Fluorescence Microscopy Data

Figure 4.17 is a plot of the median relative Rhodamine 123 intensity as a function of time for the bcl2 transfected CHO cells cultured in tissue culture flasks with 10% FBS. Note that there is not a statistically significant difference between the control and the cells that were pumped through the contractional flow device. One possible reason for this is that there were only a small percentage of apoptotic and/or necrotic bcl-2 cells.

Figure 4.18 is an ungated dot plot of Draq5 (FL4) fluorescence vs. Rhodamine 123 fluorescence taken from WT CHO-K1 cells cultured in a spinner flask and in serum free media. The two gating regions represent events with high or "bright"

Draq5 fluorescence levels (most likely nucleated cells) and the other region for low or "dim" Draq5 fluorescence (most likely debris). Figure 4.19 is forward vs. side scatter dot plot of the events in the Draq5 "bright" gating region, and Figure 4.20 is a forward vs. side scatter dot plot of the events in the Draq5 "dim" gating region. Figures 4.19 and 4.20 show that the forward versus side scatter gating region utilized in these experiments are nucleated cells and not large pieces of debris, etc.

Figure 4.21 is an overlay of histograms of the bcl-2 overexpressing cells, cultured in the bioreactor and in T-flasks, stained with an anti – human bcl2 antibody. Obviously, at some point during the serum free media and suspension adaptation, the cells lost the ability to express bcl-2.

Figures 4.22 A and B are microscope pictures, taken at 100X magnification, of bcl2 expressing CHO cells cultured in T-flasks and stained with the anti-bcl2 antibody and Hoechst 33342.

4.4 Discussion

4.4.1 Early Apoptosis

A brief inspection of figures 4.6 through 4.10 indicates that exposure to transient high levels of hydrodynamic force does not elicit a high level of apoptosis, if at all. Also the level of apoptosis peaks approximately 6 hours after the cells were pumped through the torture chamber. However there are some differences between the plots. Cells grown in suspension and in serum free media appear to be less susceptible to apoptosis than cells cultured anchorage dependent with serum containing media. As can be seen in figure 4.6 the WT CHO cells cultured with serum and are anchorage dependent

displayed some level of apoptosis at all of the EDR levels tested, whereas the WT CHO cells cultured in suspension and in serum free media only displayed low levels of apoptosis at the highest rates tested (figures 4.7 and 4.8). This data indicates that WT CHO cells adapted to grow in suspension and in serum free media are more robust, with respect to apoptosis, than cells cultured with serum and anchorage dependent. The cells over expressing the bcl-2 gene, regardless of the culture conditions, also only display low levels of apoptosis at the highest EDR levels tested (figures 4.9 and 4.10). The bcl-2 transfected CHO cells cultured in a bioreactor did have a decrease in bcl-2 expression, as seen in figure 4.21, which may explain the increase in early apoptosis, why this occurred at 12 hours instead of 6 hours is not readily explainable.)

4.4.2 Late apoptosis/necrosis

The late apoptosis/necrosis data from the WT CHO cells follows similar patterns of that of Ma *et al.* (2002), in that only the highest EDR tested (approximately 10^8 W/m³) produced a significant level of cell death. WT CHO cells cultured in suspension and in serum free media displayed trends regarding necrosis as the anchorage dependent WT CHO cells; there was not a significant level of necrosis at EDR levels below 10^8 W/m³. However, a higher percentage of WT CHO cells became necrotic at 10^8 W/m³, possibly indicating that the WT CHO cells cultured in suspension "skipped" apoptosis and died via necrosis instead. The bcl-2 transfected cells, on the other hand, did not display a similar trend – the bcl-2 transfected cells cultured in suspension and in serum free media appear to be less susceptible to necrosis than the cells cultured in tissue culture flasks and with serum containing media. Another unusual aspect of the necrosis data for the

bcl-2 CHO cultured in T-flasks cells is the necrosis "peaks" at 4 hours and then deceases. Earlier data, using propidium iodide (PI) as well as 7-AAD, indicated that the bcl-2 cells were more resistant to necrosis, although this data was only taken two hours after the cells were pumped through the contractional device (see figure 4.23).

4.4.3 Other Flow Cytometric and Fluorescence Microscopy Data

As can be seen from figure 4.17, the difference between the abused and the control cells is not statistically significant, which is counter intuitive since apoptotic cells have a lower reported level of mitochondrial activity (Shapiro, 2003; Cossarizza, 1994). These cells were also stained with Annexin V and 7-AAD, and there was no correlation found between the apoptotic cells and the relative fluorescence of Rhodamine 123.

Figures 4.18 through 4.20 indicate that the events located in the lower left portion of a Forward vs. side scatter dot plot are not nucleated (see figure 4.19), as indicated by the low level of Draq5 fluorescence and most of the remaining events on a forward and side scatter plot are nucleated (see figure 4.18), thus indicating that most of the events in the lower left potion of the forward vs. side scatter dot plot are not cells but debris. This assertion is further supported by the fact that the Draq5 "dim" population of figure 4.18 is also Rhodamine 123 "dim".

Figure 4.21 highlights the importance of maintaining selective pressure on the cells during adaptation to serum free media and suspension, since only 39% of the bcl-2 cells that were cultured in suspension and serum free media were expressing bcl-2, whereas 91% the bcl-2 cells that were cultured in T-flasks are expressing bcl-2.

Figures 4.22 A and B were created to determine where the bcl-2 is localized

in the cell. According to Arden and Betenbaugh (2004) and Harris and Thompson (2000) the bcl-2 gene product is localized only in the mitochondria and possibly nuclear envelop. It appears, that the bcl-2 gene product is expressed in more than just the mitochondria and the nuclear envelop. Fluorescence microscope pictures of the isotype control show very little fluorescence above the background, indicating that the red color seen in figures 4.22 A and B are anti-human bcl-2 – PE antibodies specifically bound to the bcl-2 gene product.

4.5 Conclusion

Fabricating certain microfluidic devices is a viable alternative to the photoresist method typically used; the data from the stainless steel contractional flow device is similar to the data produced using the thick photoresist and the stainless steel is more robust. Hydrodynamic stress is not a potent initiator of apoptosis, only low percentages of cells became apoptotic after a single pass through the contractional flow device. To measure the possible cumulative effects of stress, the same population of cells should be passed through the contractional flow device multiple times. The cells expressing the bcl-2 gene did have a lower level of apoptosis, and the wild type cells that were cultured in serum free media and in suspension also had a lower level of apoptosis. However, at high levels of stress ($> 10^8$ W/m³), the wild type cells cultured in serum free media and in suspension had higher levels of necrosis than the cells cultured in serum containing media.

Flow rate (mL/min)	median max. EDR (W/m^3)
10	2.87E+05
30	2.27E+06
50	6.45E+06
70	2.60E+07
90	1.09E+08

Table 4.1: Summary of median maximum particle EDR for each of the simulated flow Rates.

Figure 4.1: Photograph of the contractional device

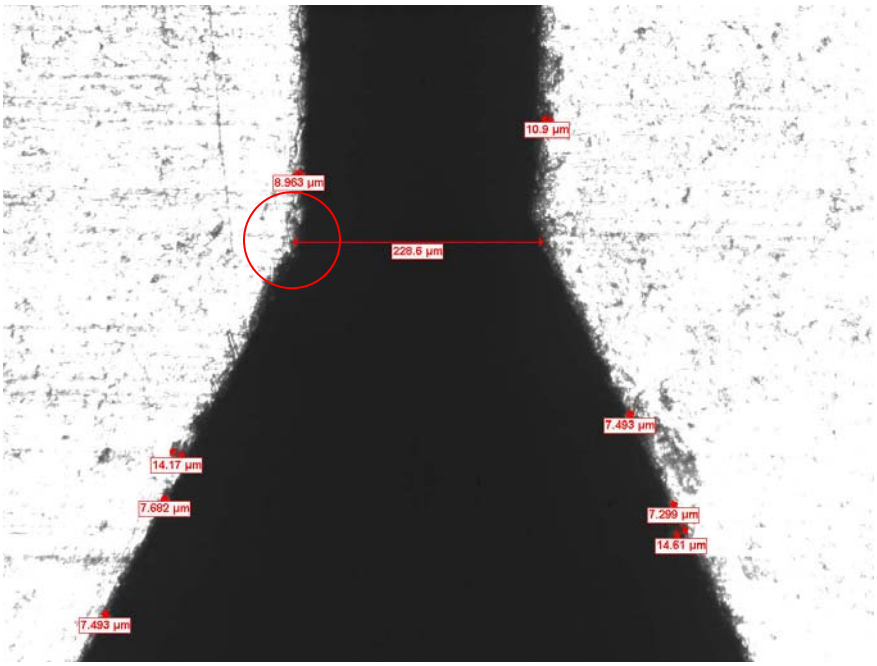

Figure 4.2: Microscope picture of the constricted region of the contractional device

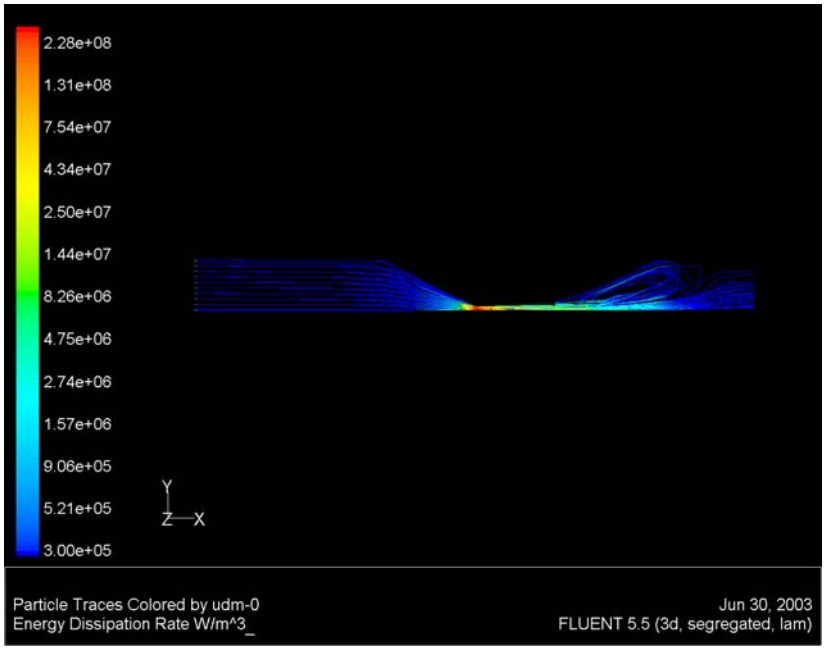

Figure 4.3: Representative particle tracks colored by EDR (in W/m³), from FLUENT simulation.

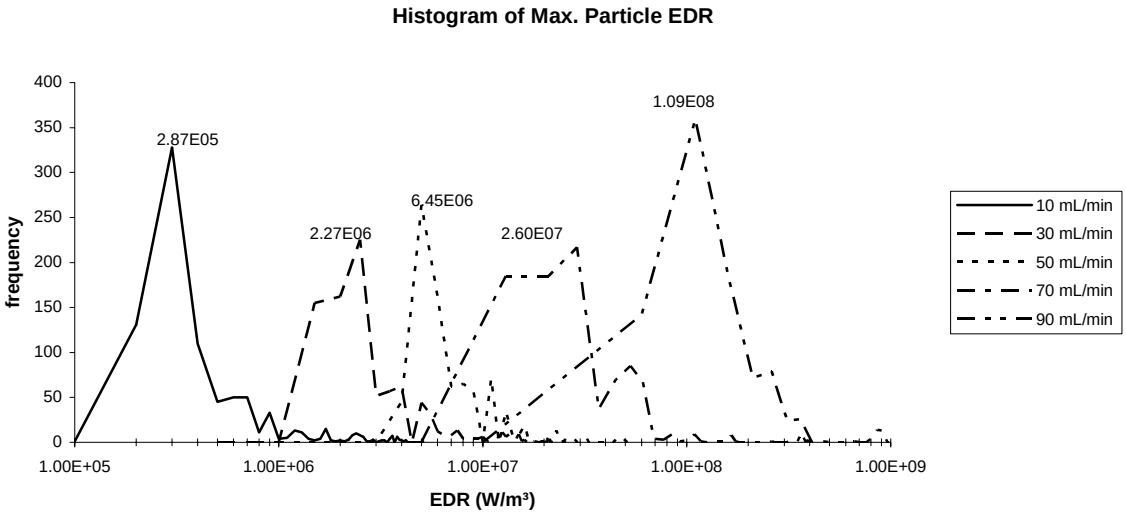

Figure 4.4: Histogram of simulated maximum EDR each particle received for every flow rate; median values are included.

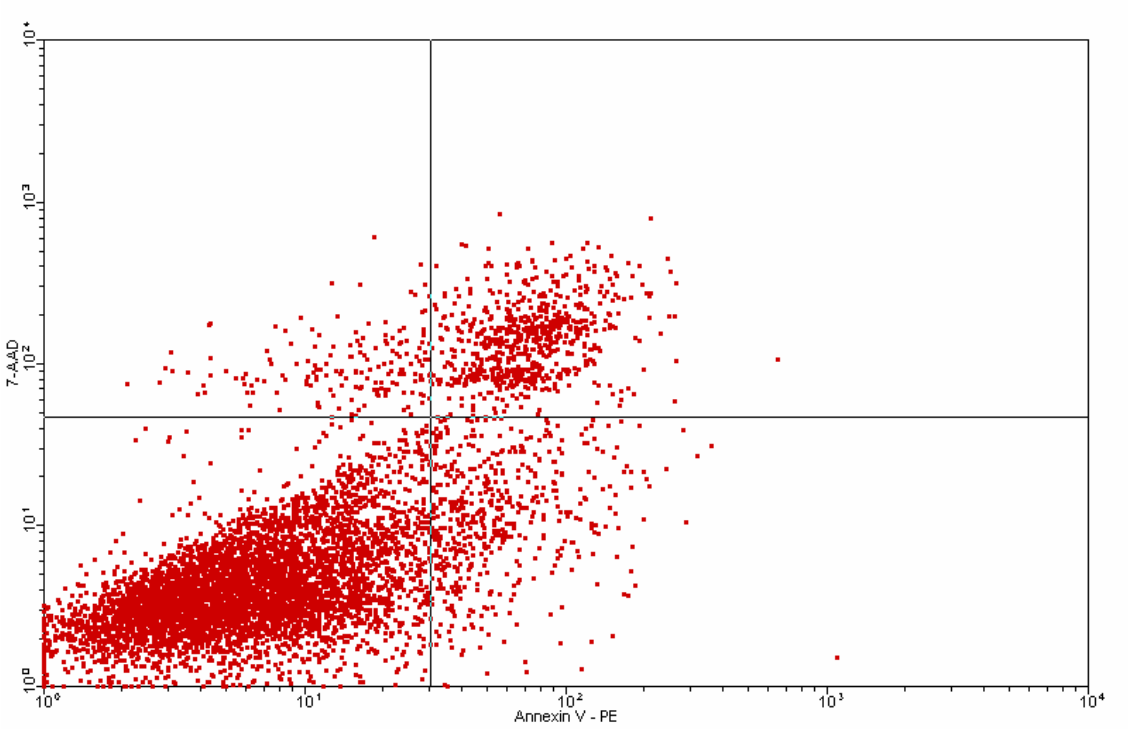

Figure 4.5: Representative dot plot of 7-AAD vs. AV-PE, from WT CHO-K1 cells cultured in T-flasks with 10% FBS, events in the lower left quadrant are healthy, events in the lower right quadrant are early apoptotic, and events in the upper right quadrant are late apoptotic or necrotic.

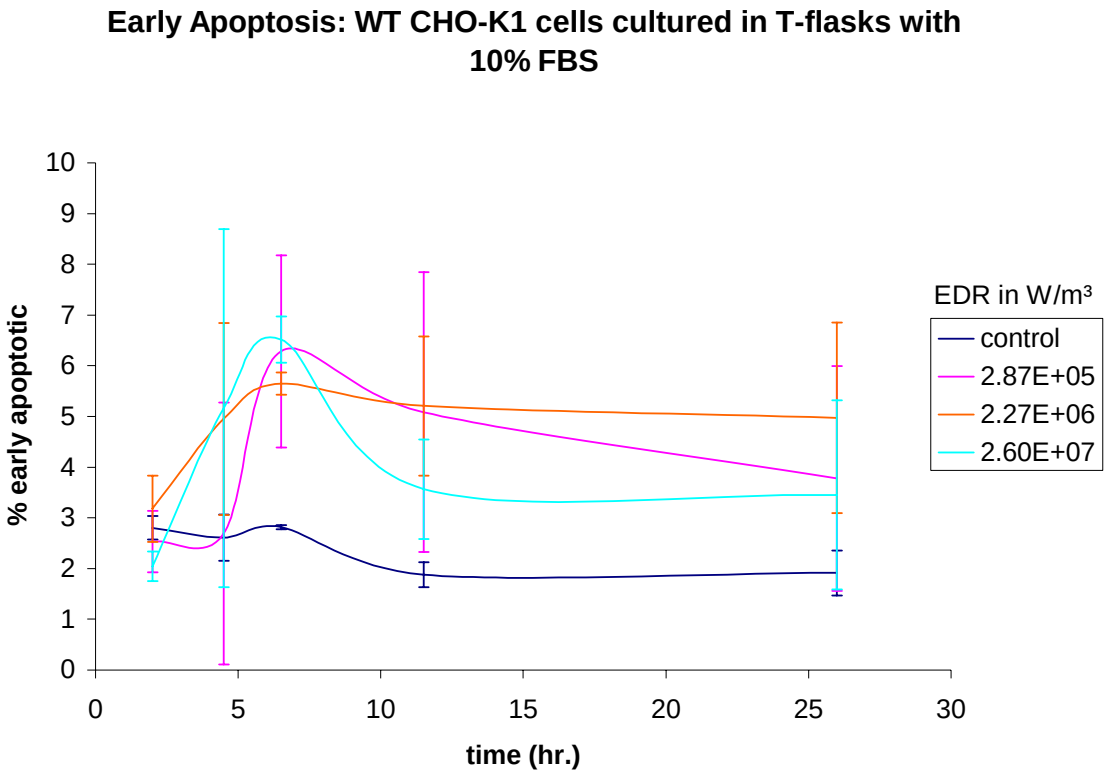

Figure 4.6: Early Apoptosis (lower right quadrant): WT CHO-K1 cells cultured in T-flasks with 10% FBS

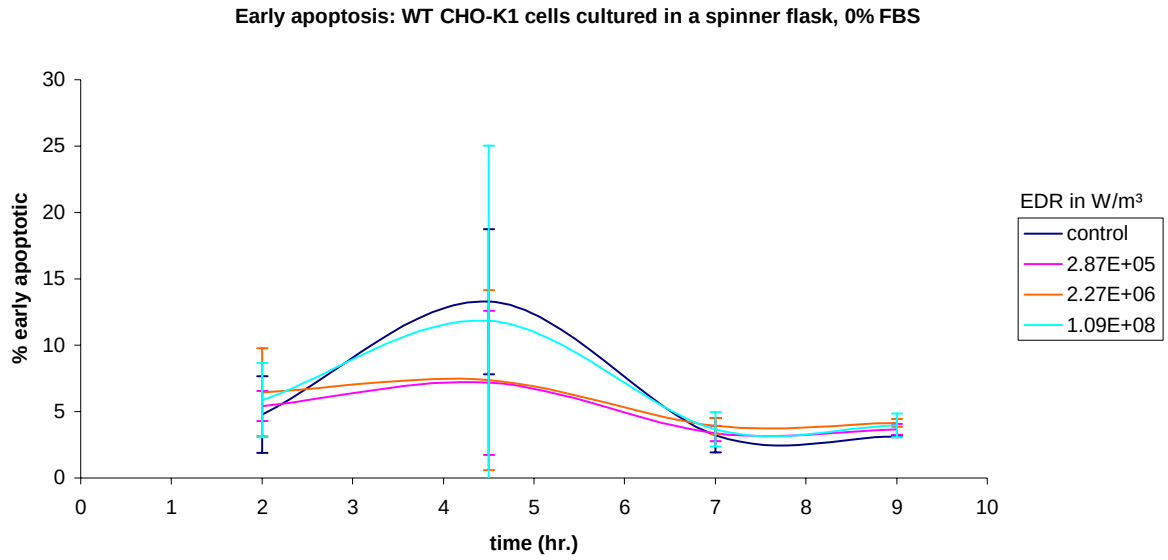

Figure 4.7: Early apoptosis (lower right quadrant): WT CHO-K1 cells cultured in a spinner flask, 0% FBS.

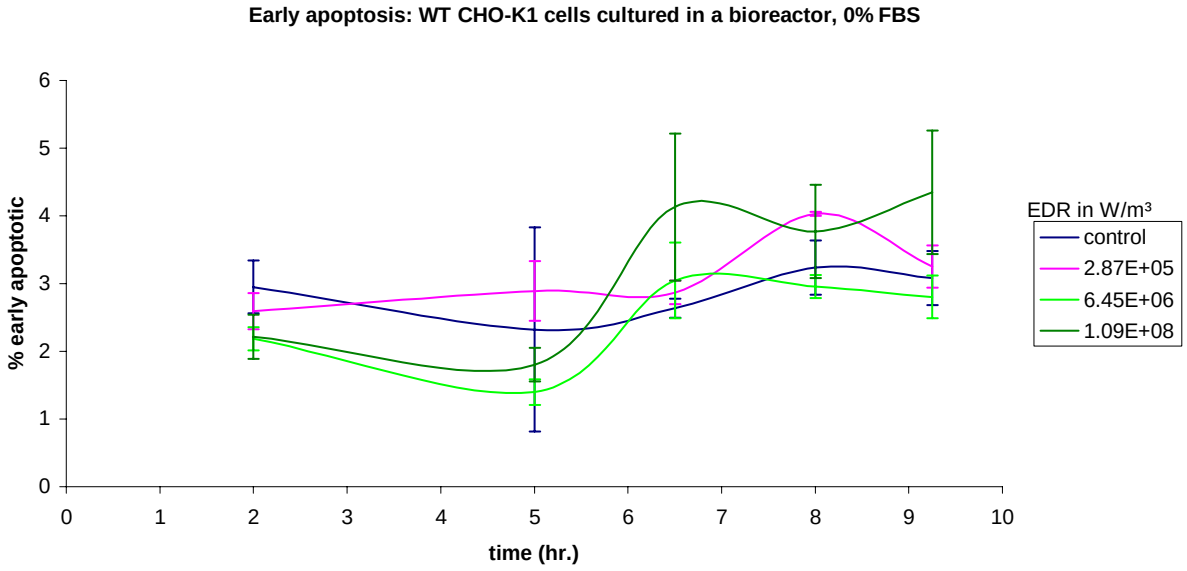

Figure 4.8: Early apoptosis (lower right quadrant): WT CHO-K1 cells cultured in a bioreactor, 0% FBS

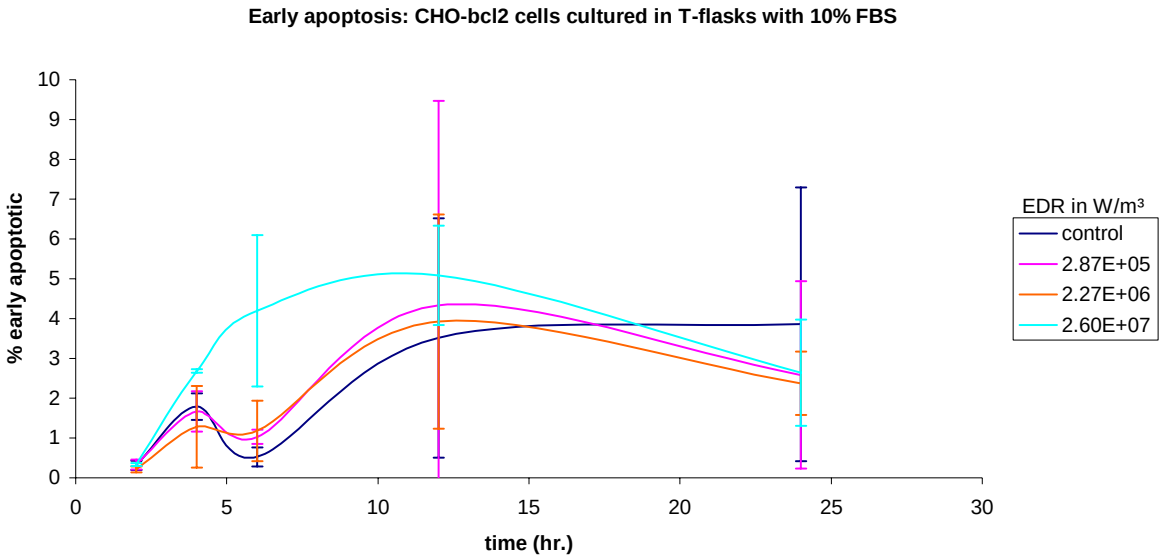

Figure 4.9: Early apoptosis (lower right quadrant): CHO-bcl2 cells cultured in T-flasks with 10% FBS

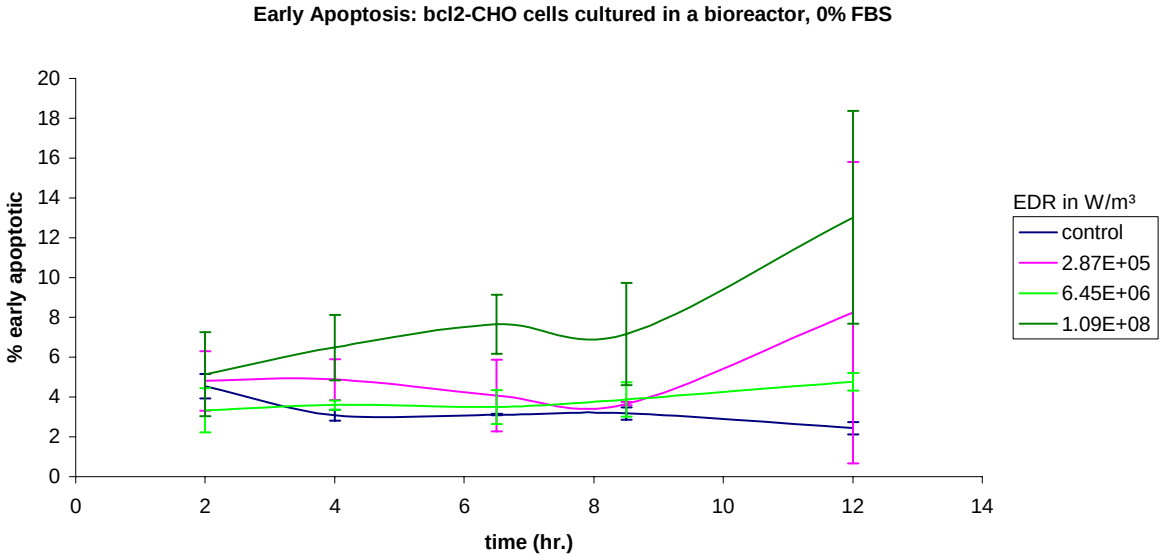

Figure 4.10: Early Apoptosis (lower right quadrant): bcl2-CHO cells cultured in a bioreactor, 0% FBS

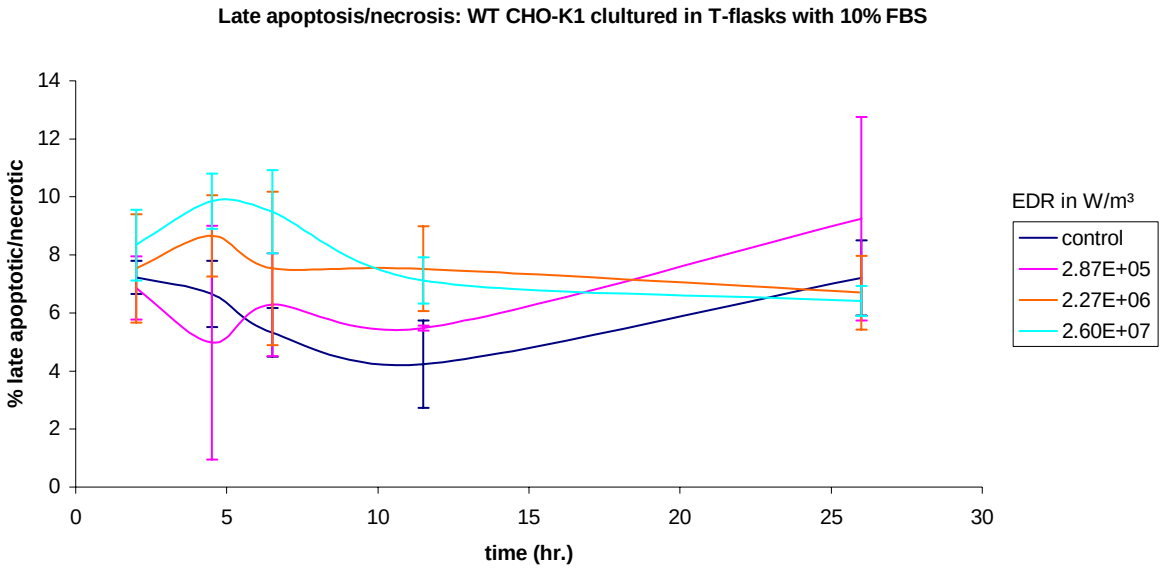

Figure 4.11: Late apoptosis/necrosis (upper right quadrant): WT CHO-K1 cultured in T-flasks with 10% FBS.

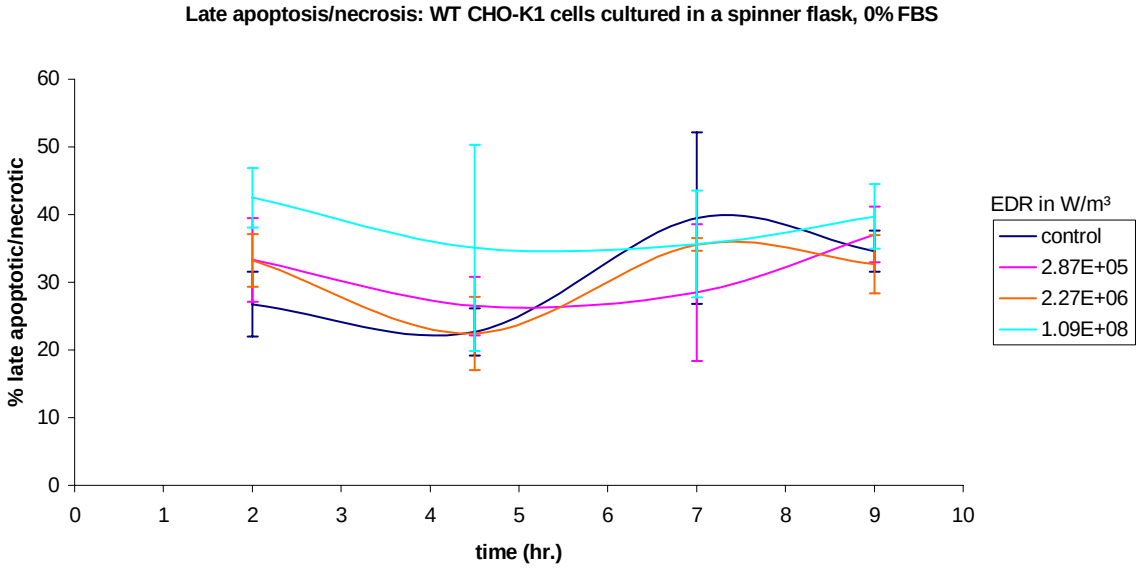

Figure 4.12: Late apoptosis/necrosis (lower right quadrant): WT CHO-K1 cells cultured in a bioreactor, 0% FBS.

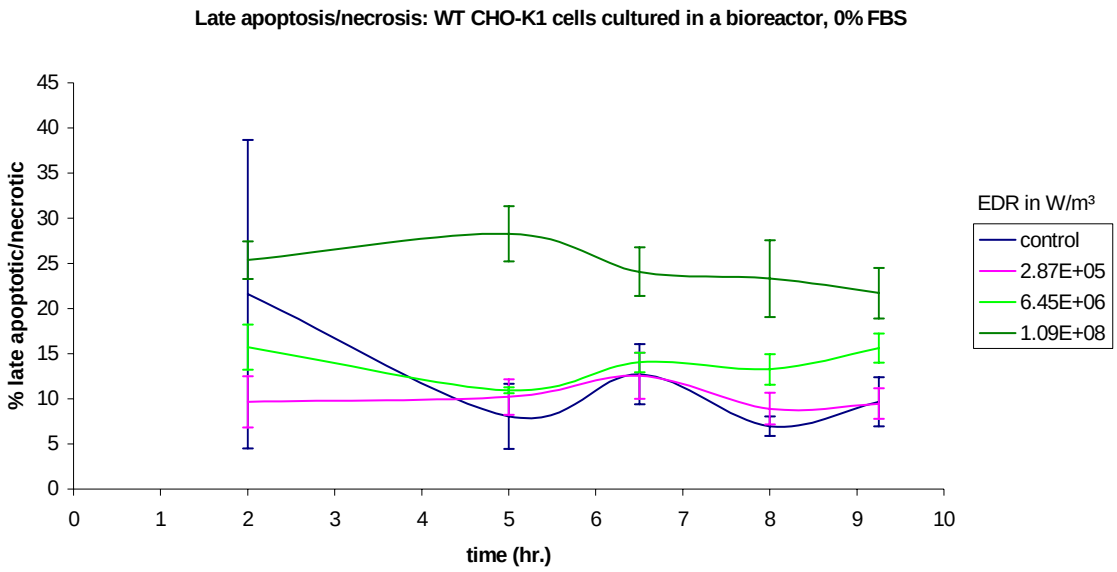

Figure 4.13: Late apoptosis/necrosis (lower right quadrant): WT CHO-K1 cells cultured in a bioreactor, 0% FBS.

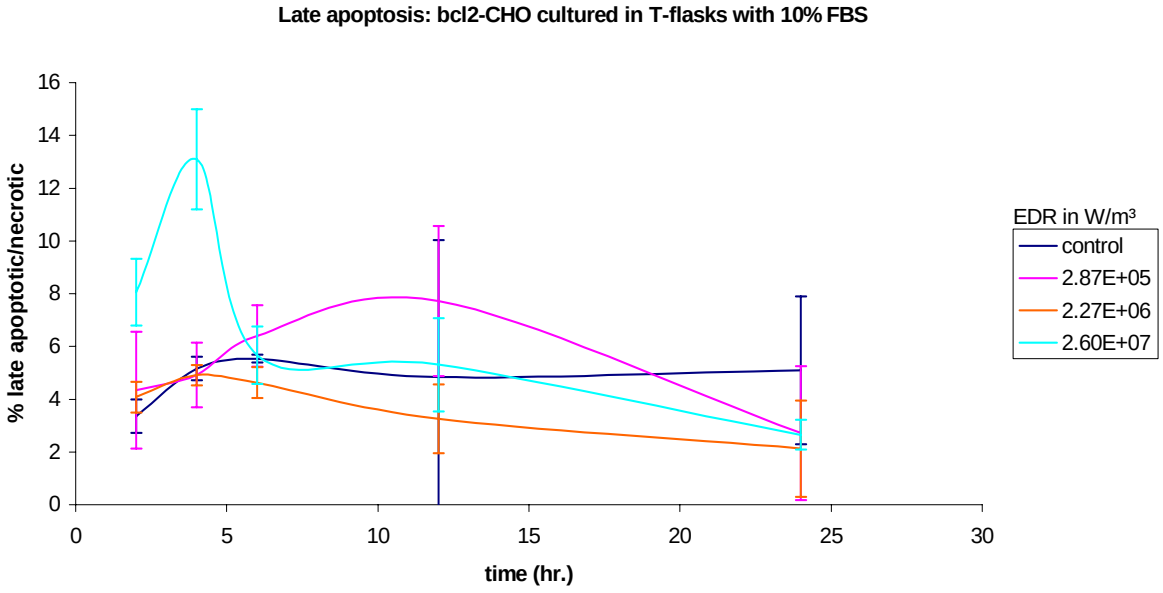

Figure 4.14: Late apoptosis/necrosis (lower right quadrant): bcl2-CHO cultured in T-flasks with 10% FBS.

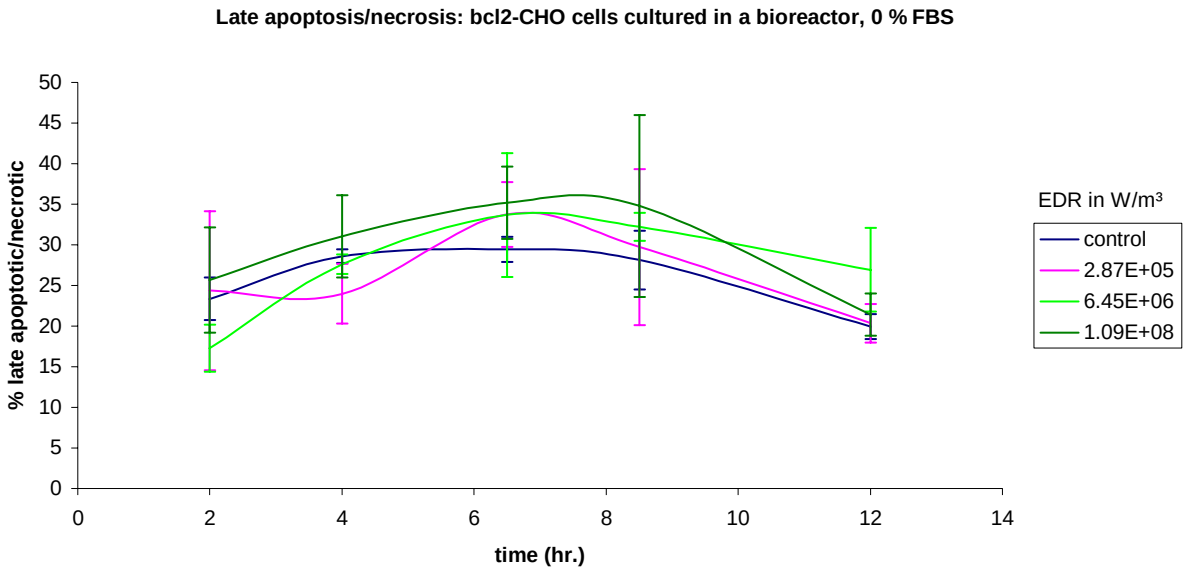

Figure 4.15: Late apoptosis/necrosis (lower right quadrant): bcl2-CHO cells cultured in a bioreactor, 0 % FBS.

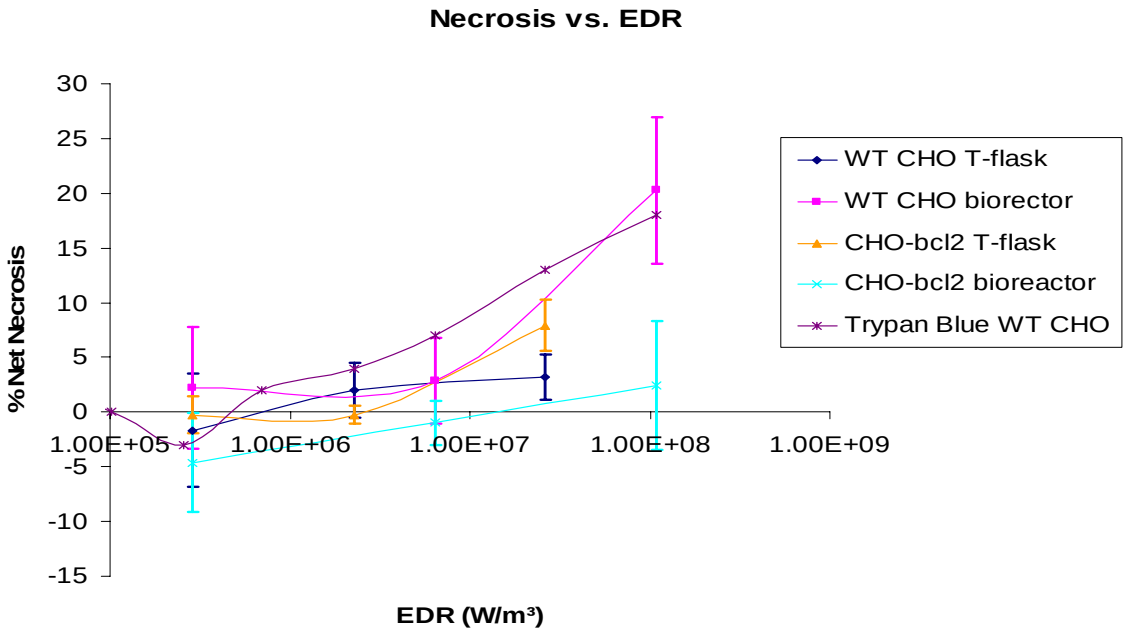

Figure 4.16: Summary of necrosis data, relative to each sample's corresponding control.

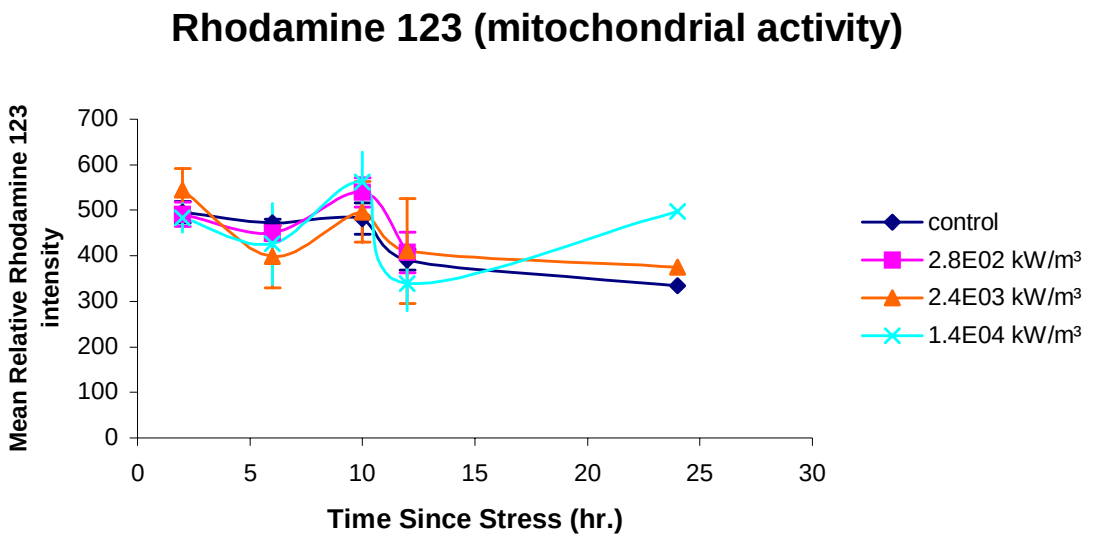

Figure 4.17: Relative median Rhodamine 123 fluorescence as a function of time for WT CHO-K1 cells cultured in spinner flasks with 0% FBS.

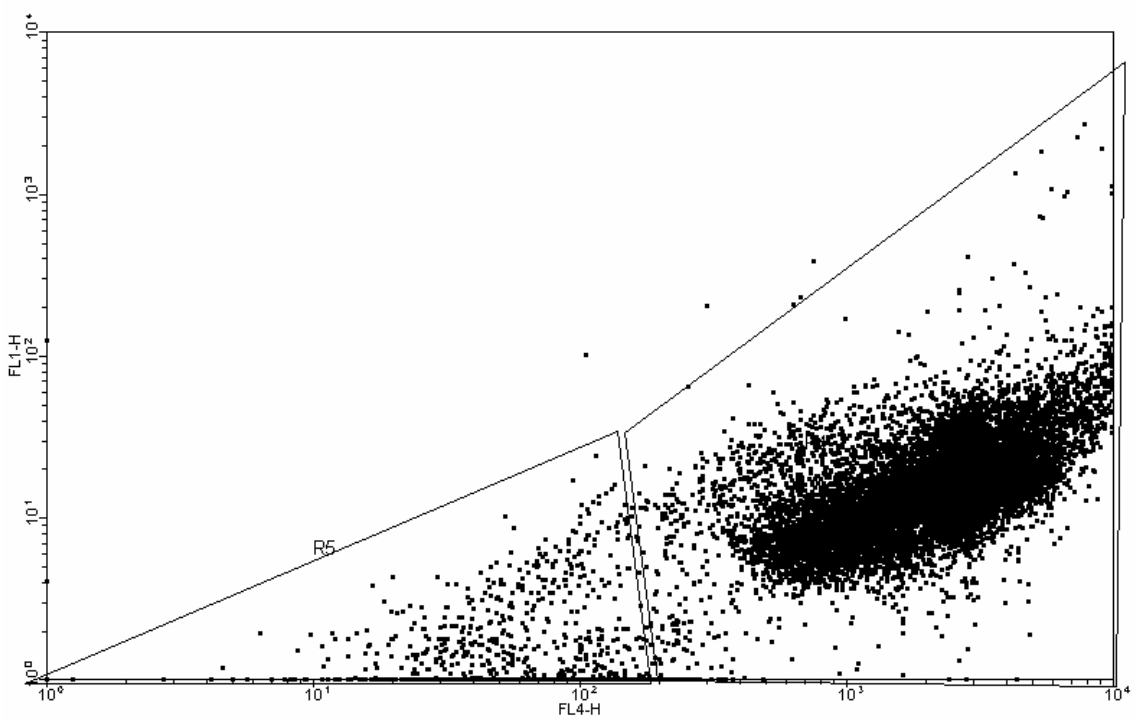

Figure 4.18: Rhodamine 123 fluorescence (FL1-H) vs. Draq5 fluorescence (FL4-H), for the WT CHO-K1 cells cultured in serum free media and in suspension in a 250 mL spinner flask.

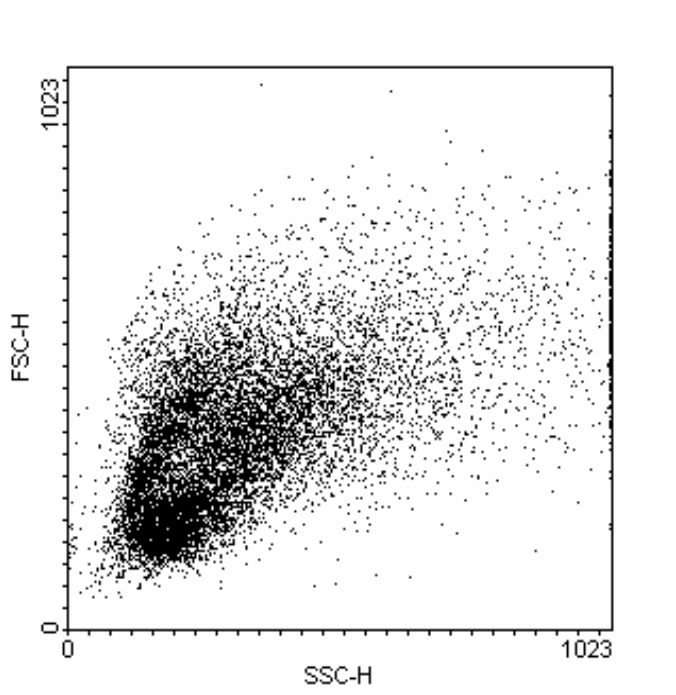

Figure 4.19: Forward vs. Side scatter dot plot of the events in the Draq5 "bright" gating region of figure 4.18.

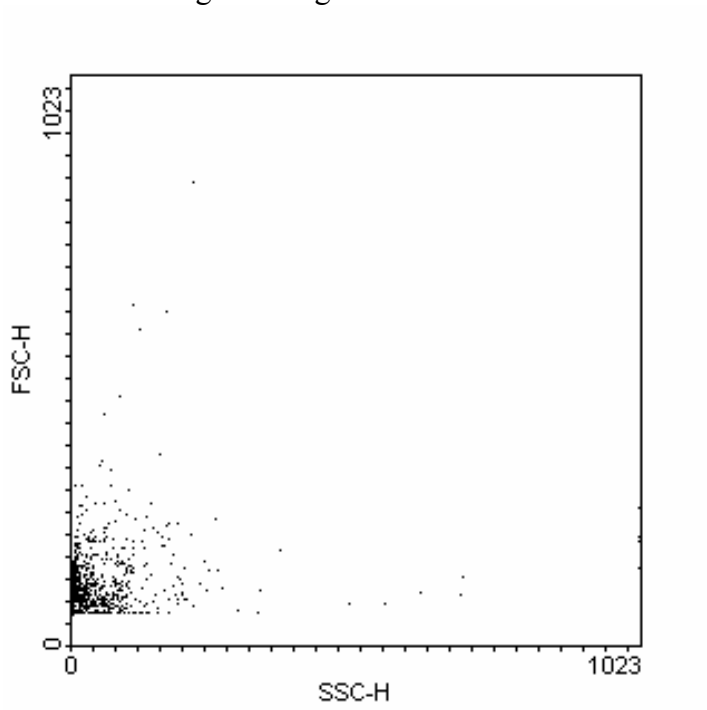

Figure 4.20: Forward vs. Side scatter dot plot of the events in the Draq5 "dim" gating region of figure 4.18

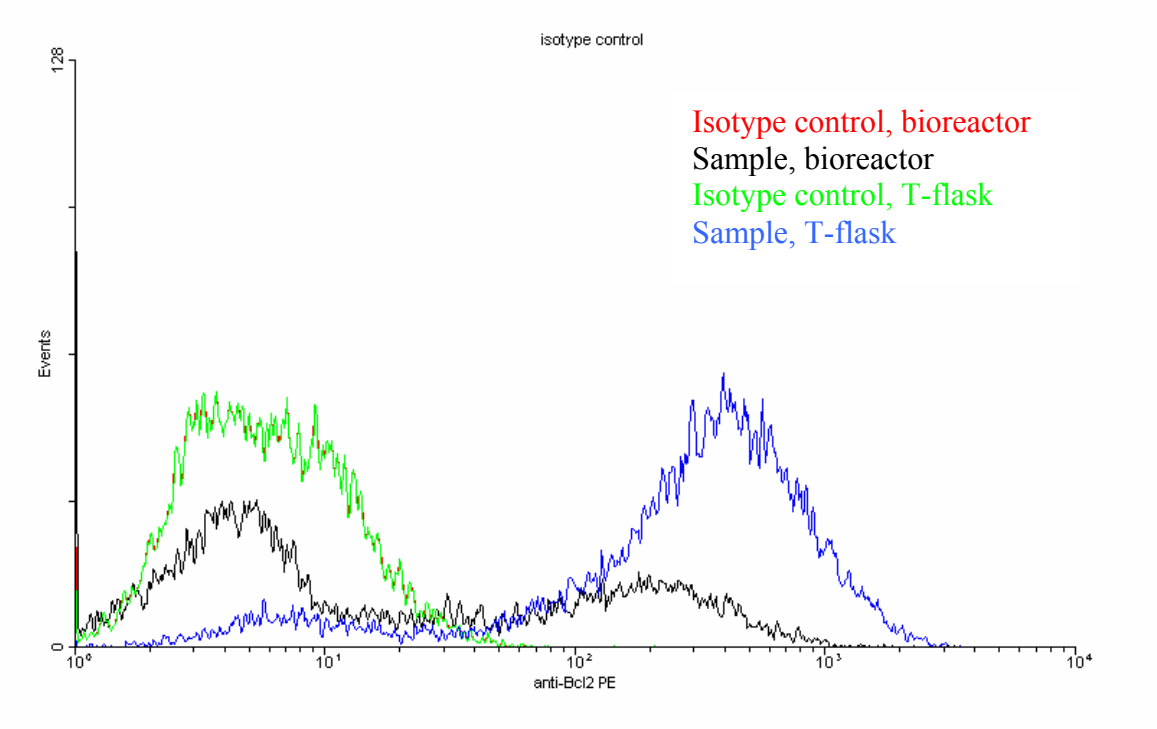

Figure 4.21: Histogram overlays of bcl2 over expressing cells stained with an anti-human bcl2 antibody conjugated to PE.

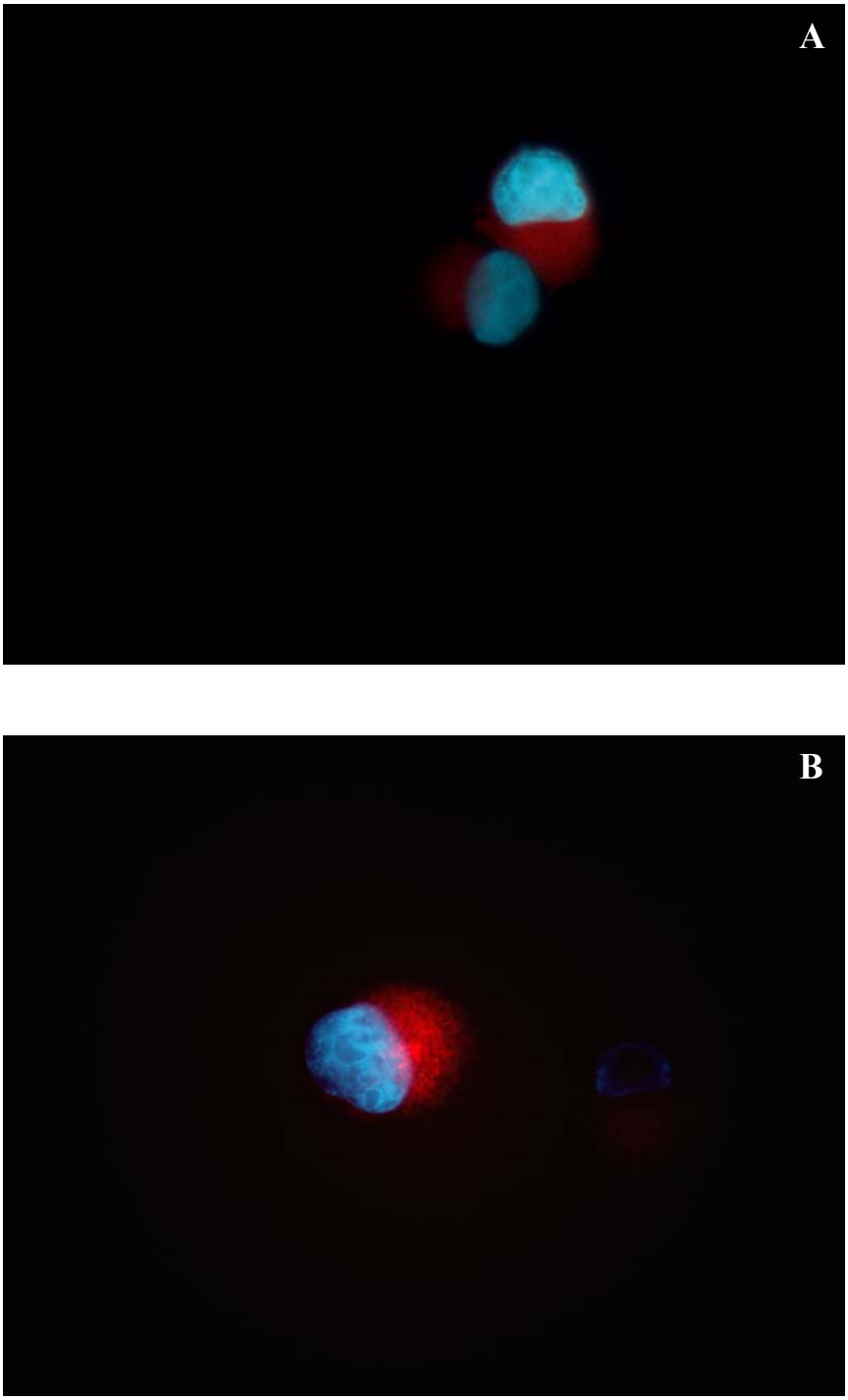

Figure 4.22 (A and B): Fluorescent Microscope pictures, taken at 100X, of bcl-2 expressing cells, red color is the anti-bcl-2 PE antibody, and the blue is the Hoechst 33342 nuclear stain.

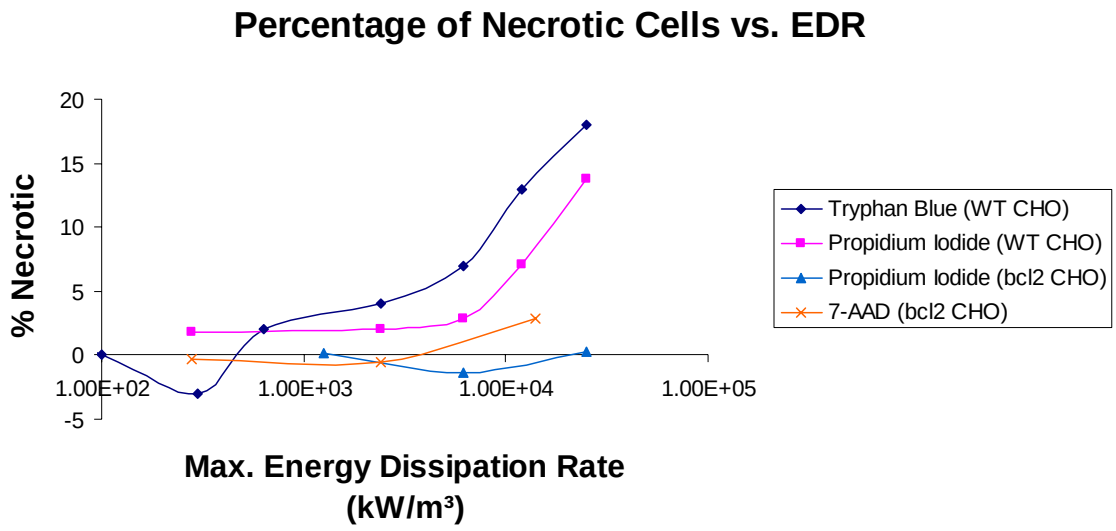

Figure 4.23: Percentage of necrotic WT and bcl2 expressing CHO cells, as a function of EDR (in kW/m³). Data recorded shortly after cells' passage through the contractional flow device.

Chapter 5

Cell Damage in FACS Instruments

5.1 Introduction

Fluorescence activated cell sorting (FACS) is a widely used method to sort subpopulations of cells rapidly and at high purities. FACS is an integral part of many biological and medical research projects as well as in cell line development at biotechnology and pharmaceutical companies. However, there is very little information available in the literature regarding cell death in FACS devices as a result of hydrodynamic forces. One of the few studies on the subject of cell damage in FACS instruments discovered a significant increase in necrosis and apoptosis in BT474 tumor cells after FACS (Seidl *et al.,* 1999).

In general, there are two primary pathways for cell death: necrosis and apoptosis. Necrosis is passive cell death or "cell murder"; some external factor causes the cell to die (Darzynkiewicz, *et al.*, 1997). Typically, when cells die via necrosis their membrane swells, and eventually the cell membrane ruptures. Apoptosis, on the other hand, is programmed cell death or "cell suicide"; cells undergo a series of events, which ultimately lead to the cells' demise. For non-receptor mediated apoptosis, cytochrome C is released from the mitochondria, which initiates the caspase cascade and

phosphatidylserine translocates from the interior of the cell membrane to the exterior. The caspase cascade ultimately initiates endonuclease activity within the nuclease and the enzymatic degradation of the cytoskeleton. Eventually the cell membrane starts to form bulges or "blebs", these blebs break away from the membrane forming apoptotic bodies containing intact organelles and small pieces of DNA, approximately 180 bp long (Cotter and Al-Rubeai, 1995).

Apoptosis can be initiated by events such as radiation, toxins, hypoxia, and nutrient starvation (Fussenegger and Bailey, 1998; Cotter and Al-Rubeai, 1995). Several researchers have noted that hydrodynamic force can initiate apoptosis (Al-Rubeai *et al.*, 1995; Perani *et al.*, 1998; Graf *et al.*, 2003). One commonly used parameter to represent hydrodynamic force is shear stress. Shear stresses arise from shear flows, which are one half rotational and one half extensional (Aris, 1962; Brodkey, 1967). Due to the non-zero vorticity in shear flows, cells rotate; because of this no one point along the cell-water interface experienced the maximum strain for very long. Regarding suspended cells, for pure extensional flows it is possible for a relatively large amount of strain to occur at one point on a cell, whereas for pure shear flow the cells can rotate away from the principle straining direction (Gregordias, *et al.*, 2000). Another parameter used to represent hydrodynamic force is the energy dissipation rate (EDR). The energy dissipation rate represents the rate at which work is done on a fluid element or, for this research, a cell (Clay, 1997). Bird *et al.* (1960) defined the energy dissipation rate as the irreversible rate of internal energy increase per unit volume. The energy dissipation rate accounts for both shear and extensional components of the flow; therefore regardless of the type of flow cells encounter the energy dissipation rate can be used as a predictor of cell

damage. For an incompressible, Newtonian fluid, the following equation can be used to determine the EDR (ε):

$$\varepsilon = \mu[\nabla U + (\nabla U)^T] : \nabla U \tag{1}$$

where μ is the dynamic viscosity, U is the velocity vector, ∇U is the velocity gradient tensor, and $(\nabla U)^T$ is the transpose of ∇U. Equation (1) is valid for any flow regime (i.e. laminar, transient or fully turbulent). The velocity gradient tensor, in Cartesian coordinates, is defined as:

$$\nabla U = \begin{bmatrix} \frac{\partial U_x}{\partial x} & \frac{\partial U_y}{\partial x} & \frac{\partial U_z}{\partial x} \\ \frac{\partial U_x}{\partial y} & \frac{\partial U_y}{\partial y} & \frac{\partial U_z}{\partial y} \\ \frac{\partial U_x}{\partial z} & \frac{\partial U_y}{\partial z} & \frac{\partial U_z}{\partial z} \end{bmatrix} \tag{2}$$

where U_x, U_y, and U_z are the x, y, and z velocity components, respectively. The second order tensor scalar product, also known as the double dot product, is defined in this case as:

$$[\nabla U + (\nabla U)^T] : \nabla U = \sum_i \sum_j [\nabla U + (\nabla U)^T]_{ij} \nabla U_{ji} \tag{3}$$

As can be seen by the above equations, once the velocity vectors are determined, the energy dissipation rate can be calculated. There are a variety of methods to determine velocity vectors. In laminar flow systems with simple geometries, the velocity vectors can be determined analytically from the momentum balance equation (Bird *et al.*,

1960). Examples of such systems are pipe flow and annular flow. For a more complete explanation of how to calculate the EDR see Mollet *et al.* (2004) or chapter 3. Most systems, however, are too complex to use either of the aforementioned analytical methods; therefore the flow is simulated using computational fluid dynamics software (CFD). The velocity vectors calculated from CFD in a laminar flow system are generally accepted, in turbulent systems; however the results are not as well received (Ma *et al.*, 2004b). FACS instruments operate within the laminar flow regime.

The EDR is well suited to describe the hydrodynamic conditions in FACS devices, because the cells are in suspension and the cells are forced through a nozzle, which creates nearly extensional flow. Also, under normal operating conditions, the suspended cells in a FACS instrument are not in contact with the wall of the nozzle, thereby reducing the shear component of the flow the cells experience.

Ma *et al.* (2002) developed a micro-fluidic contractional flow device to determine the maximum amount of energy dissipation cells can withstand before the onset of necrosis. The channel resembles a flattened hourglass (see figure 4.1). Ma *et al*. (2002) utilized FLUENT, a commercial CFD program, to simulate the velocity vectors at various volumetric flow rates. The local energy dissipation rate is then determined using equation 1. Cell suspensions were pumped through the channel at the flow rates tested in FLUENT and the cell viability was determined using a lactate dehydrogenase (LDH) assay. Ma *et al.* (2002) performed several experiments on CHO, HB-24, SF-9 and MCF-7 cell lines, and found that the cells can withstand high levels of energy dissipation, approximately 10^4-10^5 kW/m³ (or 10^7-10^8 W/m³). Using a similar microfluidic contractional flow device, the percentage of apoptotic and necrotic CHO cells were

determined using an Annexin V flow cytometric assay as well as microscopy assays (see chapter 4). The data in chapter 4 for anchorage dependent, wild type (WT) CHO cells cultured with 10% FBS showed low levels of apoptosis at 3×10^5 W/m³, whereas WT and bcl-2 transfected CHO cells cultured in suspension do not display even low levels of apoptosis until 1×10^8 W/m³.

Most FACS instruments operate by forcing suspended cells to flow in a relatively single file line where the cells are interrogated by a laser. The cells are forced into a single file line via hydrodynamic focusing, where the cell suspension is injected into flowing sheath fluid (see figure 2.2). Changing the air pressure in the sheath tank controls the flow rate of the sheath fluid. The sheath pressure reading on the instrument is actually the air pressure in the sheath tank, and is not easily correlated to the sheath fluid pressure at the nozzle due to the various constrictions in the sheath tubing (e.g. the sheath fluid filter, compression fittings, valves, etc.). The sample flow rate is controlled by altering the air pressure within the sample test tube, via the sample differential pressure. The sample differential is the amount of pressure above the sheath pressure, for example a sample differential of 0.5 psi and a sheath pressure of 25 psi would mean there is 25.5 psi of pressure over the cell suspension in the tube. Figures 5.1 A through C detail the fluidic system of a FACS instrument. Flow cytometer analyzers (e.g. FACS Calibur) operate similarly; the sheath tank and the sample tube are pressurized, forcing fluid through a focusing nozzle. Most flow cytometer analyzers, however, operate under much lower sheath pressures, typically 31 kPa or 4.5 psi, and the exit orifice is much larger, typically 430 × 180 μm (Graves, *et al*., 2002), therefore the EDR cells experience in these systems is most likely not very large.

5.2 Materials and Methods

5.2.1 CFD Simulations

The dimensions of a nozzle, also called a flow cell, from a Becton-Dickinson (BD) FACS Vantage SE were determined using a micrometer as well as diagrams obtained from BD. The dimensions were entered into Gambit, the preprocessor included with FLUENT, to create the geometry and mesh of node points of the flow cell (nozzle). A trigonal, unstructured mesh with 182,000 node points was used to model the flow through the flow cell. Due to the axial symmetry of the nozzle, only half of a two dimensional nozzle was simulated in axi-symmetric mode (see figures 5.2 A and B). The white area in Figure 5.2A is the wall of the stainless steel sample capillary. Two different nozzle diameters were used, 70 and 100 μm. The geometry and mesh were imported into FLUENT, and the sheath and sample inlet velocities, at various sheath and sample differential pressures, were entered into FLUENT as well. The sheath velocities were determined earlier by measuring the volumetric flow rate, at various sheath pressures, of the sheath fluid flowing out of the nozzle while the fluidics control knob was set to standby. The sample inlet velocity was determined by calculating the sample uptake rate, at various sample differential and sheath pressures, at the sample injection port (SIP). Figures 5.3-5.5 summarize the sample and sheath flow rate data. After FLUENT converged on a solution for each condition, a user-defined function was implemented to determine the EDR at every node point, using equation 1 (see Appendix A). A particle tracking technique was employed to determine the maximum EDR cells encounter in the

nozzle (see appendices B and C). Two hundred 10 μm diameter particles were released from the inlet of the sample tube and tracked through the entire geometry. The maximum EDR each particle experienced in the nozzle was exported to Excel for analysis.

5.2.2 FACS Experiment

Wild type (WT) CHO-K1 cells were adapted to grow in serum free media by gradually reducing the serum concentration in Gibco's (Carlsbad, CA) CD CHO-A serum free media. The WT CHO cells were cultured in T-75 flasks and harvested via trypsinization. Six samples of approximately 2.5×10^6 cells, suspended in 250 μL of CD CHO A media (each sample had 1.0×10^7 cells/mL) were sorted using a BD FACS Vantage SE with a 100 μm nozzle and a sheath pressure of 17 psi. Three of the samples were sorted with a sample differential pressure of 0.5 psi, and the remaining three were sorted with a sample differential pressure of 1.5 psi. Two samples containing cells at the same concentration were used as controls. The cells were collected in polypropylene 12×75 mm tube with 1 mL of CD CHO A media initially. After sorting, the cells were centrifuged at 250 × g for 7 minutes, and then resuspended in 20 mL of CD CHO-A media. While the cells were being sorted, a separate population of the same cell type was passed through the contractional flow device as described in chapter 4. The contractional flow device was operated such that three samples received a maximum EDR of 2.6×10^7 W/m³ and three samples received a maximum EDR of 1.1×10^8 W/m³.

All of the cell suspensions were placed in a 37ºC incubator-shaker. Approximately every two hours, 2 mL aliquots (5×10^5 cells) were removed from each cell suspension; the cells were washed twice in PBS and resuspended in 0.5 mL of 1X Annexin V binding buffer. A 100 μL aliquot was taken from each of the washed cell suspensions. The cells in this aliquot were stained with 5 μL of Annexin V-PE and 5 μL of 7-AAD; both reagents are from BD Biosciences (San Jose, CA). The cells were then analyzed using a BD FACS Calibur. The appropriate single color controls were produced earlier using heat-shocked cells – cells exposed to a 42ºC water bath for 45 minutes.

5.3 Results

5.3.1 CFD simulations

The results of the CFD simulations and particle tracking are summarized in table 5.2. Figure 5.6 is an example of the particle tracking data, after the Perl program determined the maximum EDR each particle encountered. Figure 5.7 is a contour plot of the particles as they approach the 70 μm diameter nozzle outlet. The results of the simulation appear to be consistent with the available literature, namely the diameter of the core stream determined from FLUENT is close to the diameter predicted by Pinkel and Stoval (1985). Pinkel and Stoval (1985) developed equation 4 based using mass balance equations to approximate the core stream diameter.

$$d = 1130 \times \sqrt{\frac{q}{v}} \tag{4}$$

Where d is the core stream diameter (in μm), q is the volumetric flow rate (in mL/s), and v is the exit velocity (in m/s). Table 3 is a summary of the core stream diameters calculated by FLUENT and the some of the core streams calculated using equation 4.

5.3.2 FACS Experiment

Figure 5.6 is a typical dot plot of 7-AAD relative fluorescence versus Annexin V-PE relative fluorescence; the events on this plot were gated based on a region of the forward versus side scatter plot that would exclude debris. Events in the lower left quadrant are negative for both 7-AAD and Annexin V-PE and are considered healthy cells. Events in the lower right hand quadrant positive for AV binding and are considered in the early stages of apoptosis because they are expressing PS on the exterior. Events in the upper right quadrants are positive for 7-AAD and are considered necrotic or late apoptotic; these cells have a compromised cell membrane and are no longer viable. Unfortunately, one cannot determine how these cells died, because cells with a compromised membrane may also have AV binding the PS on interior of the cell membrane. Due to the time scale of apoptosis (typically hours), events detected in the upper quadrants shortly after sorting are most likely necrotic not late apoptotic. Figure 5.8 is a plot of the mean percentage of cells in the lower right quadrant (early apoptosis) versus the amount of time that has past since being sorted or pumped through the contractional flow device. Figure 5.9 is a plot of the mean percentage of cells in the upper right hand quadrant (late apoptosis/necrosis). The error bars in both figures represent one standard deviation above and below the mean.

5.4 Discussion

5.5.1 CFD Simulations

The data from the CFD simulations indicate that the FACS Vantage is quite likely to damage cells. The high level of EDR calculated in the FACS Vantage nozzle was found to cause apoptosis and necrosis in various cell lines (see chapter 4 and Ma *et al*., 2002). The design of the nozzle is partly responsible for the high EDR values; the abrupt constriction at the exit of the nozzle causes large changes in the velocity gradient, which results in high EDR values. Also, the CFD simulation results follow Pinkel and Stovel's (1985) heuristic regarding the relationship between the core stream diameter and the sample volumetric flow rate in that increasing the volumetric flow rate by a factor of four increases the core stream diameter by a factor of two.

5.5.2 FACS Experiment

As can be seen in figure 5.8, FACS does not cause significant levels of apoptosis in the cell investigated in this study. Necrosis, however, is significant at both sorting conditions tested, as can be seen in figure 5.9. Seidl *et al.* (1999) found significant levels of both necrosis and apoptosis after FACS. One possible explanation for the reduced levels of apoptosis in this study is that the cells used were cultured in serum free media, which some have found to make the cells less robust (Castilho and Anspach, 2003). This observation indicates that instead of the cells sustaining an injury and then becoming apoptotic, the cells died immediately via necrosis. The cells in this study were

cultured in serum free media to eliminate the possibility of the cells dying during the sort due to a lack of serum. A common practice among FACS operators (Trotter, 2003; Atzberger, 2000) is to add media containing a large percentage of serum (usually 20%) to the collection tube, in an effort to improve the viability of the cells after sorting.

5.5 Conclusion

The results, overall, indicate that the FACS Vantage is causing significant levels of cell death to hydrodynamic forces. Since engineering the cells to become more robust would be impractical to the users of this instrument, a better designed flow nozzle would most likely alleviate the problems associated with cell loss due to hydrodynamic forces. More specifically an elongated nozzle with a less abrupt constriction would greatly reduce the velocity gradients just prior to the exit and thereby reduce the EDR in the exit region. Also, an elongated nozzle would reduce the onset of turbulence in the nozzle, because the fluid velocity would decrease as well as the incidence of boundary layer separations, which cause vortices. Reducing turbulence and vortices allow for higher, more stable sort rates. More studies are required with different cell lines and flow conditions to validate the occurrence of cell damage resulting from FACS sorting. Possible future work regarding this portion of the study would be to investigate other cell lines, the effect of serum has on the cells in the collection tube, and to use a LDH assay to determine the number of cells ruptured during the sorting process.

nozzle diameter (μm)	Sheath pressure (psi)	sample differential (psi)	max. EDR (W/m^3)
100	8	1.0	9.69E+06
100	8	2.0	1.76E+07
100	17	0.5	1.98E+08
100	17	1.0	1.00E+07
100	17	1.5	1.14E+07
100	17	2.0	2.18E+07
100	25	0.5	1.98E+08
100	25	1.0	4.08E+07
100	25	1.5	1.69E+07
100	25	2.0	1.86E+07
100	35	0.5	5.74E+08
100	35	1.0	5.58E+07
100	35	1.5	3.74E+07
100	35	2.0	2.20E+07
100	45	0.5	7.16E+08
100	45	1.0	1.34E+08
100	45	1.5	2.58E+07
100	45	2.0	4.68E+07

Table 5.1: Summary of maximum EDR produced in a 100 μm diamter FACS nozzle.

nozzle diameter (μm)	Sheath pressure (psi)	sample differential (psi)	max. EDR (W/m^3)
70	8	1.0	4.54E+06
70	8	1.5	1.16E+07
70	8	2.0	8.07E+06
70	17	0.5	2.86E+08
70	17	1.0	1.55E+07
70	17	1.5	1.83E+07
70	17	2.0	1.56E+07
70	25	0.5	5.97E+08
70	25	1.0	2.61E+07
70	25	1.5	1.83E+07
70	25	2.0	5.16E+07
70	35	1.0	4.26E+07
70	35	1.5	2.08E+07
70	35	2.0	4.03E+07

Table 5.2: Summary of maximum EDR produced in a 70 μm diameter FACS nozzle.

nozzle diameter (μm)	sheath pressure (psi)	sample diff (psi)	FLUENT core radius (μm)	Equation 4 core radius (μm)
70	8	1	15.1	17.7
70	8	1.5	16.4	
70	8	2	24.3	
70	17	1	10.7	
70	17	1.5	14.9	
70	17	2	17.2	
70	25	0.5	2.6	4.1
70	25	1	8.5	
70	25	1.5	15.0	17.4
70	35	1	5.7	
70	35	1.5	14.4	
70	35	2	16.0	
100	8	1	10.0	11.8
100	8	2	18.4	
100	17	1	10.7	
100	17	1.5	14.9	16.0
100	17	2	17.2	
100	25	1.5	18.6	
100	25	2	22.0	
100	35	0.5	3.8	3.2
100	35	1	5.7	
100	35	1.5	14.4	
100	35	2	16.0	

Table 5.3: FACS core stream diameters determined analytically and from FLUENT.

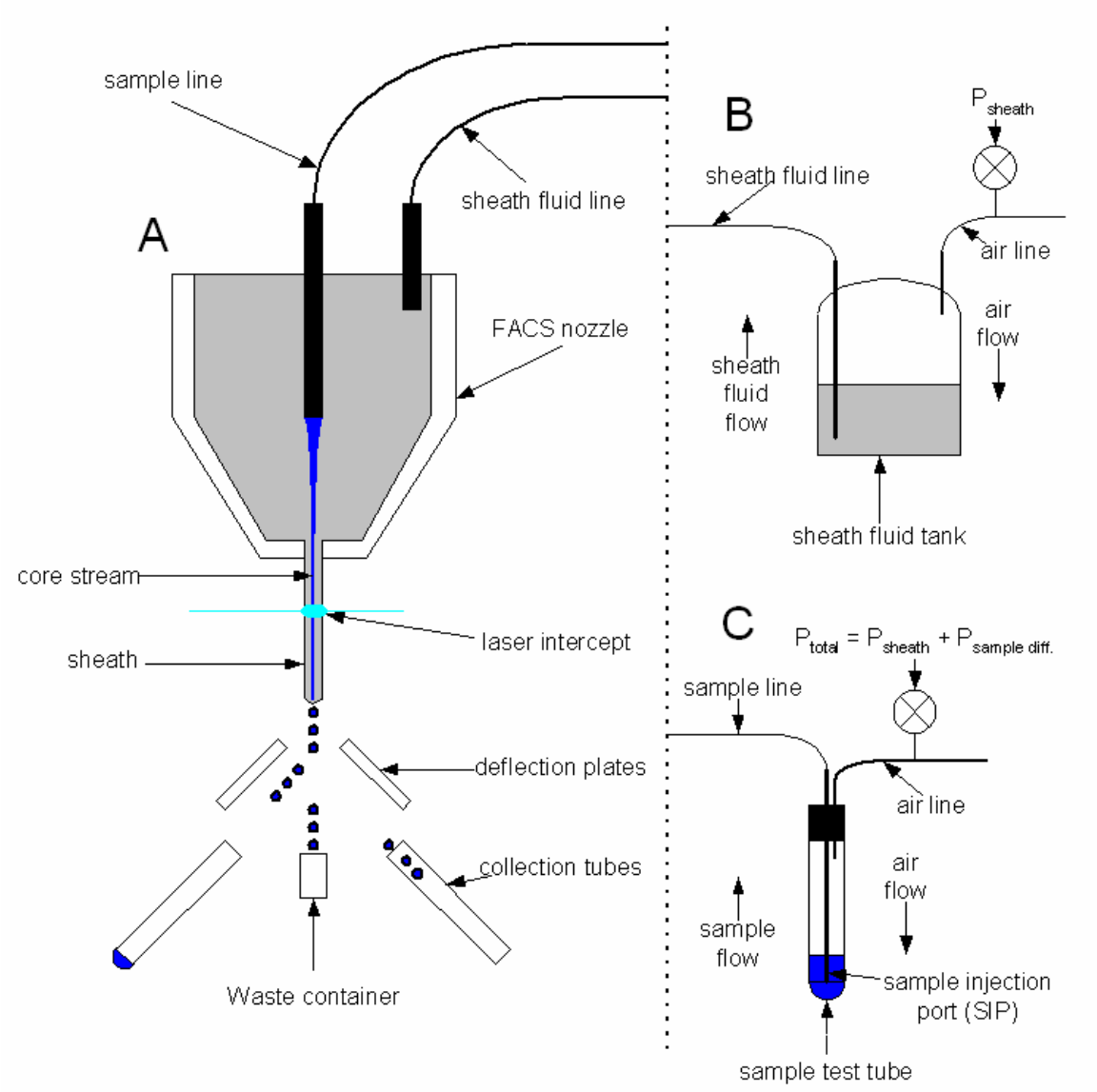

Figure 5.1: Schematic detailing the fluidics of a FACS instrument; the gray areas are sheath fluid and the blue are the sample fluid (A) cutaway of the FACS nozzle, (B) sheath tank, and (C) sample tube.

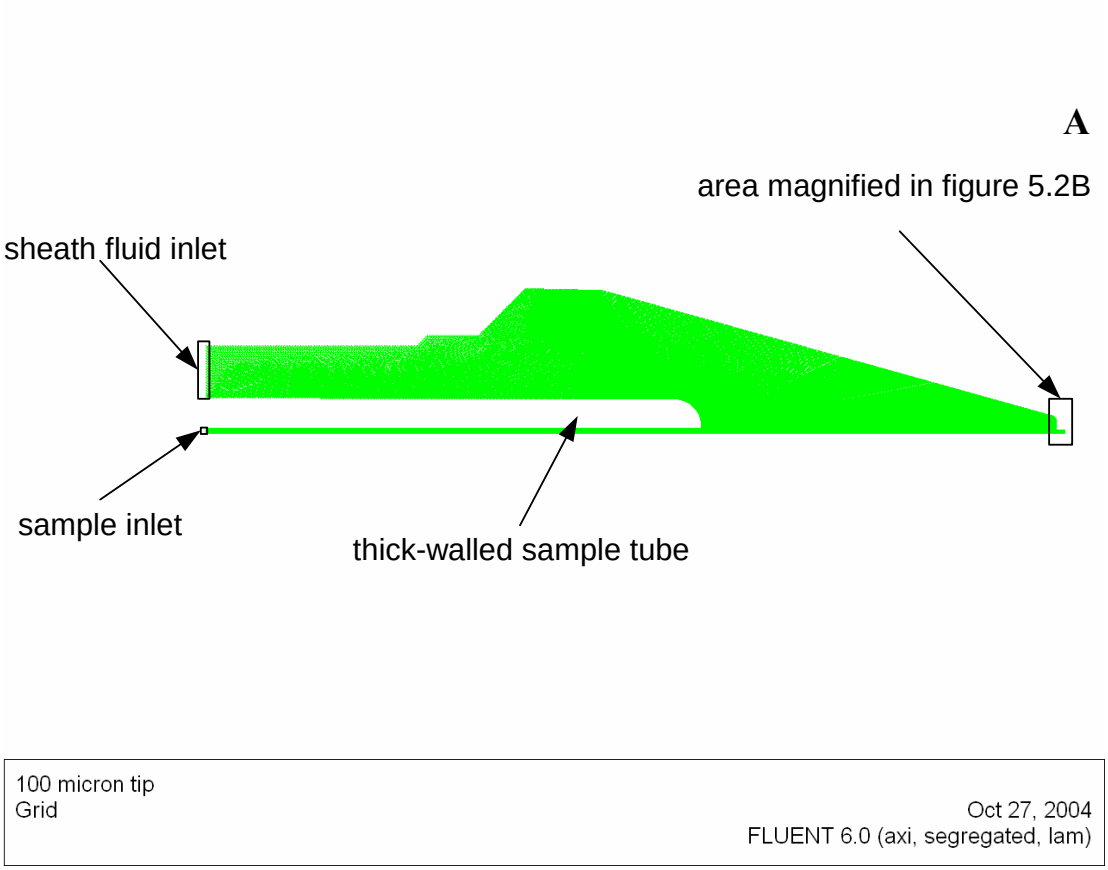

Continued

Figure 5.2: Geometry and mesh of node points for FACS instrument nozzle, (A) entire geometry, (B) magnified exit.

Figure 5.2 Continued

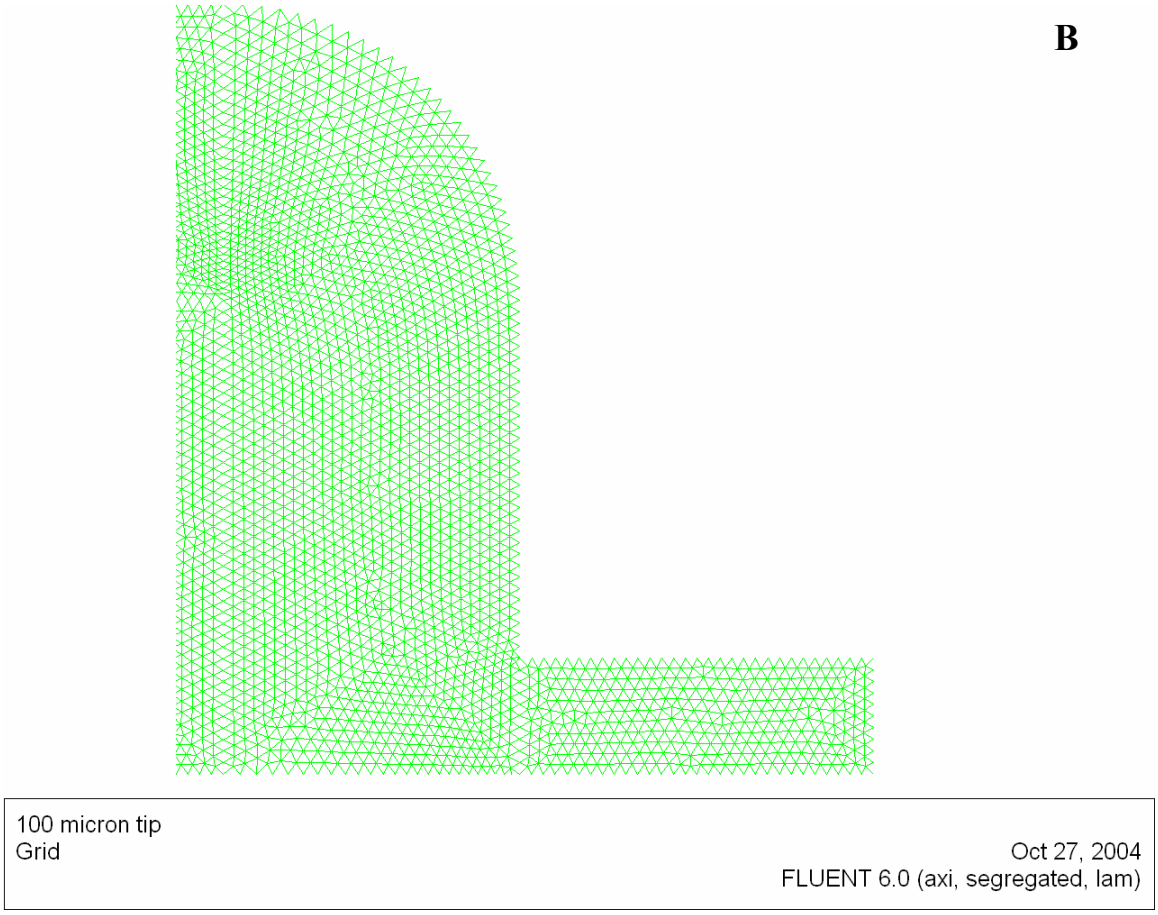

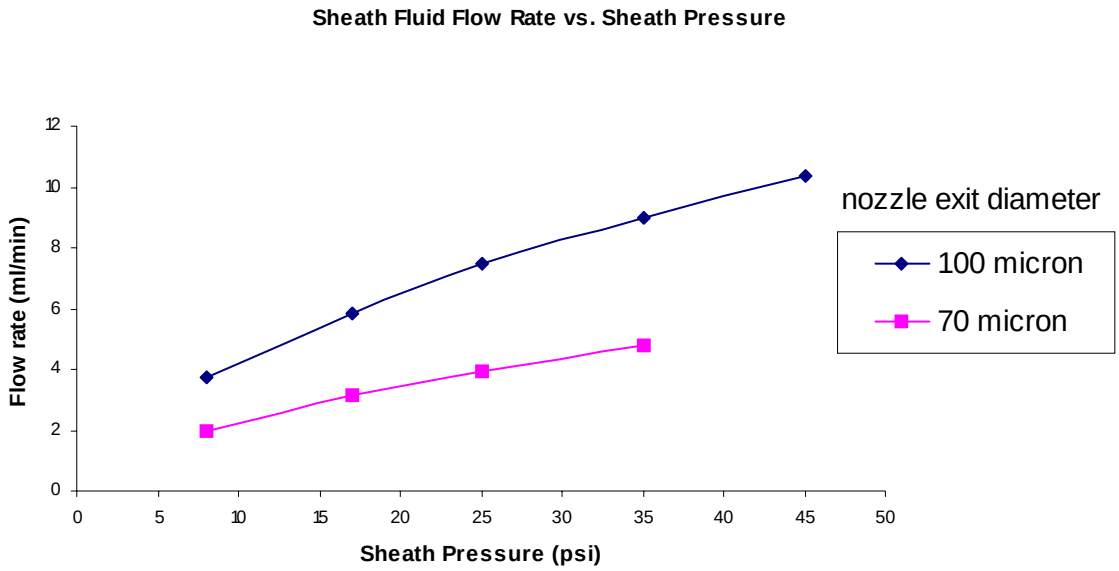

Figure 5.3: Measured volumetric flow rate versus sheath pressure for a BD FACS Vantage.

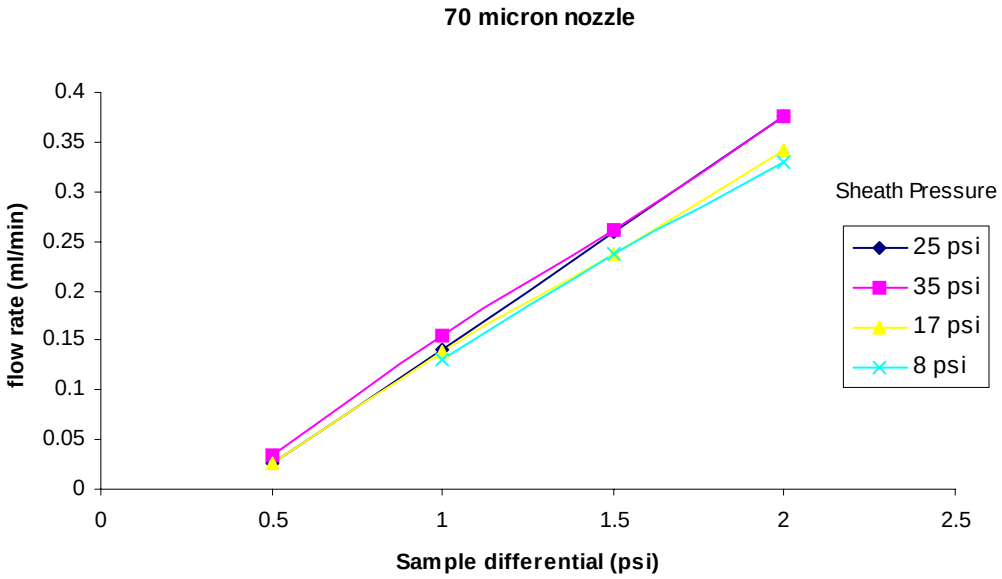

Figure 5.4: Measured sample uptake rate versus sample differential pressure, for the 70 µm diameter nozzle.

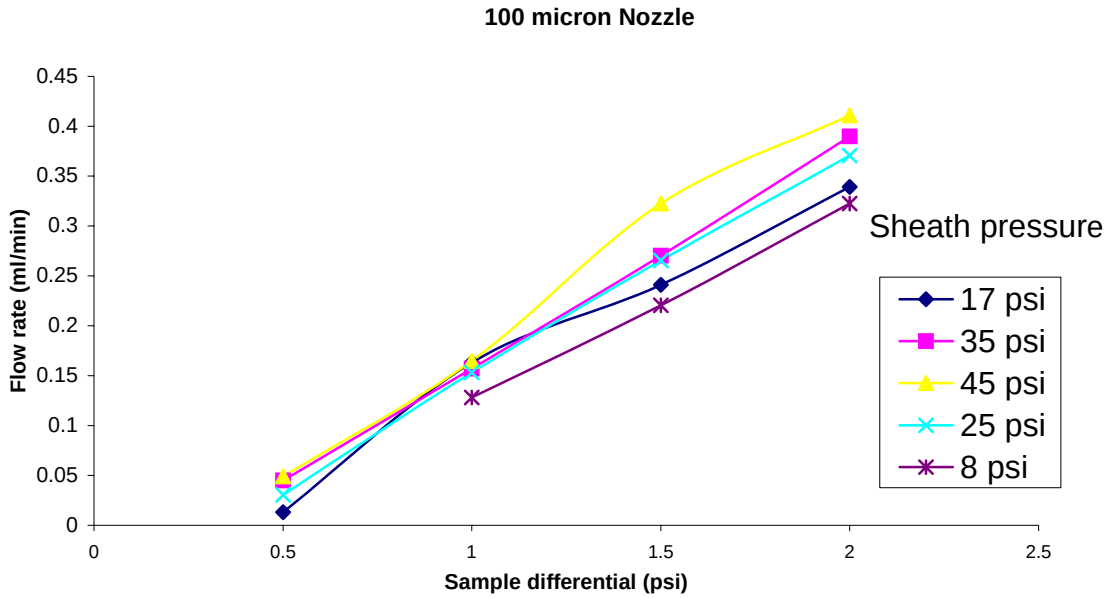

Figure 5.5: Measured sample uptake rate versus sample differential pressure, for the 100 µm diameter nozzle.

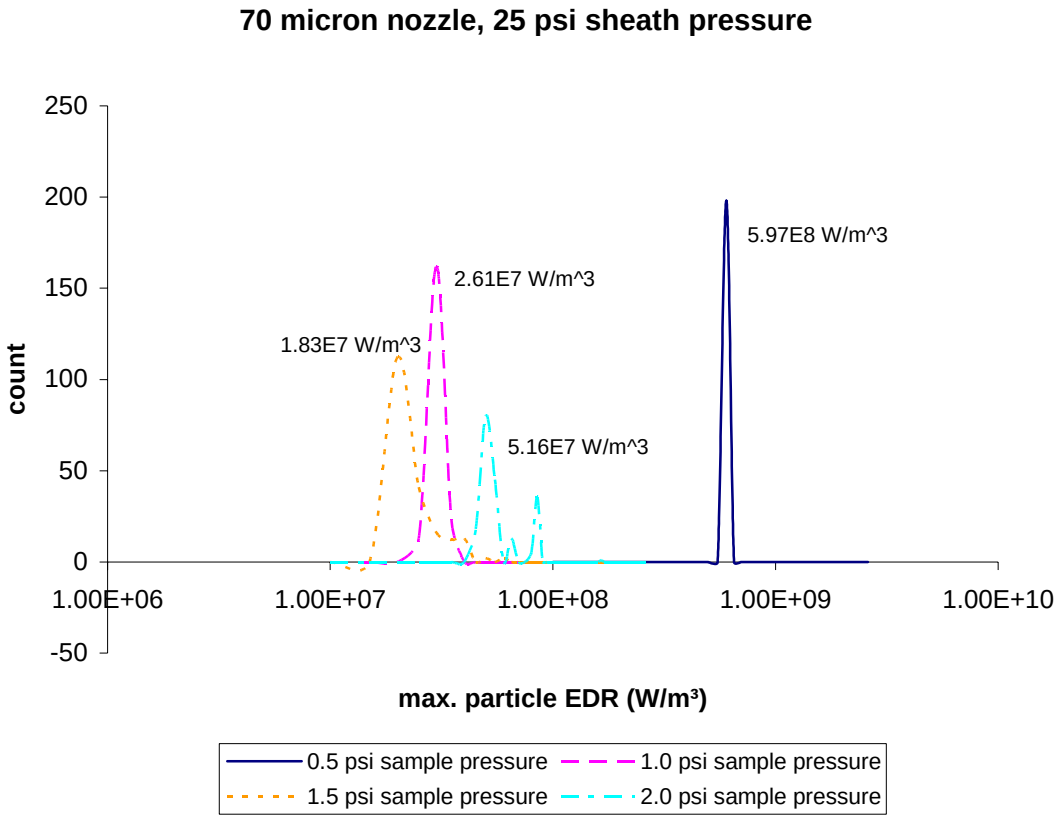

Figure 5.6: Representative histogram of maximum particle EDR versus count for the 70 µm diameter nozzle at 25 psi sheath pressure for various sample differential pressures.

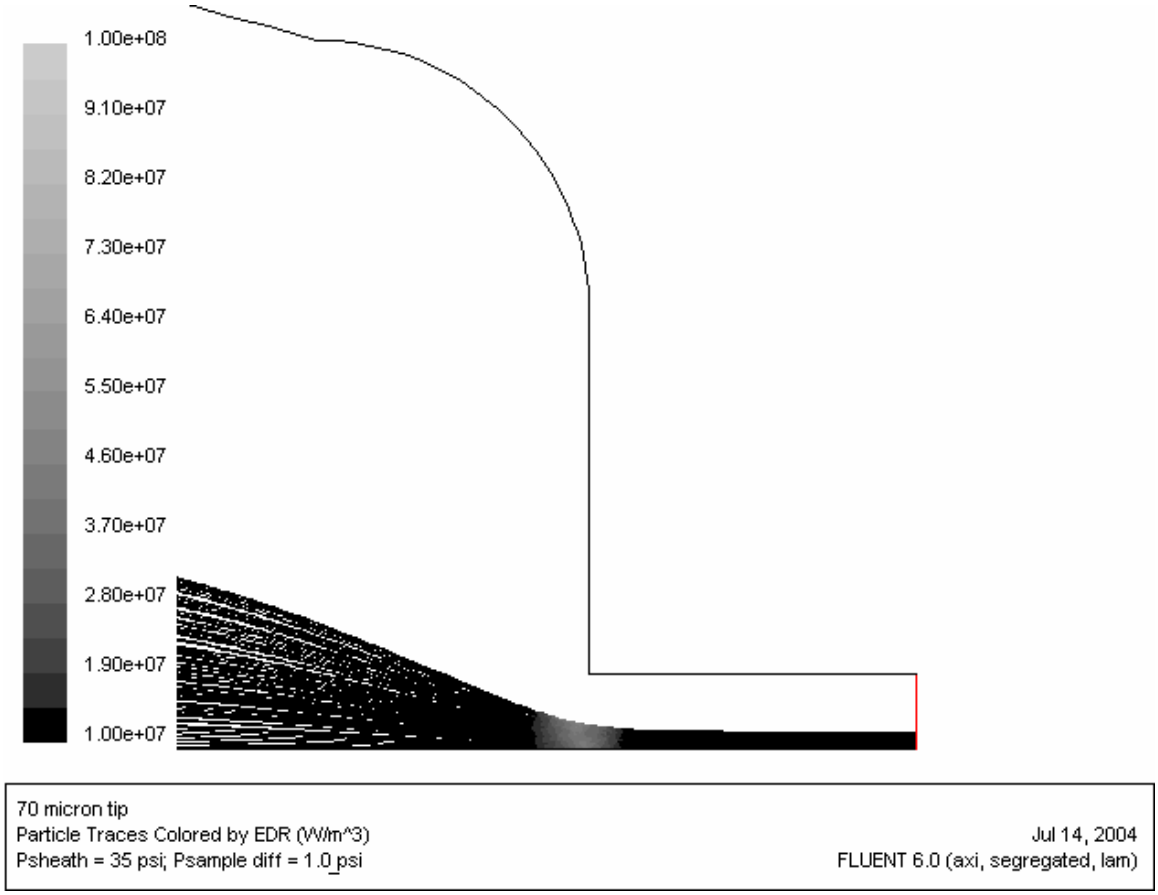

Figure 5.7: Counter plot of particle tracks, colored by EDR at the exit of the 70 µm diameter nozzle with a 35 psi sheath pressure and a 1.0 psi sample differential pressure.

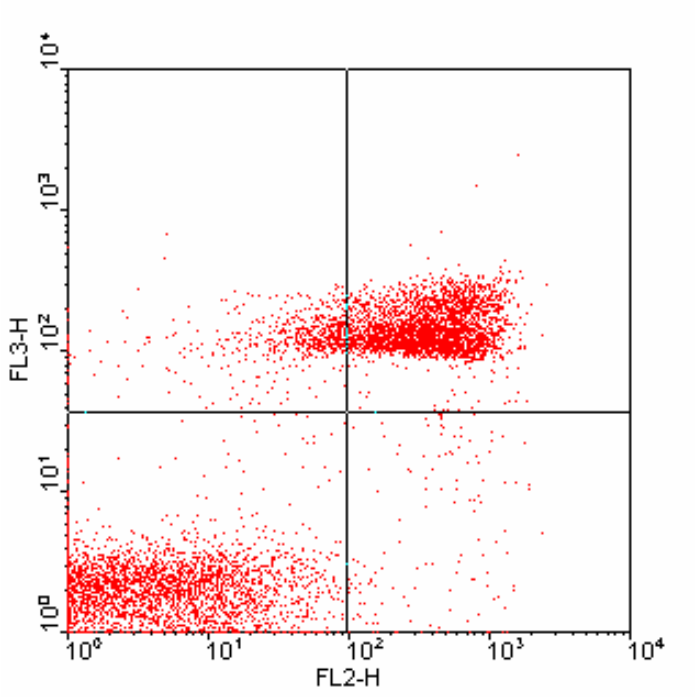

Figure 5.8: Representative dot plot of 7-AAD relative fluorescence (FL3-H) versus Annexin V-PE relative fluorescence (FL2-H), events in the lower left quadrant are healthy, events in the lower right quadrant are early apoptotic, and events in the upper right quadrant are late apoptotic or necrotic.

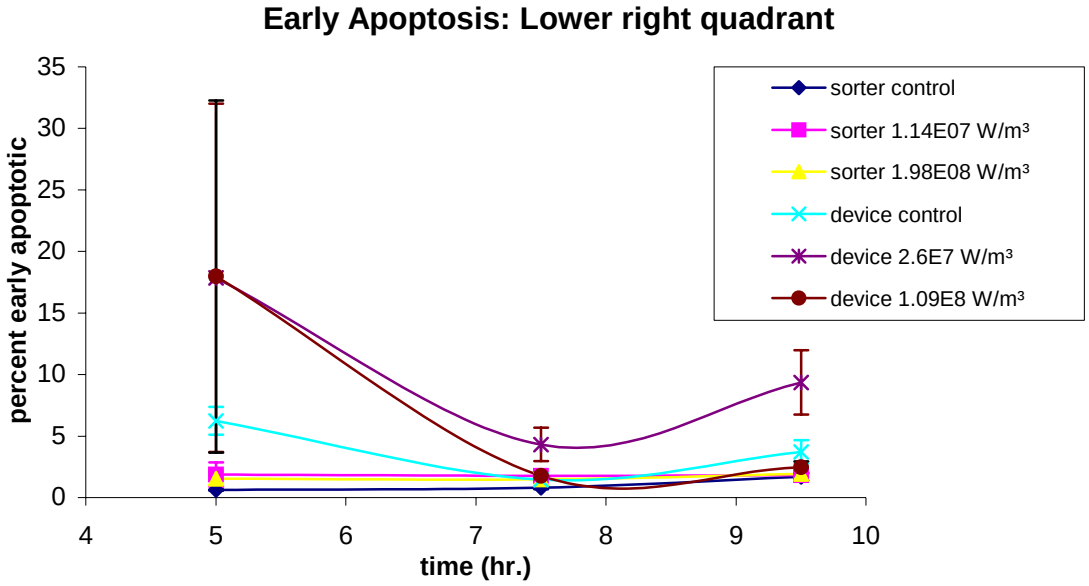

Figure 5.9: Percent of early apoptotic (lower right quadrant) versus time (hr.) since sorting or passage through the contractional flow device.

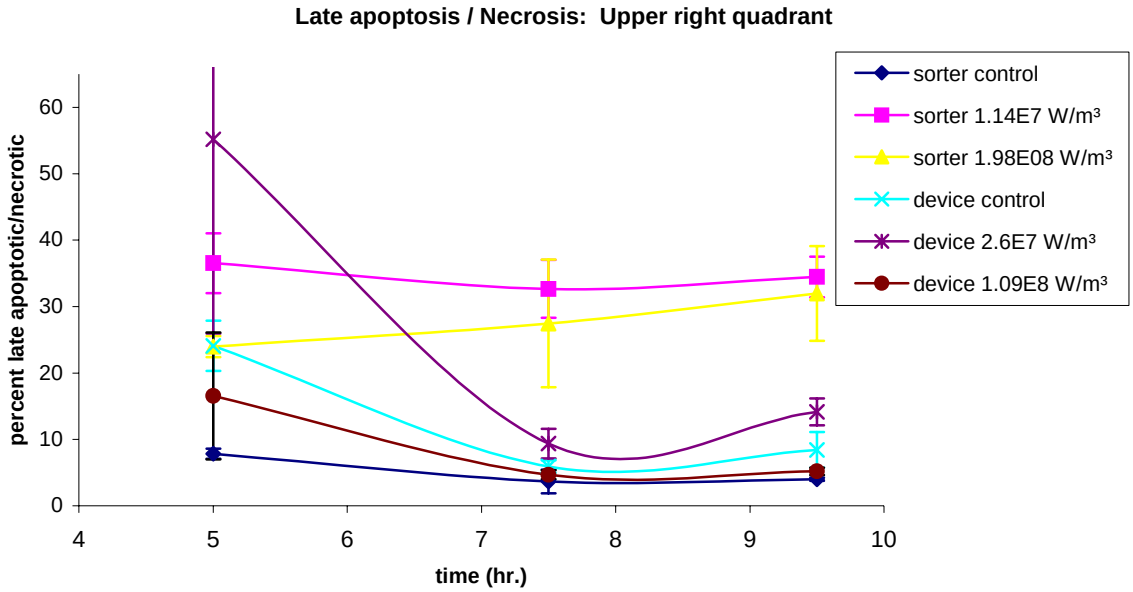

Figure 5.10: Percent of late apoptotic/necrotic (upper right quadrant) versus time (hr.) since sorting or passage through the contractional flow device.

Chapter 6

Conclusions and Future Work

The primary goals of this research were to determine cells' response to high levels of transient energy dissipation rate (EDR), and to determine the maximum local EDR cells experience in various pieces of bioprocess equipment. To accomplish the former goal, I developed an improved contractional flow device to measure cells' susceptibility to brief bursts of intense energy dissipation. To accomplish the latter goal, we (Ningning Ma and I) utilized experimental as well as analytical techniques to determine the EDR distribution in a bench scale stirred tank bioreactor and in laminar flow in a duct. I also examined the level of EDR cells encounter in a FACS (Fluorescent Activated Cell Sorter) instrument and performed experiments to determine the level of cellular damage.

Analytical and experimental techniques were employed to calculate the maximum local EDR in some bioprocess equipment. Using velocity profile equations derived for pressure driven flows, the maximum local EDR was determined for a variety of duct geometries and over a wide range of volumetric flow rates. The EDR for flow through standard pipettes was simulated using FLUENT. The results of the two aforementioned analysis led to similar conclusions: cell death in laminar flow in ducts and pipettes is

unlikely because a combination of small dimensions (on the order of a few μm) in conjunction with high volumetric flow rates are required to produce EDR levels sufficient to cause cell lysis. Based on the data presented in chapter 4, a similar conclusion can be drawn for cells becoming apoptotic as well. Ningning Ma used Particle tracking velocimetry (PTV), an experimental technique, to determine the velocity vectors and the EDR at several points throughout a bench scale stirred tank bioreactor. Ningning Ma's data indicates that even at very high agitation rates, cell rupture and apoptosis is unlikely caused by the action of the impeller. Future work for this topic would include investigating other bioprocess equipment such as pumps, filtration systems, centrifuges, and valves. Since most of the aforementioned equipment has complex flow geometries, computational fluid dynamics (CFD) simulations and/or experimental observations (i.e. PTV) would be required to adequately determine the EDR.

An improved contractional flow device was developed to determine the amount of physical abuse cells could withstand before undergoing apoptosis or necrosis. The device was fabricated out of stainless steel using a non-traditional machining technique, wire EDM (electrical discharge machining), and the flow was simulated in FLUENT, a commercial CFD program. A particle tracking technique was used to better describe the level of EDR a cell would encounter. Two different cell lines were investigated: wild type (WT) CHO-K1 cells and CHO-K1 cells engineered to overexpress the human bcl-2 gene, an anti-apoptosis gene. Both cell lines were cultured in two different conditions: attached to tissue culture flasks and in serum containing media, and freely suspended in serum free media. The WT CHO-K1 cells cultured in tissue culture flasks and in serum containing media were the most likely to undergo apoptosis, although the WT

CHO cells did not display high levels of apoptosis, typically 5% to 10% above the control values. The WT CHO cells cultured in suspension and in serum free media displayed low levels (approximately 2% above the control) of apoptosis at the highest EDR tested (10^8 W/m³), however high levels of necrosis were observed for these cells, 30% compared to 10% for the WT CHO cells cultured in tissue culture flasks and in serum containing media. CHO cells tansfected with the bcl-2 gene did not display high levels of apoptosis or necrosis. The data from this portion of the study indicates that: hydrodynamic stress is not a potent initiator of apoptosis and that high levels of EDR are required to elicit a small apoptotic response in the cells. Future work for this part of the investigation would include additional apoptosis assays, such as Hoechst 33342 and acridine orange fluorescent microscopy assays, to support the flow cytometry data, and to determine the effects of multiple passes through the contractional flow device of the same population of cells to ascertain possible cumulative effects of stress on cells.

Fluorescence activated cell sorting (FACS) is a very common technique used in the biopharmaceutical industry as well as in biological research to sort cells that display certain characteristics. However, FACS instruments have not been extensively studied with respect to cell damage. Several operating conditions of a common FACS instrument, a BD FACS Vantage, were modeled using FLUENT. A simulated particle tracking technique, similar to the technique used to simulate the contractional flow device, was employed to determine the level of EDR cells would experience in the FACS instrument. Potentially damaging, high levels of EDR were observed for all of the operating conditions investigated. WT CHO cells were sorted using the FACS Vantage at a few of the conditions simulated earlier, and these cells were tested for

apoptosis and necrosis. A high percentage of necrotic cells and a low percentage of apoptotic cells were observed. These data indicate that sorting cells using the FACS Vantage kills a significant portion of the cells; therefore the FACS operator might be inadvertently selecting the more robust cells. Future work for this study would include investigating other cell lines and growth conditions, and would simulate other commercial cell sorters such as the FACS Aria.

Bibliography

Al-Rubeai, M., Singh, R., Emery, A., and Zhang, Z. 1995. Cell Cycle and Cell Size Dependence of Susceptibility to Hydrodynamic Forces. *Biotechnology and Bioengineering*. **46**: 88-92.

Al-Rubeai, M., Singh, R. P., Goldman, M. H. and Emery, A. N. 1995. Death mechanisms of animal cells in conditions of intensive agitation. *Biotechnology and Bioengineering*. **45**: 463-472.

Aloi, L.E., Cherry, R.S. 1996. Cellular response to agitation characterized by energy dissipation at the impeller tip. *Chem. Eng. Sci.* **51**: 1523-1529.

Arden, N. and Betenbaugh, M. 2004. Life and death in mammalian cell culture: strategies for apoptosis inhibition. *TRENDS in Biotechnology*. **22(4)**: 174-180.

Aris, R. 1962. *Vectors, Tensors, and the Basic Equations of Fluid Mechanics*, Dover Publications, NY.

Arnst, C., Barrett, A., Arndt, M. and Carey, J. 2004 The Waning of the Blockbuster Drug. Businessweek Oct. 18, 2004

Aslam1, I., Robins, A., Dowell, K., and Fishel, S. 1998. Isolation, purification and assessment of viability of spermatogenic cells from testicular biopsies of azoospermic men. *Human Reproduction*. **13(3)**: 639–645.

Atzberger, A. 2000. Purdue Cyometry Laboratories Email Archive, www.cyto.purdue.edu.

Bavarian, F., Fan, L., and Chalmers, J. 1991. Microscopic visualization of insect cell-bubble interactions I: Rising bubbles, air-medium interface, and the foam layer. *Biotechnology Progress*. **7**: 140-150.

Bernard, P. and Wallace, J. 2002. *Turbulent Flow: Analysis, Measurement and Prediction.* Wiley, NY.

Bird, B. R., Stewart, W.E., Lightfoot, E.N. 1960. *Transport Phenomena.* John Wiley & Sons, NY.

Bluestein, M., and Mockros, L.F. 1969. Hemolytic effects of energy dissipation in flowing blood. *Med. Biol. Eng*. **7**: 1-6.

Boulton, G., and Blake, J. 1993. Gas bubble bursting at a free surface. *J. Fluid Mech.* **154**: 437-466.

Brodkey, R.S. 1995. *The Phenomena of Fluid Motions*. Dover Publishing, NY.

Brodkey, R.S., Hershey, H.C. 1988. *Transport Phenomena, A Unified Approach*. McGraw-Hill, NY.

Castilho, L. and Anspach, F. 2003. CFD-Aided Design of a Dynamic Filter for Mammalian Cell Separation. *Biotechnology and Bioengineering*. **83(5)**: 514-524.

Chattopadhyay, D., Rathman, J., and Chalmers, J. 1995. The protective effect of specific medium additives with respect to bubble rupture. *Biotechnology and Bioengineering*. **45**: 473-480

Chattopadhyay, D., Rathman, J., Chalmers, J. 1995. A thermodynamic explanation for cell adhesion to gas-liquid interfaces. *Biotechnology and Bioengineering*. **48**: 649-658.

Chisti, Y. 2001. Hydrodynamic damage to animal cells. *Critical Reviews in Biotechnology*. **21(2)**: 67-110.

Choi, W-C, Guezennec, YG, Brodkey, RS. 1992. In situ calibration and stereo matching for 3-D particle image Velocimetry. *Bull Am Phys. Soc*. **36**.

Clay, J. D. 1997. *Molecular Degradation of Polymer Solutions in Fast Transient Extensional Flow*, Dissertation, The Ohio State University.

Cossarizza, A., Kalashnikova, G., Grassilli, E., Chiapelli, F., Salvioli, S., Capri, M., Barbieri, D., Troiani, L., Monti, D., Franceshi, C. 1994. Mitochondrial modifications during rat thymocyte apoptosis: A study at the single cell level. *Exp Cell Res* **214**: 323-30.

Cotter, T. and Al-Rubeai, M. 1995. Cell death (apoptosis) in cell culture systems. *TIBTECH* **13**: 150-155

Croughan, M.S. and Wang, D.I.C. 1989. Growth and death in overagitated microcarrier cell cultures. *Biotechnology and Bioengineering*. **33**: 731-744.

Cruz, P.E., Cunha, A., Peixoto, C.C., Clemente, J., Moreira, J.L., Carrondo, M.J.T. 1998. Optimization of the Production of Virus-like Particles in Insect Cells. *Biotechnology and Bioengineering.* **60**: 408-418.

Darzynkiewicz, Z., Juan, G., Li, X., Gorczyca, W. Murakami, T. and Traganos, F. 1997. Cytometry in Cell Necrobiology: Analysis of Apoptosis and Accidental Cell Death (Necrosis). *Cytometry* **27**: 1–20 .

Davies, P., Dewey, C., Bussolari, S., Gordon, G., and Gimborne, M. 1984. Influence of Hemodynamic Forces on Vascular Endothelial Function In Vitro Studies of Shear Stress and Pinocytosis in Bovine Aortic Cells. *J. Clin. Invest.* **73**: 1121-1129.

Dewey, C., Bussolari, S., Gimbrone, M., and Davies, P. 1981. The Dynamic Response of Vascular Endothelial Cells to Fluid Shear Stress. *J. of Biomech. Eng*. **103**: 177-185.

Fan, S. and Graf-Hausner, U. 2002. Gentle delivery of flowing cell culture with various pumps. *Bioforum* **25(9)**: 541-542.

Fussenegger, M. and Bailey, J.E. 1998. Molecular regulation of cell-cycle progression and apoptosis in mammalian cells: implications for biotechnology. *Biotechnology Progress*. **14**: 807-833.

Garcia-Briones, M., Brodkey, R., and Chalmers, J. 1994. Computer simulations of the rupture of a gas bubble at a gas-liquid interface and its implications in animal cell damage. *Chem. Eng. Sci*. **49**: 2301-2320.

Garcia-Briones, M. and Chalmers, J. 1992. Cell-bubble interactions: mechanisms of suspended cell damage. *Ann. N. Y. Acad. Sci*. **665**: 219-229.

Garcia-Briones, M.A, Chalmers, J.J., Flow Parameters Associated with Hydrodynamic Cell Injury, *Biotechnology and Bioengineering,* **44**: 1089-1098, 1994.

Givan, A.L. 2001. *Flow Cytometry First Principles*. Wiley-Liss, New York.

Goswami, J., Sinskey, A. J., Steller, H. Stephanopoulus, G. N., and Wang, D. I. C. 1999. Apoptosis in batch cultures of Chinese Hamster Ovary cells. *Biotechnology and Bioengineering*. **62**: 632-640.

Graf, R., Apenberg, S., Freyberg, M. and Friedl, P. 2003. A common mechanism for the mechanosensitive regulation of apoptosis in different cell types and for different mechanical stimuli. *Apoptosis*. **8**: 531–538.

Graves, S., Nolan, J., Jett, J., Martin, J., and Sklar, L. 2002. Nozzle Design Parameters and Their Effects on Rapid Sample Delivery in Flow Cytometry. *Cytometry*. **47**: 127-137.

Gregoriades, N., Clay, J., Ma, N., Koelling, K., Chalmers, J.J. 2000. Cell Damage of Microcarrier Culture as a Function of Local Energy Dissipation Created by a Rapid Extensional Flow. *Biotechnology and Bioengineering*. **69**: 171-182.

Guezennec, Y.G., Brodkey, R.S., Trigui, N., Kent, J.C., 1994. Algorithms for fully automated three-dimensional particle tracking velocimetry. *Exp. Fluids*. **17**: 209-219.

Haldar, S., Negrini, M., Monne, M., Sabbioni S., and Croce, C. 1994. Down-regulation of bcl-2 by p53 in breast cancer cells. *Cancer Res*. **54**: 1818-1824.

Handa, A., Emary, A., and Spier, P. 1987. On the evaluation of gas-liquid interfacial effects on hybridoma viability in bubble column bioreactors. *Dev. Biol. Stand*. **66**: 241-253.

Harris, M. and Thompson, C. 2000. The role of the Bcl-2 family in the regulation of outer mitochondrial membrane permeability. *Cell Death & Differentiation.* **7(12)**: 1182-1192.

Hiemenz, P. C. and Rajagopalan, R. 1997. *Principles of Colloid and Surface Chemistry*, Marcel Dekker, Inc., New York.

Hochmuth, R. 2000. Micropipette aspiration of living cells. *J. Biomechanics* **33(1)**: 15-22.

Iverson, K. 2003. Troubleshooting tangential flow filtration. *Chemical Engineering Progress*. **99(6)**: 54-56.

Jaouen, P., Vandanjon, L., and Quemenuer, F. 1999. The shear stress of microalgae cell suspensions (*Tetraselmis suecica*) in tangential flow filtration systems: the role of pumps. *Bioresource Technolgy* **68**: 149-154.

Jones, R., Ping T., Lee, G., Kelley, S., Hochmuth, R., Guilak, F. 1999. Alterations in the Young's modulus and volumetric properties of chondrocytes isolated from normal and osteoarthritic human cartilage. *J. Biomechanics*. **32(2)**: 119-127.

Kioukia, N. Nienow, A., Emery, A., Al-Rubeai, M. 1992. The impact of fluid dynamics on the biological performance of free suspension animal cell culture: further studies. *Food and Bioproducts Processing*. **70 (C3)**: 143-148.

Kresta, S. 1998. Turbulence in Stirred Tanks: Anisotropic, Approximate, and Applied. *Canadian J. of Chem. Eng*. **76**: 563-576.

Kresta, S., Krens, R., and Martin, Y. 2004. The Future of Mixing Research. *Chem. Eng. Technol*. **27(3)**: 208-214.

Kunus, KT., and Papoutsakis, E.T. 1990. Damage mechanisms of suspended animal cells in agitated bioreactors with and without bubble entrainment. *Biotechnology and Bioengineering*. **36**: 476-483.

Laken, H. A. and Leonard, M. W. 2001. Understanding and modulating apoptosis in industrial cell culture. *Current Opinion in Biotechnology*. **12**:175–179.

Levine B, Huang Q, Isaacs, JT, Reed LC, Griffin DE, and Hardwick, JM. 1993. Conversion of lytic to persistent alphavirus infection by the bcl-2 cellular oncogene. *Nature.* **361**: 739-742.

Ma, N., Chalmers, J., Aunins, J., Zhou, W., and Xie, L. 2004a. Quantitative Studies of Cell-Bubble Interactions and Cell Damage at Different Puronic F-68 and Cell Concentrations. *Biotechnology Progress*. **20**: 1183-1191.

Ma, N., Mollet, M., Chalmers, J. 2004b. "Aeration, Mixing and Hydrodynamics in Bioreactors." *Cell Culture Technology for Pharmaceutical and Cellular Therapies*, Ed. Ozturk, S. and Hu, W. New York, NY: Marcel Dekker.

Ma, N., Koelling, K., and Chalmers, J.J. 2002. The Fabrication and Use of A Transient Contraction Flow Device to Quantify the Sensitivity of Mammalian and Insect Cells to Hydrodynamic Forces, *Biotechnology and Bioengineering* **80**: 428-437.

Macosko, C. 1994. *Rheolgy Principles, Measurements, and Applications.* Wiley, NY.

Martin, R., Dewitz, T., and McIntire, L. 1979. "Alterations in Leukocyte Structure and Function Due to Mechanical Trauma," in *Quantitative Cardiovascular Studies Clinical and Research Applications of Engineering Principles*, eds. Hwang, N., Gross, D., and Patel, D., University Park Press, Baltimore, MD.

Mastrangelo AJ, Hardwick JM, Bex F, and Betenbaugh MJ. 2000. Part I. Bcl-2 and Bcl-Xl limit apoptosis upon infection with alphavirus vectors. *Biotechnology and Bioengineering*. **67(5)**:544-554.

Mastrangelo, A., Hardwick, J., Zou, S., and Betenbaugh, M. 2000. Part II. Overexpression of bcl-2 Family Members Enhances Survival of Mammalian Cells in Response to Various Culture Insults. *Biotechnology and Bioengineering*. **67(5)**: 555-564.

McDowell, C.L. and Papoutsakis, E.T. 1998. Increased Agitation Intensity Increases CD13 Receptor Surface Content and mRNA levels, and Alters the Metabolism of HL60 Cells Cultured in Stirred Tank Bioreactors. *Biotechnolology and Bioengineering*. **60**: 239-250.

McQueen A. and Bailey, J. E. 1989. Influence of serum level, cell line, flow type and viscosity on flow-induced lysis of suspended mammalian cells. *Biotech. Lett*. **11(8)**: 531-536.

McQueen, A., Meilhoc, E., and Bailey, J. E. 1987. Flow effects on the viability and lysis of suspended mammalian cells. *Biotech. Lett.* **9(12)**: 831-836.

Merten, O. 2000. Constructive improvement of the ultrasonic separation device ADI 1015. *Cytotechnology* **34**: 175–179.

Michaels, J. Kunas, K., and Papoutsakis, E. 1992. Fluid-mechanical damage of freely suspended animal cells in agiated bioreactors: effects of dextran, derivatized celluloses and polyvinyl alcohol. *Chemical Engineering Communications*. **118**: 341-360.

Miyazaki, H., Hasegawa, Y., and Hayashi, K. 2000. A newly designed tensile tester for cells and its application to fibroblasts *J. Biomechanics.* **33(1)**: 97-104.

Mollet, M., Ma, N., Zhao, Y., Brodkey, R., Taticek, R., and Chalmers, J. 2004. Bioprocess Equipment: Characterization of Energy Dissipation Rate and its potential to Damage Cells. *Biotechnology Progress*. **20(5)**: 1437-1448.

Molowa, D. 2002. The state of biologics manufacturing: Part 2, JP. Morgan Securities Feraury 22, 2002.

Morrone, S. 1997. Annexin V, Purdue Cytometry CD-ROM Series, Volume 4. J. Watson, Guest Ed., J.Paul Robinson, Publisher. Purdue University Cytometry Laboratories, West Lafayette, IN.

Nienow, A. W. 1997. On impeller circulation and mixing effectiveness in the turbulent flow regime. *Chemical Engineering Science*. **52(15)**: 2557-2565.

Nienow, A. W., Langheinrich, C., Stevenson, N. C., Emery, A.N., Clayton T.M., and Slater, N. K. 1996. Homogenisation and oxygen transfer rates in large agitated and sparged animal cell bioreactors: Some implications for growth and production. *Cytotechnology* **22(6)**: 87-94.

Ozturk, S. 1996. Engineering challenges in high density cell culture systems, *Cytotechnology* **22**: 3-16.

Papadaki, M. and Eskin, S. 1997. Effects of fluid shear stress on gene regulation of vascular cells. *Biotechnology Progress*. **13(3)**: 209-221.

Perani, A., Singh, R. P., Chauhan, M., and Al-Rubeai, M. 1998. Variable functions of bcl-2 in mediating stress-induced apoptosis in hybridoma cells. *Cytotechnology* **28**: 177-188.

Pinkel, D. and Stovel, R. 1985. "Flow Chambers and Sample Handling," in *Flow Cytometry: Instrumentation and Data Analysis*, eds. Van Dilla, M., Dean, P., Laerum, O., and Melamed, M.

Ranjan, V., Waterbury, R., Xiao, Z., and Diamond, S.L. 1996. Fluid shear stress induction of the transcriptional activator c-fos in human and bovine cells, HeLa, and Chinese hamster ovary cells. *Biotechnology and Bioengineering* **49**: 383-390.

Rao, M. A. and Brodkey, R. S. 1972. Continuous flow stirred tank turbulence parameters in the impeller stream. *Chem. Eng. Sci*. **27**: 137-156.

Roberts, R.M., Gray, M.R., Thompson, B., and Kresta, S.M. 1995. The Effect of Impeller and Tank Geometry on Circulation Time Distributions in Stirred Tanks. *Trans IChem*. **73**: 78-86.

Rose, S., Black, T., and Ramakrishnan, D. 2003. "Mammalian Cell Culture: Process Development Considerations," in *Handbook of Industrial Cell Culture: Mammalian, Microbial, and Plant cells*. Eds.: Vinci, V.A. and Parekh, S.R. Human Press, Totwa, NJ. p 69-146.

Seidl, J.,Knuechel, R., and Kunz-Schughart, L.A. 1999. Evaluation of Membrane Physiology Following Fluorescence Activated or Magnetic Cell Separation. *Cytometry* **36**: 102–111.

Senger, R. and Nazmul, K. 2003. Effect of shear stress on intrinsic CHO culture state and glycosylation of recombinant tissue-type plasminogen activator protein. *Biotechnology Progress* **19(3)**: 119-1209.

Shapiro, H. 2003. *Practical Flow Cytometry*. Wiley-Liss, New York.

Simpson, N. H., Milner, A. E., and Al-Rubeai, M. 1997. Prevention of cell death by bcl-2 during suboptimal culture conditions. *Biotechnology and Bioengineering*. **54(1)**: 1-16.

Song, X., Throckmorton, A., Wood, H., Antaki, J. and Olsen, D. 2003. Computational Fluid Dynamics Prediction of Blood Damage in a Centrifugal Pump. *Artificial Organs* **27(10)**: 938–941.

Spedding G. R. and Rignot E. J. M. 1993. Performance analysis and application of grid interpolation techniques for fluid flows. *Experiments in Fluids* **15**: 417-430.

Stoots, C.M., and Calabrese, R.V. 1995. Mean Velocity Field Relative to a Rushton Turbine Blade. *AIChE J.* **41**: 1-11.

Suzuki, E., Terada, S., Ueda, H., Fujita, T., Komatsu, T., Takayami, S., and Reed, J. 1997. Establishing apoptosis resistant cell lines for improving protein productivity of cell culture. *Cytotechnology*. **23**: 55-59.

Tatterson, G.B. 1991. *Fluid Mixing and Gas Dispersion in Agitated Tanks*. McGraw-Hill Inc. New York.

Taylor, G. I., 1934. The formation of emulsions in definable fields of flow. *Proc. Royal Soc. London A*. **146(501)**: .

Tebbe, H., L¨utkemeyer, D., Gudermann, F., Heidemann R., and Lehmann, J. 1996. Lysis-free separation of hybridoma cells by continuous disc stack. *Cytotechnology* **22**: 119–127.

Thomas, C.R., and Zhang, Z. 1998. The effect of hydrodynamics on biological materials. In: *Advances in bioprocess engineering II*, Galindo E, Ramirez, OT, editors, The Netherlands: Kluwer Academic Pub. p.137-170.

Thomas, C., Zhang, Z., and Cowen, C. 2000. Micromanipulation measurements of biological materials. *Biotech Lett*. **22**: 531–537.

Trinh, K., Garcia-Briones, M., Hink, F., and Chalmers, J. 1994. Quantification of damage to suspended insect cells as a result of bubble rupture. *Biotechnology and Bioengineering*. **43**: 37-45.

Trotter, J. 2003. Purdue Cyometry Laboratories Email Archive, www.cyto.purdue.edu.

Van't Riet, K. and Smith, J.M. 1975. The Trailing Vortex System Produced by Rushton Turbine Agitators. *Chem. Eng. Sci*. **30**:1093-1105.

Varley, J. and Birch, J. 1999. Reactor design for large scale suspension animal cell culture. *Cytotechnology* **29**: 177–205.

Venkat, R.V., Stock, L.R., and Chalmers, J.J. 1996a. Study of Hydrodynamics in Microcarrier Culture Spinner Vessels: A Particle Tracking Velocimetry Approach. *Biotechnology and Bioengineering*. **49**:456-466.

Venkat, R.V., and Chalmers, J.J. 1996b. Characterization of agitation environments in 250 ml spinner vessels, 3 L and 20L reactor vessels used for animal cell microcarrier culture. *Cytotechnology*. **22**: 95-102.

Veselska, R and Janisch, R. 2001. Reaction of the Skin Fibroblast Cytoskeleton to Micromanipulation Interventions. *J. Structural Biology* **136**: 110–118.

Vogel, J. and Kroner, K. 1999. Controlled Shear Filtration: A Novel Technique for Animal Cell Separation. *Biotechnology and Bioengineering*. **63(6)**: 663-674.

Walsh G., Dewson, G., Wardlaw, A., Levi-Schaffer, F., and Moqbel, R. 1998. A comparative study of different methods for the assessment of apoptosis and necrosis in human eosinophils. *Journal of Immunological Methods.* **217**: 153–163.

Wernersson, E. S. and Tragardh C. 1999. Scale-up of rushton turbine-agitated tanks. *Chem. Eng. Sci.* **54**: 4245-4256.

White, F. M. 1974. *Viscous Fluid Flow*. McGraw-Hill Inc., New York.

Wu, H., and Patterson, G. 1989. Laser-doppler measurements of turbulent flow parameters in a stirred mixer. *Chem. Eng. Sci*. **44**: 2207-2221.

Yianneskis, M., Popiolek, Z., and Whitelaw, J. 1987. An experimental study of the steady and unsteady flow characteristics of stirred reactors. *J. Fluid Mech.* **175**: 537-555.

Zanghi, J. A., Renner, W. A., Bailey, J. E., and Fussenegger, M. 2000. The growth factor inhibitor saramin reduces apoptosis and cell aggregation in protein-free CHO cell batch cultures. *Biotechnology Progress*. **16**: 319-325.

Zhao, Y. and Brodkey, R. S. 1998. Averaged and Time-Resolved, Full-Field (Three-Dimensional), Measurements of Unsteady Opposed Jets. *Can. J. Chem. Eng*. **76**: 536-545.

Zhou, G., and Kresta, S.M. 1996a. Distribution of Energy Dissipation Between Convective and Turbulent Flow For Three Frequently Used Impellers. *Trans IChemE*, **74**: 379-389.

Zhou, G., and Kresta, S.M. 1996b. Impact of Tank Geometry on the Maximum Turbulence Energy Dissipation Rate for Impellers. *AIChE J.* **42**: 2476-2490.

Appendix A

User Defined Function (UDF) to calculate EDR

A.1 Calculating the EDR in three dimensions

Use edr.c to calculate the energy dissipation rate (in W/m³) for fluid flow in three dimensional geometries.

Contents of edr.c:

```
#include "udf.h"
Domain *d;
DEFINE_ON_DEMAND(edr)
{
        float maxedr = 0.0;
        float epsilon, mu, dudx, dudy, dudz, dvdx, dvdy, dvdz, dwdx, dwdy, dwdz;
        Thread *t;
        cell_t c;
        d = Get_Domain(1);
        thread_loop_c(t, d)
        {
                /*computes the edr at every cell and stores it in user defined memory, location index 0*/
                begin_c_loop(c,t)
                {
                        mu = C_MU_L(c,t);
                        dudx = C_DUDX(c,t);
                        dudy = C_DUDY(c,t);
                        dudz = C_DUDZ(c,t);
                        dvdx = C_DVDX(c,t);
                        dvdy = C_DVDY(c,t);
                        dvdz = C_DVDZ(c,t);
                        dwdx = C_DWDX(c,t);
```

```
                        dwdy = C_DWDY(c,t);
                        dwdz = C_DWDZ(c,t);
                        epsilon = mu*(2*dudx*dudx + dudy*(dvdx + dudy) + dudz*(dwdx
+ dudz) + dvdx*(dvdx + dudy) + 2*dvdy*dvdy + dvdz*(dwdy +dvdz) + dwdx*(dudz
+dwdx) + dwdy*(dvdz + dwdy) + 2*dwdz*dwdz);
                        C_UDMI(c,t,0) = epsilon;
                        if (epsilon > maxedr) maxedr = epsilon;
                }
                end_c_loop(c,t)
        printf("\n Max EDR = %g W/m^3 \n", maxedr);
        }
}
```

A.2 Calculating the EDR in two dimensions

Use edr2d.c to calculate the energy dissipation (in W/m³) for fluid flow in two dimensional geometries.

Contents of edr2d.c:

```
#include "udf.h"
Domain *d;
DEFINE_ON_DEMAND(edr2d)
{
        float maxedr = 0.0;
        float epsilon, mu, dudx, dudy, dvdx, dvdy;
        Thread *t;
        cell_t c;
        d = Get_Domain(1);
        thread_loop_c(t, d)
        {
                /*computes the edr at every cell and stores it in user defined memory, location index 0*/
                begin_c_loop(c,t)
                {
                        mu = C_MU_L(c,t);
                        dudx = C_DUDX(c,t);
                        dudy = C_DUDY(c,t);
                        dvdx = C_DVDX(c,t);
                        dvdy = C_DVDY(c,t);
                        epsilon = mu*(2*dudx*dudx + dudy*(dvdx + dudy) + dvdx*(dvdx + dudy) + 2*dvdy*dvdy);
                        C_UDMI(c,t,0) = epsilon;
                        if (epsilon > maxedr) maxedr = epsilon;
                }
                end_c_loop(c,t)
        printf("\n Max EDR = %g W/m^3 \n", maxedr);
        }
}
```

Appendix C

Particle Tracking in FLUENT

1 Launch FLUENT

2 Load the appropriate user defined function detailed in Appendix A, by:

a. Clicking on Define → User-Defined → Memory…; increase "Number of User-Defined Memory Locations" to at least one, and then click OK.

b. Then click on Define → User-Defined → Functions → Interpreted; next to source name, enter the complete path to the correct UDF (e.g. Z:edr.c). Check the box next to "Display Assembly Listing", and then click Interpret.

3 Load the mesh or case file, set the initial conditions (i.e. inlet velocity, pressure, etc.), and define a particle injection.

4 Run the simulation, and after FLUENT converges on a solution, calculate the EDR by clicking on Define → User-Defined → Execute on Demand, select the appropriate file and click execute.

5 Determine the EDR each particle encounters by:

a. Clicking on Display → Particle Tracks

b. Click on the box next to "XY Plot", under Y-axis function, select User-defined memory

c. Click on the box next to “Write to file”

d. Select the appropriate particle injection under “Release From Injection”

e. Click Write…; enter the appropriate file name to save the data (i.e. condition1)

f. After FLUENT completes writing the file, go to Windows Explorer and change the file extension of the file created above to .txt file.

g. Run the Perl program detailed in Appendix C to determine the maximum EDR each particle experienced. Make sure the file has the correct name prior to executing the Perl program.

Appendix C

Perl script to determine the maximum EDR for each particle

The following Perl script was written by Ruben Godoy.

```
# This is my third program in perl in the second season
# This program was written on february 2nd, 2004 by Ruben Dario Godoy
# This program was named reader3.pl
# This program is intended to read a file from Fluent and send data on EDR
# to a new file.

print ("Please, do not forget to modify the program to correct the input and output
files\n");
print ("Did you correct the file name? y/n");
$MODIF = <STDIN>; # This line ask you if you corrected the file names
chop ($MODIF);
unless ($MODIF eq "y") {
        die ("please, write down the rigth names for tho input/output files\n");
}
unless (open(EDR, "C:\Documents and Settings\mollet\Desktop\input1.txt")) {
        die("cannot open input file input1.txt\n");
}
#if the program gets this far, the input file was opened succesfully
print ("Input file was opened succesfully\n");
unless (open(salida, ">>C:\Documents and Settings\mollet\Desktop\output1.txt")) {
        die("cannot open output file output1.txt\n");
}
#if the program gets this far, the output file was opened succesfully
print ("Output file was opened succesfully\n");
$LINE = <EDR>;
while ($LINE ne "") {
        chop ($LINE);
        @EDR = split (/[\t ]+/, $LINE);
        if ($EDR[1] eq "") {
                print salida ("empty\n");
```

```
        } else {
                print salida ($EDR[1],"\n");
        }
        $LINE = <EDR>;
}
print ("End of program part to create the edr file");
close (salida);
# If the program gets this far, it just created a file containing the edr values
# and a line identifying particle numbers.
unless (open(EDRMAX, "C:\Documents and Settings\mollet\Desktop\output1.txt")) {
        die ("cannot open input file C:\WINDOWS\Desktop\output1.txt");
}
print ("Input file was opened succesfully\n");
# if the program gets this far, the output file was opened succesfully and
# it is going to start looking for the maximum edr. Line 40
unless (open(salidaedr, ">>C:\Documents and Settings\mollet\Desktop\output2.txt")) {
        die("cannot open output file output2.txt\n");
}
#if the program gets this far, the output file was opened succesfully
print ("Output file was opened succesfully; edr maximum for the particles\n");
print ("can be found in C:\WINDOWS\Desktop\output2.txt as default\n");
$LINEMAX = <EDRMAX>;
chop ($LINEMAX);
$NPART=0;
$Ald=0;
$L=0;
while ($LINEMAX ne "") {
        if ($LINEMAX == 0) {
                if ($L == 0) {
                        $NPART = $NPART + 1;
                        if ($NPART > 1) {
#                               print salidaedr (" EDR particle No ",$NPART," =");
                                print salidaedr ($Ald,"\n");
                                $Ald=0;
                        }
                $L = 1;
                }
                print ("Analyzing particle No. ",$NPART,"\n");
        } else {
                if ($L == 1) {
                $Ald = $LINEMAX;
                $L = 0;
                }
                if ($LINEMAX > $Ald) {
                $Ald = $LINEMAX;
                }
```

```
        }

        $LINEMAX = <EDRMAX>;
        chop ($LINEMAX);
}
if ($L==0) {
        print salidaedr ($Ald,"\n");
}
print ("The program analized ", $NPART, " particles succesfully","\n");
print ("End of program part to find maximum EDR\n");
# THE PROGRAM FUNCTIONED PERFECTLY FOR THE PROVIDED SAMPLE OF
THE FLUENT PROGRAM.
# RECOGNIZES THE NUMBER OF ELEMENTS OF EVERY LINE, SEPARATES
THE EDR AND RECOGNIZE
# THE NUMBER OF PARTICLES. IT NEEDS TO BE MODIFIED IF THE EDR IS IN
ANOTHER COLUMN
# (IN WHICH CASE SHOULD CHANGE ONLY THE NUMBER IN $EDR[1]), AND
IF THERE IS A VARIATION
#IN THE HEADINGS OF THE OUTPUT.
```

Appendix D

Annexin V (AV) assay procedure

1. Perform trypan blue dye exclusion assay to determine cell count and viability.
2. Harvest cells, centrifuge at 1600 rpm for 5 minutes, resuspend in at least 120 mL fresh media (without serum), the cell concentration should be approximately 1-5×10^5 cells/mL.
3. Divide cell suspension into four equal volumes.
4. Place three of those volumes into 50 mL syringes.
5. Take 4 mL of cell suspension from one of the volumes and place in a 42ºC water bath for 45 minutes.
6. Pump the three syringes worth of cell suspension through the narrow (200 μm wide) contractional flow device at 10, 50, and 90 mL/min (2.9×10^5, 6.5×10^6, and 1.0×10^8 W/m^3, respectively).
7. Collect all of the effluent into a 50 mL conical tube, add FBS if necessary, and place in a 37ºC incubator-shaker.
8. Take a 4 mL aliquot from each 50 mL tube, place cell suspension in a 15 mL conical tube.

9. Perform trypan blue dye exclusion assay on the cells in each conical tube.
10. Add 20 μL of Rhodamine 123 solution (0.1 mg/mL final concentration) to each aliquot.
11. Centrifuge at 1600 rpm for 5 minutes.
12. Remove supernatant with a pipette (do not decant the supernatant), resuspend in 1 mL of PBS, centrifuge again, and resuspend in 1 mL Annexin V labeling buffer.
13. Repeat steps 11 and 12 for the heat shocked cells.
14. Take 100 μL of the heat shocked cell suspension and place in a FACS tube (repeat three times).
15. Add 5 μL of Annexin V-PE to one of the heat shocked FACS tubes.
16. Add 5 μL of 7-AAD to one of the heat shocked FACS tubes.
17. Take 100 μL from each of the abused and control suspensions and place in a FACS tube (repeat for the control).
18. Set one of the control FACS tubes aside.
19. Add 5 μL of Annexin V-PE and 7-AAD to each of the FACS tubes.
20. Analyze on the flow cytometer.
21. Use the FACS tubes created in steps 15 and 16 and the control FACS tube that were set aside as single color controls.
22. Repeat steps 8 through 20 every two hours.